Title
Cellular organization in Agrobacterium tumefaciens

Author
Cameron, Todd A.

Publication Date
2013

Peer reviewed|Thesis/dissertation

Cellular organization in *Agrobacterium tumefaciens*

By

Todd A. Cameron

A dissertation submitted in partial satisfaction of the

requirements for the degree of

Doctor of Philosophy

In

Microbiology

in the

Graduate Division

of the

University of California, Berkeley

Committee in charge:

Professor Patricia C. Zambryski, Chair
Professor Arash Komeili
Professor David G. Drubin

Fall 2013

Abstract

Cellular organization in *Agrobacterium tumefaciens*

by

Todd A. Cameron

Doctor of Philosophy in Microbiology

University of California, Berkeley

Professor Patricia C. Zambryski, Chair

Bacterial cell structures are macromolecular features found among all types bacteria. They often serve essential or specialized functions, and are important contributors to the widespread diversity and success of bacteria. I have focused my research on the formation and localization of two of these structures in the plant pathogen *Agrobacterium tumefaciens*: the type IV secretion system (T4SS) and the bacterial cell envelope.

A. tumefaciens is an α-proteobacterium uniquely capable of genetically transforming plant host cells during its infection process. DNA and protein substrates are transferred into plant cells via the T4SS, which forms multiple complexes around the bacterial circumference. To understand the mechanisms driving T4SS positioning, I assessed their spatial distribution by quantitative analysis and modeling. My findings indicate that these secretion complexes localize in a non-random periodic pattern along the cell perimeter. These results, along with additional plant infection studies, suggest this spatial organization serves to promote efficient delivery of substrates into host cells

A potential mechanism behind this periodic arrangement is the unipolar cell growth recently described for *A. tumefaciens*. To better understand this unusual growth mechanism, I carefully scrutinized growing cells, nascent peptidoglycan, and peptidoglycan synthesis components by electron and fluorescence microscopy. My results indicate that the unipolar growth process is surprisingly dynamic, multi-dimensional, and involves both novel and familiar components. These findings thus represent a significant departure from the canonical growth mechanism of *E. coli* and other well-studied bacilli.

Table of Contents

List of Figures and Tables

Acknowledgements

I thank my graduate advisor Dr. Pat Zambryski for her guidance and mentoring throughout my graduate career. I have learned much about the scientific process, discourse, and writing through our work together. I also thank Dr. Arash Komeili for his assistance and many insights, during both committee meetings and informal discussions. I am further grateful for the guidance of the additional faculty that helped shape my dissertation research through the qualifying exam and subsequent committee meetings: Dr. David Drubin, Dr. David Zusman, and Dr. Kathleen Ryan.

I wish to thank the current and past members of the Zambryski lab. Dr. John Zupan has especially been a great mentor and collaborator on many projects. I also appreciate and enjoyed the collaborations with Dr. Julieta Aguilar, James Anderson-Furgeson, and Justin Zik. I am grateful for the advice and comments from Dr. Tessa Burch-Smith, Dr. Solomon Stonebloom, Jacob Brunkard, and Anne Runkel.

I also thank the many researchers outside of the Zambryski lab who have facilitated this work. Dr. Marcus Roper made especially important contributions to the analysis and modeling of type IV secretion system localization. Dr. Steven Ruzin and Dr. Denise Schichnes of the Biological Imaging Facility at the University of California, Berkeley provided vital assistance and fundamentally enabled these microscopic studies. I am grateful for the critical assessment of this work by Dr. Yihfen Yen and Dr. Barbara Bensing, as well as additional collaborations with members of the Sullam lab at the University of California, San Francisco. I appreciate the insight and assistance of Dr. Sloan Siegrist and the Bertozzi lab in the study of bacterial cell growth, and thank Dr. Sharik Khan, Dr. Stephen Farrand, and Dr. Joe Lutkenhaus for supplying plasmids or antibodies critical to this work.

Finally, I thank my wife, my family, and my friends for their support, encouragement, and understanding as I have worked on this dissertation.

CHAPTER 1

Introduction

This chapter includes material from:

1. **Cameron TA, Zambryski PC**. 2012. Disarming Bacterial Type IV Secretion. Chemistry & Biology **19**:934–936.

2. **Cameron TA, Roper M, Zambryski PC**. 2012. Quantitative Image Analysis and Modeling Indicate the *Agrobacterium tumefaciens* Type IV Secretion System Is Organized in a Periodic Pattern of Foci. PLoS ONE **7**:e42219.

1.1 Type IV Secretion

1.1.1 Introduction and relevance

The type IV secretion system (T4SS) is an evolutionarily conserved bacterial secretion apparatus. T4SSs are highly diversified, and capable of secreting DNA and/or protein substrates. They play an essential role in conjugation between bacteria and in effector protein secretion during interactions between pathogenic bacteria and their eukaryotic hosts (for review, see ref 1). The T4SS is a significant contributor to the rapid spread of antimicrobial resistances, as bacteria utilize conjugation to transfer resistance genes on plasmids and other mobile genetic elements. The system plays a more direct role in disease by mediating the delivery of effector proteins into the host cells of bacterial pathogens. It is an important virulence factor of pathogens that cause many notable human diseases, including peptic ulcers *(Helicobacter pylori)*, Legionnaires' disease *(Legionella pneumophila)*, whooping cough *(Bordetella pertussis)*, typhus fever *(Ricksettsai prowazekii),* Q fever (*Coxiella burnetii*), cat-scratch disease (*Bartonella henselae*), and Malta fever (*Brucella sp.*) (2-4).

One of the earliest and best characterized T4SSs is that of the soil-dwelling plant pathogen *Agrobacterium tumefaciens.* The T4SS of *A. tumefaciens* serves as a general model for T4SS structure and function, and is uniquely capable of injecting plant cells with a specific DNA sequence (T-DNA) that becomes integrated directly into the host genome. Although *A. tumefaciens* is a significant agricultural pathogen, it is also an exceptionally important tool for plant research; ever since it was found that any sequence could be placed within the T-DNA element for transfer into plants (5, 6), *A. tumefaciens*-mediated plant transformations have been a staple of plant biotechnology and research.

A. tumefaciens is not rigorously associated with any specific human or animal diseases, aside from rare catheter-linked infections in immunocompromised patients (7). In popular culture, *A. tumefaciens* is sometimes linked with controversy for to its use in genetic engineering. It is also associated with the enigmatic Morgellons disease, due to an irreproducible report that identified *A. tumefaciens* genes in lesions of several patients (8). Additional research has demonstrated that, under specific laboratory conditions, *A. tumefaciens* is able to transfer DNA into yeast and human cell lines (9, 10). However, this occurs at a very low frequency and is extremely unlikely to occur in natural settings given the strict regulation of T4SS expression by plant-specific phenolic compounds. This particular capability is not unique to *A. tumefaciens*; the related zoonotic pathogen *B. henselae* was also shown capable of utilizing its T4SS to transfer plasmids carrying GFP into human cells (11, 12). However, a role for this capability in the natural infection process of *B. henselae* has not yet been demonstrated (13).

1.1.2 *vir* induction and transformation

A. tumefaciens cells undergo virulence (*vir*) induction when stimulated simultaneously by several signals, including lowered pH, certain sugars, and phenolic compounds such as acetosyringone released from wounded plant tissues (14-18). Phenolics are absolutely required for activation of virulence, whereas sugars act to lower the threshold required for activation (15). These signals are detected by the VirA and VirG two-component phosphor-relay, and the activated VirG transcription factor subsequently drives expression of numerous *vir* genes (19).

Among the *vir*-induced proteins are the VirB proteins composing the T4SS secretion channel, T-pilus, and secreted effector proteins. The proteins VirB1-VirB11 form the large cell envelope-spanning T4SS complex and extracellular T-pilus (20-23). The secreted single-stranded DNA substrate, the T-strand (16), is amplified up to 50 times within the bacterium (24), then directed by VirD4 to T4SS channels for export. Various effector and chaperone proteins, including VirD2, VirE2, VirE3, VirF, and VirD5, are targeted to the T4SS by C-terminal secretion signals, and secreted into the plant cell to facilitate the integration of the T-DNA directly within the plant genomic DNA (25-27). Genes expressed from the integrated DNA disrupt the balance of the plant hormones auxin and cytokinin, leading to the formation of crown gall tumors: hardened masses of plant tissues emerging from the stem at the soil line (25, 28). Additional genes carried by the T-strand promote the synthesis of opines, unusual N-carboxyalkyl amino acids that serve as carbon and nitrogen sources specifically metabolized by *A. tumefaciens* (29, 30).

1.1.3 T4SS structure and function

Crystallography and cryo-electron microscopy (EM) analyses of the T4SS of the conjugative plasmid pKM101 have substantially improved our understanding of the architecture of individual complexes. VirB7, VirB9, and VirB10 are each present as a tetradecamer, and form a ~20x20x20 nm core complex about 1.05 megadalton in size (Figure 1-1A) (31, 32). Although VirB9 and the lipoprotein VirB7 are strictly OM-associated, VirB10 stretches from the cytoplasm to the cell surface, and forms an alpha-helical outer membrane (OM) pore (32). This structure is highly unusual, and only one other alpha-helical OM pore is known to exist (32). In a recently published crystal structure, the ATPase VirB4 was also found bound to the core complex at the cytoplasmic interface (33).

The other VirB proteins have not yet been crystalized in a multiprotein complex, but their general arrangement and roles have inferred through fractionation and other studies. In the periplasm and inner membrane are VirB8, a bitopic inner membrane (IM) protein with a short cytoplasmic tail and a larger periplasmic domain, VirB6, a polytopic IM protein, and VirB3, a small membrane protein. VirB8, VirB6, and VirB3 likely form the IM-associated inner layer of the secretion complex. The secretion process and T-pilus assembly is powered by three cytoplasmic IM-associated ATPases, VirB4, VirB11 and VirD4 that induce conformational changes at the OM pore through VirB10 (34-36).

The T-pilus consists of covalently cyclized subunits of VirB2, which form a hollow structure with a 10 nm diameter (37, 38). VirB5 caps the pilus, and is suspected to play a role in initial host cell interactions (39). It is unknown whether the T-pilus serves as only an attachment and anchoring factor, or if it is actually the conduit for the transferred DNA. VirB3 exists in the IM, and contributes to both the formation of the T-pilus and to substrate secretion (20, 40-44). VirB1 has two domains which are cleaved apart in the periplasm (45); the N-terminal portion forms a lysozyme-like lytic transglycosylase that interacts with VirB8 in the periplasm, to provide localized peptidoglycan degradation, whereas the C-terminal third, termed VirB1*, promotes pilus formation (23).

Studies of the translocation route of the T-DNA have also been informative in piecing together the overall structure of the T4SS. Using a clever assay, cells were fixed with formaldehyde while translocating the T-DNA, then the individual components were purified and the association of the T-DNA with each protein was detected by PCR (21).

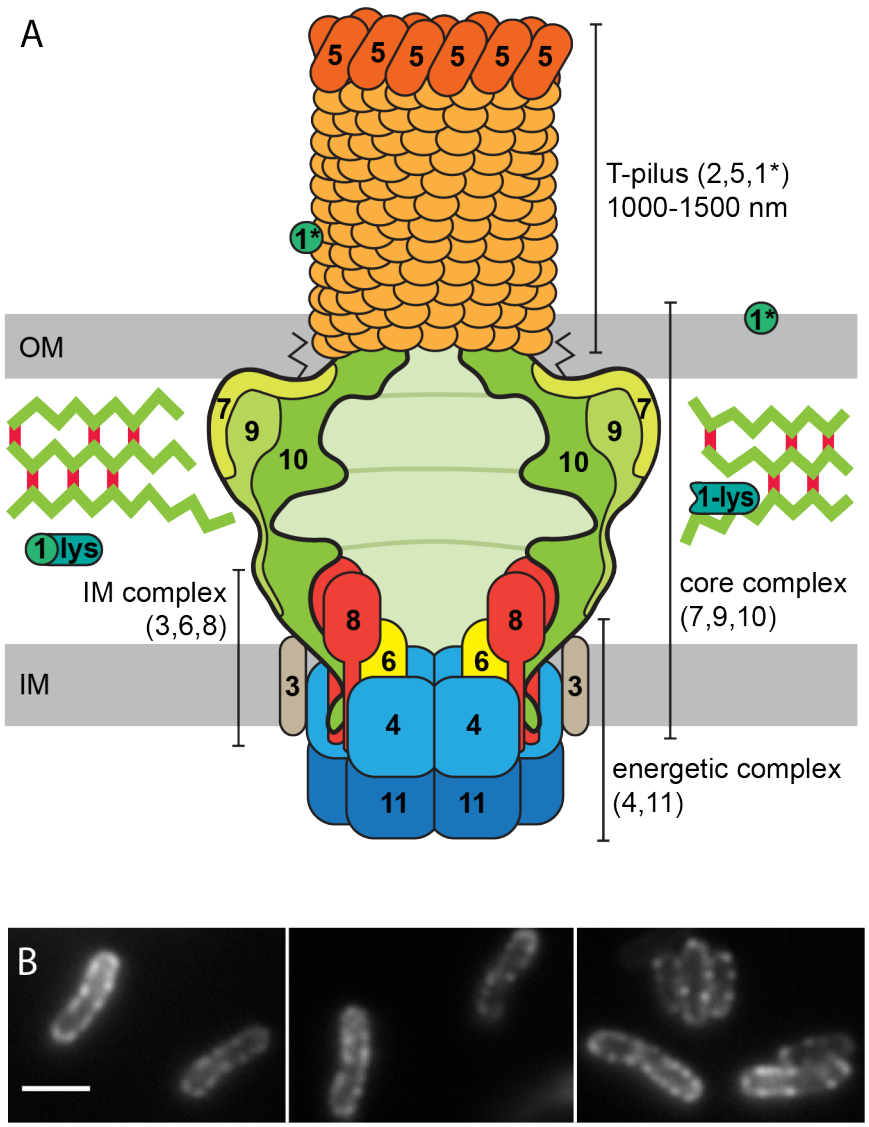

Figure 1-1 A model of the architecture of the T4SS

(A) B7-B9-B10 form the core complex (green) that spans from the inner membrane (IM) to the outer membrane (OM). B8 homodimers (red) are positioned to allow interaction with B4 and B10. The IM-spanning energetic complex (blue) is comprised of hexamers of B4 and B11. The extracellular T-pilus primarily consists of B2 (gold) with B5 (orange) at the tip. The N-terminus of B1, 1-lys, cleaves the peptidoglycan layer (green zig-zags and red crosslinks) to allow insertion of the T4SS, and the C-terminus of B1, 1*, is required for pilus assembly. The exact localization of B3 (grey) and B6 (yellow) is not known, but both are associated with the IM. The diagram is drawn approximately to scale; for example, the width of the T-pilus and B11 hexamers is 10 nm, and the core complex is ~ 18 X 18 nm. (B) The *vir* T4SS is positioned periodically around the circumference of *A. tumefaciens*. T4SS foci were visualized using a functional GFP fusion to VirB8. Scale bar is 2 mm.

By combining this technique with individual T4SS component deletions, the route of the T-DNA through the T4SS complex was established. Initial loading of the T-DNA is dependent on interaction with VirD4, as previously shown (46). VirB7 is then required, indirectly, for transfer of the T-DNA to VirB11. The two ATPases VirB11 and VirB4 pass the T-DNA to VirB6 and VirB8 in the periplasm. VirB3, VirB5, and VirB10 are then necessary for the T-DNA to reach VirB9 and VirB2. The most surprising results from this study are the requirements of VirB7 and VirB5 when they would not otherwise be expected to influence secretion. It is not clear what role VirB7 has in the early stages of secretion. There is some evidence to support a role for the T-pilus proteins VirB5 and VirB2 within the T4SS core complex. Numerous T4SS mutants have been isolated that do not generate visible pili, but still support secretion and require the presence of VirB2 and VirB5 (35, 38, 47-50).

1.1.4 T4SS as an antivirulence target

Knowledge of the T4SS structure has recently proven useful in the search for new antibiotics. While existing antibiotics inhibit overall bacterial growth by targeting essential cellular functions, an emerging alternative strategy is to directly target bacterial virulence factors without directly killing cells, in the hopes of avoiding the strong selective pressures of current antibiotics (51, 52). Bacterial secretion systems are particularly compelling targets, and there has been significant progress over the last decade in the development of inhibitors of Type III secretion systems and chaperone-usher secreted pili (53, 54).

This approach was recently applied to the T4SS of *Brucella abortus*. Dimerization of the T4SS component VirB8 is required for T4SS function (55), and this requirement served as an attractive target for high throughput screening of inhibitor molecules. Several inhibitors have since been identified that modulate VirB8 conformation by interacting with regions other than the dimerization interface (56, 57). These inhibitors could be useful in disabling T4SSs, even after they have been assembled in intracellular pathogens, and are under continued investigation. Unfortunately, no single solution would likely apply to most T4SSs, due to their highly diversified subunit composition.

1.1.5 Diversity of the T4SSs

Although the VirB system of *A. tumefaciens* serves as the archetypical of T4SS for most studies, there are many highly divergent and specialized systems throughout both Gram negative and Gram positive bacteria. Most T4SSs either transfer DNA, or transfer protein, and only a few systems such as the *A. tumefaciens* VirB T4SS are capable of transferring both types of substrates (58).

A. tumefaciens contains three T4SSs: aside from the tumor-inducing *vir* T4SS, there are also two conjugative T4SSs, the *trb* and *avh* systems found on the pTiC58 and pAtC58 plasmids, respectively. Each of the *vir*, *trb*, and *avh* T4SSs encode functionally distinct conjugative systems specific to their respective substrates (59, 60). None of these systems exhibit high amino acid sequence identity between subunit homologs, although the *avh* and *vir* systems are more closely related. VirB4 and VirB11, the two most conserved proteins of all three systems, have roughly 55% similarity to the homologs in the *avh* system, and 45% similarity to those in the *trb* system. VirB3, VirB4, VirB6, and VirB8-VirB11 have significant amino acid sequence similarity to the corresponding *avh* proteins; in the *trb* system, only VirB3, VirB4, and VirB9-VirB11 have

significant similarity. Interestingly, the *avh* system can weakly complement single deletions of any *trb* gene except *trbJ*, but there is no complementation from either *avh* or *trb* for *vir* deletions (60).

Beyond *A. tumefaciens,* there are several other notable T4SSs. *H. pylori* carries the Cag system, which is believed to contain orthologs of each of the VirB components, plus several additional proteins that adapt the system to its human hosts (61). The *E. coli* F plasmid shares eight proteins with VirB, but includes ten additional components that uniquely allow the F-pilus to dynamically extend and retract (58). The Dot/Icm T4SS found in *L. pneumophila*,*C. burnetii,* and IncI plasmids is highly divergent from the VirB system, and mainly shares homology with VirD4 and VirB4, and with fragments of VirB10 and a few additional components (58). At least one of the ATPases of this system is thought to have been co-opted from the type IV pilus biogenesis system (62). Gram positive conjugation systems are relatively poorly understood, but appear to include several components analogous to VirD4, VirB4, and VirB6, plus a variety of associated hydrolases (1).

1.1.6 Subcellular organization of the T4SS

Approximately 12-14 vir-T4SS complexes adorn the *A. tumefaciens* cell perimeter in a periodic distribution pattern (Figure 1-1B) (63). Since lateral attachment to host plant cells by *A. tumefaciens* is dependent on the presence of a functional T4SS (64), this periodic distribution of complexes likely facilitates effective host cell contact and substrate transfer concomitantly through multiple vir-T4SS complexes. The subcellular arrangement of the T4SS is discussed in more detail in Chapter 2 and Chapter 3.

The localization mechanism of T4SS complexes has not yet been identified. A similar non-random distribution was recently reported for flagella in *Bacillus subtilis.* Two proteins, FlhG and FlhF, were found to control flagellar spacing, and both had previously been identified as putative regulators of flagellar assembly or function (65). Epistatic studies revealed that FlhG, an ATPase, antagonizes FlhG, a GTPase that nucleates the assembly of new flagella. Analogous proteins are not known to exist for the T4SS. Recent efforts have focused on understanding peptidoglycan synthesis and whether this process could lead to a periodic localization of T4SS complexes.

1.2 Peptidoglycan

1.2.1 Introduction and relevance

Peptidoglycan (PG) plays a primary role in maintaining bacterial cell integrity and cell shape. The PG layer is an interconnected mesh of glycan strands covalently bonded by short, periodic peptide crosslinks in the bacterial cell envelope, and when isolated intact from a cell, the sacculus it forms retains the overall, albeit deflated, shape of the original cell. Its architecture allows bacteria to withstand significant osmotic pressure, and thicker cell walls confer greater resistance: typical Gram negative strains with ~ 6 nm PG layers can withstand pressures of several atm, whereas Gram positive strains with ~ 55 nm PG layers can withstand upwards of 20 atm (66, 67).

The PG layer is fundamental feature of most bacteria, although a few exceptions exist. Members of the phylum Tenericutes, including *Mycoplasma pneumoniae* and *Ureaplasma urealyticum*, lack PG but are able to generate protrusions and maintain rod or even spiral cell shapes through a unique network of cytoskeletal proteins (68-70).

The Chlamydiales and Planctomycetes likewise lack detectable PG, although the Chlamydiales are paradoxically still sensitive to antibiotics that target PG synthesis (71, 72). Bacteria that normally produce PG have sometimes been recovered from infected hosts as cell wall-less, osmotically sensitive "L-forms", and are likely the result of antibiotic treatments that target PG synthesis. L-forms exhibit extremely fluid cell division and fission (73), giving rise to the intriguing hypothesis that the evolution of the PG layer was a critical feature that solidified the genomes of early life and enabled specialization and speciation to occur (72, 74). These few exceptions underscore the important role that PG plays for most bacteria.

As a nearly universally conserved, bacteria-specific feature, PG serves as an excellent target for natural and synthetic antibiotics. Alexander Fleming famously identified an antibacterial compound, penicillin, produced by cultures of *Penicillium rubens* (75), which targets specific enzymes involved in PG synthesis and is broadly effective against many types of bacteria. It was later developed into a pharmaceutical agent in the 1940s (76), although at least one resistance mechanism was identified before penicillin was ever used therapeutically (51, 77). Since the advent of widespread antibiotic use, pathogenic bacteria have been under constant pressure to develop and spread resistances (often by way of type IV secretion-mediated conjugation), and commonly used antibiotics such as penicillin are largely ineffective at treating many dangerous infections (52). In recent years, the ensuing increase in antibiotic resistance has largely outpaced the production of new drugs (78), highlighting the need for novel targets and treatments (such as anti-virulence drugs, see section 1.1.4).

1.2.2 PG structure

The basic structural subunit of PG consists of a disaccharide of UDP-N-acetylglucosamine (NAG) and UDP-N-acetylmuramyl pentapeptide acid (NAM). The exact composition of the pentapeptide sidechain varies between species, but in Gram negative bacteria generally includes a L-alanine covalently linked to NAM, followed by D-glutamic acid, a meso-diaminopimelic acid (DAP), and two D-lysine residues (79). The inclusion of D-amino acids is believed to help protect the PG from non-specific degradation. This subunit is synthesized in the cytoplasm by the proteins MurA-G, attached to undecaprenol in the membrane by MraY, flipped into the periplasm by FtsW and RodA, and finally released from the undecaprenol (80).

In the periplasm, the NAG-NAM disaccharide subunits are linked together by transglycosylase enzymes to form glycan strands 10-50 disaccharides in length (81). When arranged in a glycan strand, the pentapeptide sidechains are oriented outwards in a periodic pattern that repeats every three dissacharides; looking down the length of the polysaccharide, the pentapeptides line up as if forming a three-bladed fan (82). When properly oriented towards each other, the pentapeptides of adjacent glycan strands are covalently crosslinked by various transpeptidase enzymes. Among the Gram negatives, the most common crosslink is formed by DD-transpeptidases that take the 4^{th} position D-alanine of one peptide stem and link it to the DAP of a second peptide, forming a 4-3 crosslink. LD-transpeptidases catalyze the less common 3-3 crosslink, which is made directly between the two DAP residues (83).

Through several decades of research, there have been two main models of the possible orientations of glycan strands in the cell (84). The currently favored model places the glycan strands of both Gram negative and Gram positive bacteria roughly

perpendicular to the long axis of the cell, with peptide crosslinks arranged parallel to the cell axis. This model is supported by recent cryotomography results and measurements of cell twisting under turgor changes (85-87). The alternate model oriented glycan strands out radially, with peptide crosslinks parallel to the cell surface; a counter argument to this model lies in the fact that in many bacteria the length of the glycan strands would exceed the observed thickness of their PG (81, 88).

1.2.3 Cell growth and division

To grow and divide, bacteria must also modify their PG layer in a controlled fashion. For cell division, most bacteria share the same strategy: PG is synthesized at the midcell in a decreasing diameter, until the cell is completely bisected and two separate cells are formed (89). In *Escherichia coli*, septal PG synthesis is conducted by a divisome consisting of the transpeptidase PBP3, the transglycosylase/transpeptidase PBP1b, various PG-remodeling enzymes, and an assortment of regulatory and structural proteins (79). These are all organized along a large scaffolding ring formed by the tubulin homolog FtsZ, and contraction of this ring provides the force that propels the division process (90-92). FtsZ is anchored to the cytoplasmic membrane by FtsA in most bacteria, although γ-proteobacteria such as *E. coli* utilize both ZipA and FtsA for this purpose (89).

Although bacteria employ a variety of strategies to expand their cell wall prior to division, in general new PG is inserted in either a laterally dispersed fashion along the cell length, or at specific landmarks such as the cell pole(s) (93). The most popular bacterial model systems, including *E. coli*, *Bacillus subtilis*, and *Caulobacter crescentus*, utilize the laterally dispersed mode of PG insertion, leading to a substantial body of research and understanding of this type of cell elongation. In *E. coli*, lateral PG synthesis is conducted by an elongasome primarily consisting of the transpeptidase PBP2 and the transglycosylase/transpeptidase PBP1a, plus several accessory proteins. These are likely organized by short filaments of the actin homolog MreB and associated structural proteins (94, 95).

Notably, the distinction between cell elongation and division components is not always clearly defined. For instance, PBP1a and PBP1b primarily function in their respective roles of cell elongation and division, but are partially interchangeable since only a deletion of both genes is lethal (96-99). FtsZ and MreB have also been found to facilitate the transition to cell elongation and division, respectively (100-102). Nonetheless, cell elongation and division generally function as separate processes.

1.2.4 Polar growth

In contrast, relatively little is known about the components and processes that facilitate polar growth even though this growth strategy is utilized by several orders of bacteria, notably the Actinomycetales and the Rhizobiales, and sporadically among other bacterial species (93, 103-105). Among the Gram positive Actinomycetales, polar growth has been investigated in members of *Streptomyces, Mycobacterium,* and *Corynebacterium*. In *Streptomyces coelicolor* polar growth is facilitated by three Gram positive-specific coiled-coil proteins, DivIVA, Scy, and FilP, with the former two directly organizing polar growth, and the latter providing structural support as the new pole matures (106-108). However, it is not clear which PG synthesis enzymes are necessary for polar growth in *Streptomyces* (109). In *Corynebacterium*, PBP1a, PBP1b, PBP2a,

and PBP2b all localize to the growth pole; however PBPs such as those can account for no more than 60% of the PG crosslinking activity in *Corynebacterium*, and the remaining 40% is conducted by LD-transpeptidases that were not localized (110, 111).

Polar growth in the Gram negative Rhizobiales has only recently been explored, and unlike the Actinomycetales, the Rhizobiales grow only from one pole. Although unipolar growth produces new and old cells that are roughly equivalent in size after division, some asymmetries are present; for example the old poles of *A. tumefaciens* can produce a holdfast (104). The Rhizobiales also lack the lateral PG synthesis scaffold MreB that is essential in the well-studied model systems mentioned above (104, 112). However the cell division proteins FtsA and FtsZ both localize to the growth pole and the septum in *A. tumefaciens*, suggesting that these well-known cell division components may also participate in polar growth (see Chapter 4) (113).

1.3 Dissertation Overview

The following chapters describe my dissertation research. Chapters 2 and 4 are shorter transitional chapters that facilitate a consistent research narrative and describe collaborative efforts with others in the Zambryski lab, whereas Chapters 3 and 5 describe my major dissertation research efforts in detail. Chapter 2 introduces the existing research on T4SS localization and several important findings from two published paper from the Zambryski lab in which I was second and third author. Chapter 3 rigorously explores the spatial organization of the T4SS, and encompasses a previously published manuscript where I was the lead author. Chapter 4 links T4SS localization to polar cell growth, and summarizes important findings from another publication where I was second author. Chapter 5 describes in more detail the proteins likely involved in polar cell growth. This chapter covers a second first-author manuscript that will soon be submitted for publication. Finally, Chapter 6 reviews the total findings and implications of this dissertation, and discusses future research directions.

CHAPTER 2

The Type IV secretion system of *Agrobacterium tumefaciens* is arranged as multiple foci around the bacteria cell, and mediates lateral attachment to host plant cells

This chapter briefly reviews the following publications:

1. **Aguilar J, Cameron TA, Zupan J, Zambryski PC**. 2011. Membrane and core periplasmic *Agrobacterium tumefaciens* virulence Type IV secretion system components localize to multiple sites around the bacterial perimeter during lateral attachment to plant cells. MBio **2**:e00218–11.

2. **Aguilar J, Zupan J, Cameron TA, Zambryski PC**. 2010. Agrobacterium type IV secretion system and its substrates form helical arrays around the circumference of virulence-induced cells. PNAS **107**:3758–3763.

2.1 Summary

2.1.1 Reports of polar localization

Prior to this work, polar localization of the T4SS was the most popular model in the field. This was based on a slow evolution of results and interpretations, starting in part with early SEM images showing several examples of *A. tumefaciens* cells attached, among other orientations, head-on to a carrot cells (114). Examinations of the subcellular localization of numerous VirB proteins by immunogold labeling later showed T4SS components across the entire cell surface, potentially with a slight polar bias (115, 116).

Immunofluorescence studies then indicated that the coupling protein VirD4 localized primarily at the cell poles, suggesting that the other T4SS components might have the most functionally relevant localization at the poles (117). Fluorescent protein fusions next showed that VirD4 recruited the T-DNA chaperone VirE2 to the poles (118), and that VirB6 was also at the poles (119), colocalized with VirD4 (120). To more thoroughly investigate the subcellular localization of the T4SS, Judd et al. performed immunolocalization of most of the T4SS components, and reported polar localization of VirB1 and VirB3-11 (121). These latter localizations were determined on cells grown at the physiologically relevant temperature of 20ºC, in contrast to the earlier study by Kumar et al. where cells were grown at higher temperatures. Finally, the T-DNA was also found to localize at the cell pole, through the action of VirC1, a ParA-like protein (24).

Early reports of polar attachment are likely due to the ability of *A. tumefaciens* to produce a unipolar holdfast under certain conditions. The unipolar polysaccharide (UPP) is strictly required for attachment, but is also co-regulated with the production of cellulose fibers, and could further be assisted by succinoglycan, β-1,2 glucan, and β-1,3 glucan (114, 122, 123). Like the holdfasts of *C. crescentus*, UPP binds to WGA-lectin, and may therefore consist partially of NAG polymers (124, 125). Ironically, the presence of this thick holdfast at the attached pole would most likely prevent putative polar extrusion of the fragile T-pilus and transfer of any T4SS substrates through such an attached pole.

Additional considerations cast further doubt on the conclusion that the T4SS complexes are localized to the cell poles. Many of the fluorescent protein fusions examined were expressed from the *lac* promoter by IPTG (24, 118), potentially leading to overexpression and the formation of polar aggregates (126). These exclusively polar localization results obtained by fluorescence microscopy were not reconciled with the earlier immunogold labeling data showing T4SS components across the entire cell surface (115, 116). Additionally, the conjugative T4SSs of the IncHI1 plasmid were reported to localize as multiple foci around the cell periphery, further confounding these reports of polar VirB T4SS localization (127, 128).

2.1.2 New evidence of lateral localization

In 2011 and 2012, Aguilar et al. re-examined the localization of the T4SS at high resolution using deconvolution microscopy (64, 129). A GFP-VirB8 fusion was constructed, and verified for its ability to complement a deletion of the native *virB8* gene. The VirB8-GFP fusion revealed that VirB8 localizes as multiple foci around the cell periphery, and this result was confirmed through immunolocalization of the native

protein (129). Additional GFP fusions were constructed, but these did not effectively complement their deletions. Instead, immunolocalization of the remaining T4SS components confirmed that native VirB1, VirB2, VirB4, VirB5, and VirB7-11 localize to multiple foci along the cell periphery (64). Attempts to colocalize various VirB proteins by immunofluorescence were unsuccessful, possibly due to stochastic antibody binding.

These experiments were replicated using *A. tumefaciens* strain A348, the strain used in earlier studies reporting polar localization. This control was performed to ensure that localization to multiple lateral foci was not specific to the *A. tumefaciens* strain C58 used by Aguilar et al. The two *A. tumefaciens* strains A348 and C58 are commonly used laboratory strains carrying highly homologous Ti plasmids and *virB* genes. Immunolocalization of several components (VirB2, VirB5, VirB7) and a VirB8-GFP fusion in *A. tumefaciens* strain A348 all resulted in multiple lateral foci (64).

These studies support a putative role for T-pili in the host-cell binding process. Electron microscopy of whole *A. tumefaciens* cells demonstrated that T-pili originate from the lateral cell surface, and immunolocalization studies found the major T-pilus component VirB2 localized to multiple foci around the cell (64, 129). Furthermore, attachment assays using plant protoplasts revealed that *A. tumefaciens* predominantly binds to host plant cells along its lateral surface, rather than by its poles, and that this binding is dependent on the presence of the pTiC58 plasmid carrying the *virB* T4SS genes (64). Whether T-pili are specifically required for host-cell attachment has not yet been explored.

One of the most striking aspects of the observed T4SS localization was its apparent helical nature, visualized in the middle plane of a cell as alternating puncta on either side of the membrane, often with intermediately positioned puncta or arcs seen at the upper or lower planes of the cells (see Figure 3-1A in Chapter 3). The dependence of lateral plant cell binding on the presence of the T4SS proteins, which themselves localize to lateral foci along the cell periphery, suggests that an organized distribution of T4SSs could promote efficient attachment of *A. tumefaciens* to plant cells from any orientation. Further studies of the subcellular organization of the T4SS are discussed in Chapter 3.

CHAPTER 3

Quantitative image analysis and modeling indicate the *Agrobacterium tumefaciens* type IV secretion system is organized in a periodic pattern of foci.

This chapter includes material from:

1. **Cameron TA, Roper M, Zambryski PC**. 2012. Quantitative Image Analysis and Modeling Indicate the *Agrobacterium tumefaciens* Type IV Secretion System Is Organized in a Periodic Pattern of Foci. PLoS ONE **7**:e42219.

3.1 Introduction

The type IV secretion system (T4SS) is an evolutionarily conserved bacterial secretion apparatus that is essential for conjugation and effector protein secretion during numerous pathogenic interactions between bacteria and their eukaryotic hosts (for review, see ref 1). Many notable human pathogens, including *Brucella ssp.*, *Bordetella ssp.*, *Legionella ssp.* and *Coxiella burnetii* rely on T4SSs for effective host colonization (3, 130). However, one of the first recognized and best characterized T4SS is that of the soil-dwelling plant pathogen *Agrobacterium tumefaciens.* The T4SS of *A. tumefaciens* serves as a general model for T4SS structure and function.

A. tumefaciens cells undergo virulence (*vir*) induction when stimulated simultaneously by several signals, including lowered pH, certain sugars, and phenolic compounds such as acetosyringone released from wounded plant tissues (14-17). In *vir*-induced cells, T4SS genes in the *virB* operon are expressed to produce *virB* T4SS complexes. Eleven proteins, VirB1 through VirB11, form a large cell envelope-spanning T4SS complex and extracellular T-pilus that together mediate the delivery of T4SS substrates (20-23). Recent structural analyses have established that fourteen copies of VirB7, VirB9 and VirB10 together form a large core complex approximately 20 nm in diameter and more than 1 mDa in size (31, 32). The complex is further composed of multiple copies of the ATPases VirB4 and VirB11, additional proteins of structural or functional significance (VirB1, VirB3, VirB6, VirB8), and the major and minor T-pilus components VirB2 and VirB5.

The *virB* T4SS is uniquely capable of delivering both DNA and protein substrates into the cytoplasms of host cells. The secreted single-stranded DNA substrate, the T-strand, is directed into the plant nucleus by additional secreted chaperones (VirE2, VirF), and integrated stably into the plant genomic DNA (for review, see ref 25). The T-strand carries bacterial genes that disrupt the balance of the plant hormones auxin and cytokinin, leading to the formation of crown gall tumors (28, 131). Other genes carried by the T-strand promote the synthesis of opines, unusual N-carboxyalkyl amino acids that serve as carbon and nitrogen sources specifically metabolized by *A. tumefaciens* (29, 30).

Recent results show that *vir* induced *A. tumefaciens* primarily attach laterally to host plant cells (129), yet non-*vir* induced bacteria attach to generic substrates (such as glass slides) using a polar holdfast (132). This shift to a lateral attachment orientation requires *vir* induction of *A. tumefaciens*; loss of the Ti plasmid (which carries the *virB* operon encoding the T4SS and T-pili) or lack of *vir* induction both result in cells that no longer attach laterally, suggesting that the *virB* T4SS plays a role in lateral attachment (64). To fully understand how the *virB* T4SS could participate in lateral attachment to host cells during a successful infection, it is important to determine where and how the T4SS complexes localize in the bacterial cell. Although some previous studies suggested that VirB complexes are found only at cell poles (24, 118, 121), improved microscopy techniques have demonstrated that *virB* T4SS component proteins and substrates localize as multiple lateral foci around the cell envelope (64, 129). Exemplifying these results, Figure 3-1A shows that the T4SS component VirB8 localizes as apparently regularly-spaced foci along the cell periphery when fused to green fluorescent protein (GFP). This localization pattern was confirmed by detecting native VirB proteins with immunofluorescence microscopy, which avoids potential artifacts

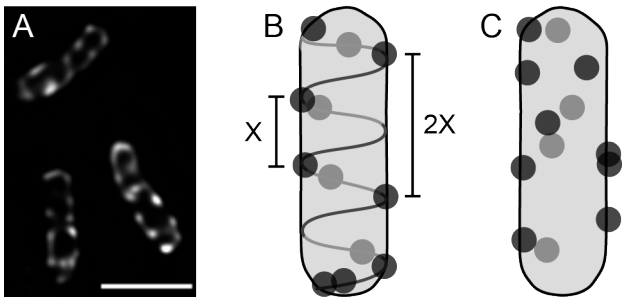

Figure 3-1 GFP-VirB8 localizes as multiple foci along the cell periphery
(A) *A. tumefaciens* expressing *vir*-inducible GFP-VirB8 on plasmid pJZ041. Image represents an average intensity z-projection of a deconvolved z-stack. Scale bar is 2 μm. B and C, two possible models of the localization of GFP-VirB8. Light and dark grey circles represent foci on the far and near sides of the cell, respectively. (B) Helical distribution model illustrating an underlying cellular scaffold directing foci localization. The fundamental period "X" is reflected in the spacing "2X" between more distant foci pairs; gaps arise occasionally as variations in foci placement on the scaffold leads to some segments without foci. (C) Random distribution model of foci along cell periphery.

generated by overexpression of fusion proteins (64, 129). Furthermore, since VirB8 is only stable when complexed with other VirB proteins (44), and GFP-VirB8 fully complements DNA transfer to plant cells (129), the VirB8 fusion proteins should represent only functional T4SS complexes. The lateral distribution of VirB foci strikingly parallels the lateral attachment observed of *A. tumefaciens* to host cells, suggesting that multiple lateral VirB complexes might facilitate lateral attachment and efficient substrate transfer from any side of contact.

Notably, the localization of T4SS components also resembles the multiple equally spaced foci of numerous bacterial proteins reported to localize in a helical fashion, including MreB, FtsZ, MinD, and the Sec translocase (112, 133-135). This similar pattern of localization suggests that VirB complexes might therefore be similarly organized, presumably mediated through an association with an underlying scaffold, or regularly repeating process in the cell such peptidoglycan synthesis (Figure 3-1B). However, recent re-examinations of MreB localization have generally concluded that the originally proposed filamentous helical model for MreB was incorrect, and instead suggest that individual MreB patches move circumferentially around the bacterial cell (94, 95, 136, 137) (also see ref 87 for an alternate interpretation). Thus, it is apparent that initial appearances of spatial organization need to be thoroughly tested. For instance, the appearance of regularly spaced T4SS foci might occur by chance when observing many cells with randomly placed foci (Figure 3-1C).

To understand if any fundamental biological mechanisms are driving T4SS positioning, we directly tested whether VirB complexes are distributed randomly or with a regular organization. Fourier analyses, nearest neighbor distances, and modeling revealed that T4SS foci conformed to a non-random distribution with predictable periodicity. Together, the data strongly support a model where T4SS complexes are systematically spaced across the bacterial cell surface, likely to help maximize effective contact and transfer of substrates to host cells.

3.2 Results

To determine whether GFP-VirB8 foci might occur in regular intervals, we examined the spacing of foci along the edges of *vir*-induced *A. tumefaciens* cells expressing GFP-VirB8. The analysis was conducted on foci along cell edges, since deconvolved z-stacks could be flattened to bring all of these foci into view without generating large ambiguities. As it is not possible to distinguish between foci originating from the top and bottom of an individual cell once the z-stack is flattened, we did not analyze foci in cell centers.

A Fourier analysis of the fluorescence signal along bacterial cell edges was performed to resolve variations in fluorescence intensity into component periodic signals, and reveal the presence of any predominant periodicities. Fluorescent profiles were collected along both sides of the visible cells, yielding linear intensity profiles suitable for one-dimensional Fourier analysis (Figure 3-2A). A Fourier analysis decomposes a temporal or spatial signal, such as a sound or image, into component sinusoidal waves of specific frequencies and phases. The distribution of wave frequencies reflects the periodicity of the signal, with sharper peaks corresponding to the wavelengths of any periodic components of the signal. Since Fourier transformations of the raw intensity profiles resulted in periodic components describing variations in both spacing as well as foci intensity, foci peaks were standardized as Gaussian distributions of similar intensities. The resulting profiles were Fourier transformed for each cell to obtain the periodicities reflecting the spatial arrangements of foci. The cumulative periodicity of the Fourier transforms indicated that GFP-VirB8 foci were loosely periodic, with the major peak present between k=1.88 and k=2.41 μm^{-1} (Figure 3-2B) corresponding to foci spaced about 0.41 to 0.53 µm apart. Furthermore, the smaller peaks at higher wavenumbers correspond to linear combinations of the

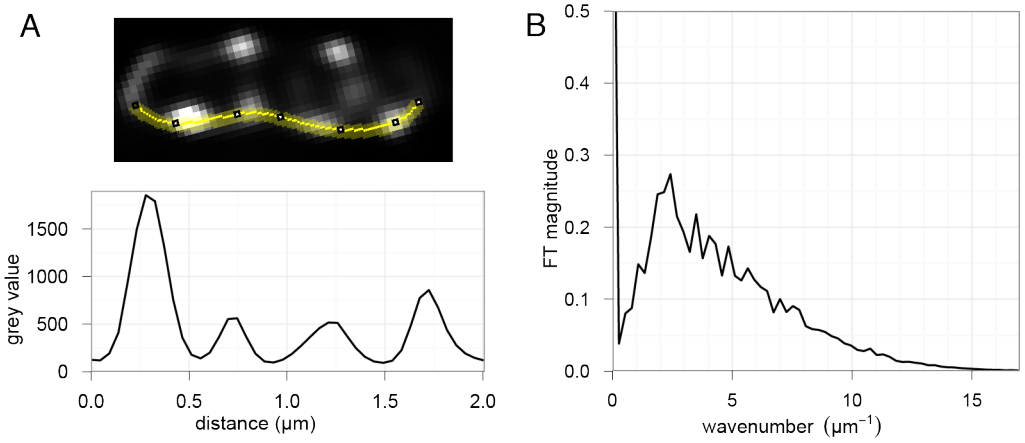

Figure 3-2 Fourier analysis reveals periodicity of GFP-VirB8 foci

(A) Example GFP-VirB8 expressing cell with the lower edge highlighted, with corresponding fluorescence profile plot used in subsequent analyses. (B) Combined Fourier transforms of each standardized fluorescence profile from 152 cell-sides. The Fourier transform peaks between k=1.88 and k=2.42, indicating the presence of a periodic element with a peak period of 0.41-0.53 µm.

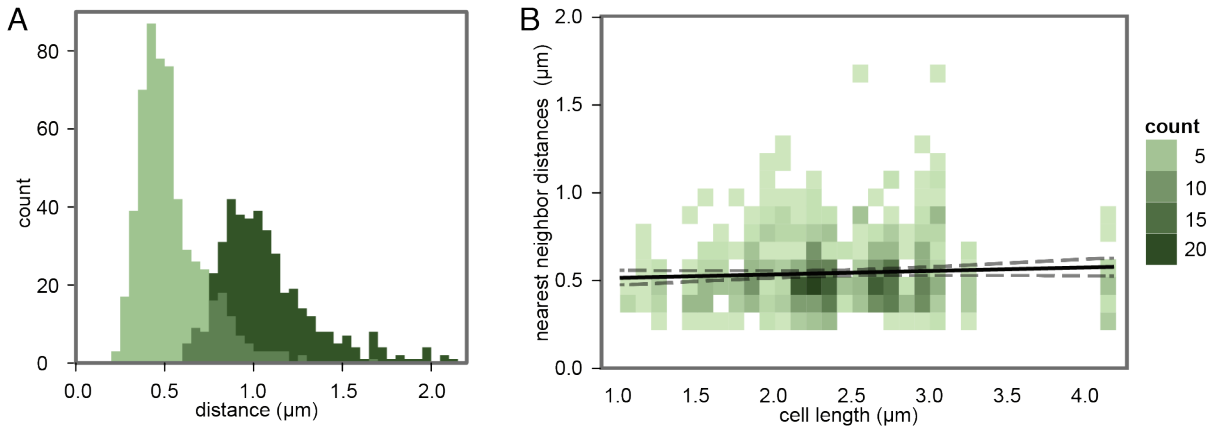

Figure 3-3 Nearest neighbor distributions of GFP-VirB8 foci

(A) GFP-VirB8 foci distances from 76 cells shown as two superimposed histograms of peak to peak distances between nearest neighbor peaks (light grey) and next nearest neighbors (dark grey), with overlap in grey. Bin size is 0.05 μm. (B) Heat map of VirB8 nearest neighbor distances versus cell length. A linear model fit (black line) with 95% confidence intervals (dashed lines) show little correlation between cell length and foci spacing.

fundamental modes k_1=1.08 μm^{-1} (0.93 μm) and k_2=2.41 μm^{-1} (0.41 μm), consistent with an overall periodic spacing.

To assess whether this periodicity could be obtained by a random localization process, a precise set of nearest neighbor distances between foci was collected and analyzed. The distances between experimentally observed pairs of neighboring GFP-VirB8 foci were manually determined by measuring peak-to-peak distances of the recorded fluorescent profiles. When plotted on a histogram (Figure 3-3A), we obtained two unimodal distributions with distinct peaks, demonstrating the median distances between nearest neighbor and next nearest neighbor VirB8 foci were 0.45 μm and 0.95 μm, respectively. The next nearest neighbor distribution peaks at twice the distance and with twice the width of the nearest neighbor distribution, indicating there is a consistent spatial separation between pairs and triplets of adjacent foci. The slight right-skew of these distributions could be explained if foci were stochastically absent along portions of a scaffold (compare 'X' and '2X', Figure 3-1B); this would result in occasional nearest neighbor measurements that span multiple periods.

Notably, the measured nearest neighbor distances and Fourier period closely agree with the simple average nearest neighbor distance (0.48 μm) that would be obtained if the 717 counted foci were distributed evenly over the total length of both sides of the measured cells (348 μm). This further demonstrates that the distribution of VirB8 foci in the cells was not biased towards any particular subcellular region or pole. For instance, if foci were found only towards one half of the cell, then these metrics would no longer coincide; the number of foci would be halved and the average distance between foci distributed over the entire cell length would be twice the average nearest neighbor distance. Furthermore, cell length did not correlate with VirB8 foci distances (Figure 3-3B), indicating that cell size and cell cycle were not factors affecting foci spacing.

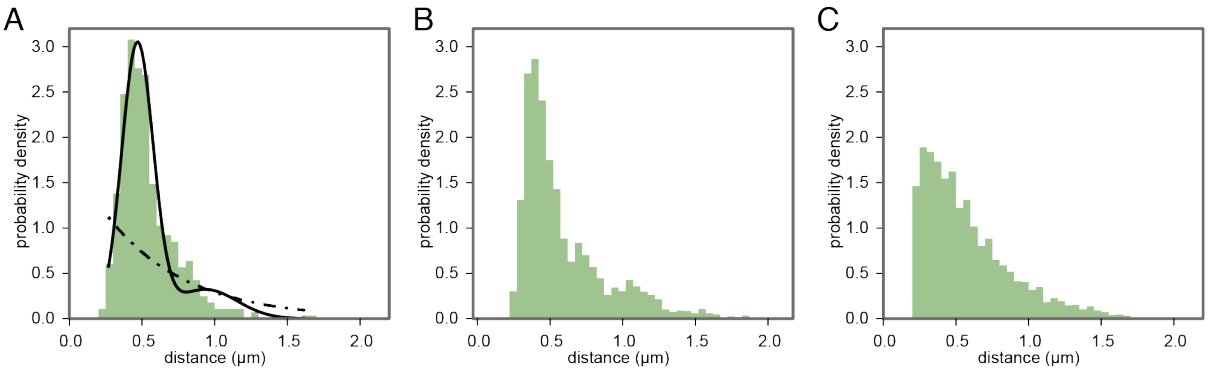

Figure 3-4 Maximum likelihood modeling and Monte Carlo simulations support periodic placement

(A) Density histogram of nearest neighbor distances for VirB8 overlayed with maximum likelihood best-fit models of periodic (—) and random (- • -) placement. Arrowhead indicates secondary peak of periodic model. B and C, density histograms of nearest neighbor distances gathered from Monte Carlo simulations of periodic helical (B) and random (C) placement.

To quantitatively evaluate if randomly distributed foci could produce the observed results, the experimental VirB8 nearest neighbor distribution (grey histogram, Figure 3-4A) was fit with hypothetical distributions that would arise from either random (dashed line, Figure 3-4A) or periodic (solid line, Figure 3-4A) foci placement. A uniform random distribution of points on a line produces an exponential distribution of nearest neighbor distances (see Materials and Methods for derivation, and Figure 3-4C for example); therefore an exponential distribution was used to model nearest neighbor measurements between foci along the edges of cells with randomly placed foci (dashed line, Figure 3-4A). Periodic localization of foci was modeled as a Gaussian distribution with a mean (period) of μ and standard deviation σ (solid line, Figure 3-4A). To account for the potential that nearest neighbor distances might occasionally span multiple periods, we introduced a small probability that pair distances were instead drawn from the next-nearest neighbor distribution (Gaussian with a mean of 2μ and standard deviation 2σ). This resulted in a smaller secondary peak at twice the period of the primary distribution (arrowhead, Figure 3-4A). The random and periodic models were then fit to the experimental VirB8 nearest neighbor distribution using maximum likelihood estimation; the resulting periodic model closely follows the observed distribution, while the random localization model fits the data poorly (Figure 3-4A).

These model fits were next verified via Monte Carlo simulations of random and periodic foci localization. For each simulation, equal numbers of foci were repeatedly modeled on 3D cells in either a random or periodic helical pattern, then nearest neighbor distances along each edge were gathered in consideration of the resolution (~200 nm) expected for deconvolved fluorescence microscopy. The Monte Carlo simulations (Figure 3-4B and C) produced results mirroring the maximum likelihood model fits (Figure 3-4A).

Finally, to evaluate the relative likelihoods of the periodic and random models, the Akaike information criterion (AIC) was used. The AIC allows for a quantitative comparison between two or more models with varying degrees of complexity by utilizing maximum likelihood estimates in conjunction with penalties for model complexity (138).

With this approach, the periodic model could be appropriately penalized for utilizing more parameters than the random model, thus ensuring that the better fit of the periodic model was not simply the result of over fitting the data. Given the data observed, the difference in AIC score was 841 in favor of the periodic localization model, indicating that random placement is extremely unlikely relative to the periodic model (E-value << 10^{-100}). Thus, both visually and quantitatively, a model of periodically spaced foci better fit the measured distribution of VirB complexes than a null model of random spacing.

3.3 Discussion

The localization of *virB* T4SS foci was assessed by Fourier analysis, nearest neighbor distributions, Monte Carlo cell simulations, maximum likelihood model fits and Akaike information criteria testing. Each analysis clearly indicated that the T4SS is not localized by a random process. Together, the data provide compelling evidence that VirB complexes are positioned periodically across the surface of *A. tumefaciens* cells. The data further demonstrate that the VirB complexes are distributed over the entire length of cells without bias towards any particular subcellular region, validating previous observations (64, 129).

It is not yet clear how the T4SS attains a periodic localization in *A. tumefaciens*, although one obvious possibility is that the T4SS complexes interact directly with a helical scaffold. A number of bacterial proteins have been reported to localize helically, most prominently the cytoskeletal proteins such as FtsZ and MinD (135). Surprisingly, even some metabolic proteins such as CTP synthase and YvcK have been observed forming filaments or helices, respectively (139, 140). Such proteins could serve directly as a scaffold guiding a helical, and therefore periodic, localization of T4SS complexes throughout the cell. Alternatively, structures consisting of concentric rings or multiple lateral filaments (141, 142) could also serve as scaffolds for generating regularly spaced T4SS complexes.

However, a protein scaffold is not the only way to acquire a periodic localization pattern. For instance, lipid rafts were recently implicated in heterologous protein distributions in *Bacillus subtilis* (143), and could potentially play a role in organizing the T4SS. Although not studied in *A. tumefaciens,* anionic lipids have also been reported to form regular bands or helices in *B. subtilis*, often also in conjunction with the Sec secretion system (133, 144, 145). Many proteins, such as FtsA (146), SecA (133, 147), MinD (148), and MreB (149) interact directly with anionic lipids through positively charged amphipathic α-helical domains. Several of the VirB proteins, particularly the ATPase VirB11, contain putative amphipathic helices that could interact with anionic lipids to help direct the T4SS to anionic lipid domains.

In a closely related alternate mechanism, the T4SS complexes could also be localized by the Sec secretion system. Of the eleven T4SS components, eight (VirB1-3, VirB5, VirB7-10) are putative Sec secretion substrates (like many autotransporter proteins of Type V secretion (150), several of the VirB proteins of *A. tumefaciens* possess extended N-terminal Sec signal peptides that are not readily identified by prediction tools such as SignalP). With most of the T4SS components directed through the Sec secretion system, VirB complexes could be assembled in close proximity to Sec channels. Given the association of the Sec system with anionic lipids, and in conjunction with potential amphipathic helices within the VirB proteins, a regular banded or helical localization pattern could be imparted to the final assembled T4SS complexes.

One final possibility instead relies on disruptions of the peptidoglycan layer to facilitate assembly of the T4SS. The 20 nm T4SS core complex (31) likely requires significant remodeling of local peptidoglycan to successfully assemble in the cell envelope. Although VirB1 does function as a lytic transglycosylase, it may not sufficiently disrupt the peptidoglycan on its own. Localization of the VirB complexes near sites of peptidoglycan synthesis or modification would facilitate both insertion of the complex and the subsequently required repairs to the peptidoglycan layer.

Once a characteristic spacing of T4SS complexes is established, it would need to be maintained consistently through the course of cell growth. In bacterial species such as *E. coli*, a periodic pattern of T4SS complex assembly might become distorted over time as lateral peptidoglycan synthesis during cell elongation introduces new peptidoglycan between T4SS complexes. Interestingly, no correlation was found between cell length and foci spacing in *A. tumefaciens*, so cell growth does not appear to have a major role in determining or modifying foci placement. In further support, recent evidence indicates that *A. tumefaciens* undergoes primarily unipolar growth during cell elongation (104), and therefore spatial arrangements of foci over the length of the cell would remain relatively undisturbed through successive rounds of cell division. Coupled with the dramatically slowed growth of *A. tumefaciens* under *vir*-induced conditions, periodically organized T4SS complexes most likely exist well through the duration of the infection process.

Compared to random localization, an organized distribution of the *virB* T4SS complexes could provide a variety of benefits to the bacterial cell. Fewer complexes would be required to ensure coverage of the bacterial circumference, thereby allowing cells to conserve resources spent on T4SS assembly. Furthermore, with VirB complexes evenly distributed across the cell surface and oriented in all directions, *A. tumefaciens* cells would be more likely to successfully contact a host cell and maintain stable lateral attachment for DNA and protein transport (Figure 3-5). Finally, a periodic T4SS distribution would help avoid excessive localized cell envelope stress that might occur due to complex clustering, a potential hazard given that each secretion channel is at least 20 nm in diameter (31) and spans both cell membranes and the peptidoglycan layer.

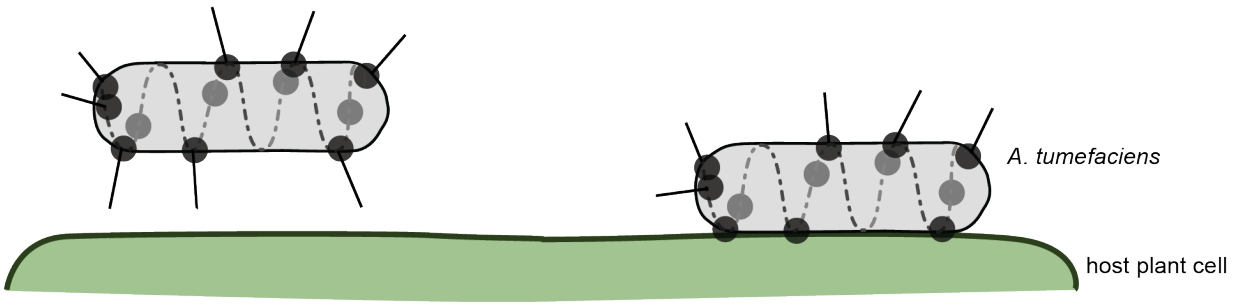

Figure 3-5 T4SS-mediated attachment of *A. tumefaciens*

An *A. tumefaciens* cell producing multiple T4SSs arranged periodically across the cell surface will likely successfully initiate and maintain contact with a target cell from any orientation. A disorganized arrangement of T4SSs could lead to 'blind spots' with few or no T4SSs and unable to initiate contact or effective substrate transfer.

Further research will be required to explore the potential mechanisms and importance of periodic T4SS localization. Ultimately, such studies will improve our understanding of the *virB*-dependent pathogenesis of *A. tumefaciens,* and more generally, of the strategies bacterial cells employ to arrange the T4SS and other large cellular components.

3.4 Materials and Methods

3.4.1 Strains and Growth Conditions

Wild-type *A. tumefaciens* strain C58 containing nopaline pTiC58 was transformed with plasmid pJZ041 containing GFP-VirB8 under control of the *vir* promoter, as described (129). Transformed cells were grown with 300 μM streptomycin and 100 μM spectinomycin under all conditions. To induce the *vir* system, an overnight culture was grown in LB at 28ºC, then diluted to an OD_{600} of 0.1 in pH 5.5 minimal AB media and grown for 5 h at 19°C (23). Cultures were plated on AB agar plates supplemented with 200 μM acetosyringone (AS) and incubated for 2 days at 19°C.

3.4.2 Fluorescence imaging and measurements

vir-induced cells were resuspended in AB media to an OD_{600} of 5, and 5 μl were placed between a slide and coverslip. Stacks of optical sections were taken with an Applied Precision Deltavision Spectris DV4 deconvolution microscope and deconvolved using Huygens Pro (Scientific Volume Imaging) as described (129). To acquire nearest neighbor distances and fluorescent profiles, deconvolved z-stacks were flattened into average intensity z-projections. To acquire fluorescent profiles, cell edges were selected manually with consideration of the corresponding brightfield images then measured over a 2-pixel thick averaged line using the profile tool in Fiji (151). All distinguishable individual cells in the field of view were included for analysis.

3.4.3 Checking for periodicity using Fourier transforms

The centers of foci were determined automatically from fluorescent profiles as follows. The fluorescence intensity values of the profiles yielded one dimensional intensity-distance data: $I=I(x)$. Foci centers were located to sub-pixel precision by interpolating a parabola to the three brightest data points at each putative peak of the fluorescent profiles. Since variations in foci size and brightness can obscure the periodicity of foci placements, the intensity curve for each focus was standardized by replacing its peak by a standard curve $I(x,x_*) \sim \exp(-(x-x_*)^2/2w^2)$, where x_* is the location of the peak, and the width of each standard curve was taken to be $w \approx \Delta x$, where Δx is the spacing of measurements. For these standardized intensity curves, Fourier transforms could be calculated exactly $\hat{I}(k,x_*) \sim \exp(-\pi w^2 k^2 - ikx_*)$. To normalize and aggregate Fourier transforms from different intensity curves, the standardized intensity curves were subsampled on a regular grid: k was restricted to take discrete values $\{k_n\} = \{2\pi n/L : n=\ldots,-1,0,1,\ldots\}$. Periodicity at any of the wave numbers k_n leads to a large value of the $|\hat{I}(k_n)|$; otherwise, the different phases of the contributions from different intensity peaks, $\hat{I}(k,x_*)$, tend to cause their Fourier transforms to cancel. To search for a signal of periodicity across many different cells, a histogram of relative frequencies was constructed by binning and averaging the discrete data $|\hat{I}(k_n)|$ across cells.

3.4.4 Hypothesis testing

The experimentally measured inter-foci separations were compared with the predicted distribution of inter-foci separations assuming that foci were spaced at random around the cell. What is the distribution of foci separations under this null hypothesis? Suppose we know that there are N foci distributed along a cell of length L. Then the locations $\{X_i\}$ of the foci can be treated as uniform random variables, i.e. $X_i \sim U(0,L)$. Each X_i therefore has the same probability density function $p_i(x) = 1/L$, $0<x<L$. Suppose we are interested in the spacing D_i between X_i and the closest member of the set $\{X_j: X_j > X_i\ ,\ j \neq i\}$. Given that $X_i=x$ (say) the likelihood that this spacing exceeds d is

$$P\left(D_i > d \middle| X_i = x\right) = P\left(\text{no } X_j \text{ in } \left[x, x+d\right]\right) = \begin{cases} \left(1-d/L\right)^{N-1} \text{ if } x < L-d \\ 0 \text{ if } x > L-d \end{cases}$$

In the first case, (N-1) random variables $\{X_j: j \neq i\}$ need to be chosen to fall outside of the interval, each, independently, with probability 1-d/L. To obtain the distribution of D_i without conditioning on the location of X_i we appeal to the law of total probability:

$$P\left(D_i > d\right) = \int_0^L P\left(D_i > d \middle| X_i = x\right) p(x) dx = \left(1-d/L\right)^N$$

From this calculation we can calculate the probability density function for the separation of foci:

$$p_D(d) = \frac{\partial P\left(D_i > d\right)}{\partial d} = \frac{N}{L}\left(1-\frac{d}{L}\right)^{N-1}$$

noting that the distribution is the same for all foci. In most cases, d is much smaller than L. We therefore consider the limit where N is allowed to tend to infinity, while keeping the mean inter-foci spacing constant $\lambda=L/N$. Then:

$$p_D(d) \sim \frac{e^{-d/\lambda}}{\lambda}$$

i.e. the inter-foci separations are exponentially distributed under the null hypothesis.

To calculate the likelihood that the measured distribution of foci separations arises from random placement, the Akaike Information Criterion (AIC) was calculated assuming (i) the null hypothesis and (ii) that foci had a preferred separation d_*, modeled statistically, by a (Gaussian) $N(\mu,\sigma)$ distribution. Based on the observed data, two modifications were made to these distributions (i) to avoid modeling inter-foci separations below the observable limits of resolution, the null hypothesis distribution was modified by imposing a cut-off length scale d', (ii) because variations in foci placement on a periodic substructure can lead to segments of this scaffold to occasionally lack foci (over the particular contours where the fluorescent profiles were collected), we allowed inter-foci separations to include pairs of foci from next nearest neighbor periods, along with pairs from neighboring periods. Accordingly, the null and alternate hypotheses were modeled statistically by distributions:

$$(i) \quad p_D(d) = \begin{cases} 0 & \text{if } d < d' \\ \dfrac{e^{-(d-d')/\lambda}}{\lambda} & \text{if } d \geq d' \end{cases}$$

$$(ii) \quad p_D(d) = \frac{p}{\sqrt{2\pi\sigma^2}} e^{-(d-\mu)^2/2\sigma^2} + \frac{(1-p)}{\sqrt{4\pi\sigma^2}} e^{-(d-2\mu)^2/4\sigma^2}$$

Here the parameter *p* represents the probability that a pair of foci is drawn from neighboring (rather than next-to-neighboring) periods. The parameters *d'*, *λ*, *σ, μ, p* were estimated by non-linear fitting to the observed data using the Matlab built-in function fminsearch (Mathworks, Waltham MA).

3.4.5 Monte Carlo simulations

For each of the periodic and random foci simulations, 1000 *A. tumefaciens* cells were modeled as 3D cylinders 2 μm in length and 0.6 μm in diameter. The pitch and variability of the helical model, and the number of foci modeled were estimated from the VirB8 nearest neighbor data. Based on the VirB8 data, these models should include approximately four foci along each edge. However, it was estimated that foci as far as 150 nm from the cell edge (in a 2D projection) would be included in the fluorescent profiles measured over a 2-pixel (~90 nm) thick averaged line, due to the inherent resolution limits of roughly 200 nm for fluorescence deconvolution microscopy (152). Consequently, the four modeled foci on each cell edge would originate from ~1/3 of the cell surface, indicating there should be twelve foci total for a cell 2 μm in length. Therefore, twelve foci were placed on the surface of each modeled cell, either at random positions along the path of a helix with a period of 0.50 μm ± 0.15 μm, or entirely at random. Nearest neighbor distances were then gathered between foci falling within 150 nm of each side of a 2D projection of each cell. To account for limits of resolution, the positions of foci falling closer than 200 nm were averaged together.

CHAPTER 4

Dynamic FtsA and FtsZ localization and outer membrane alterations during polar growth and cell division in *Agrobacterium tumefaciens*

This chapter briefly reviews the following publication:

1. **Zupan JR, Cameron TA, Anderson-Furgeson J, Zambryski PC**. 2013. Dynamic FtsA and FtsZ localization and outer membrane alterations during polar growth and cell division in *Agrobacterium tumefaciens*. PNAS **110**:9060–9065.

4.1 Summary

4.1.1 Potential T4SS localization mechanisms

Given the periodic localization observed for the T4SS, we next asked what sort of mechanism could result in an organized localization pattern. Secretion of T4SS components through the Sec system, and association of T4SS components with anionic lipid domains, cytoskeletal proteins, and regions of active peptidoglycan synthesis were all considered possible candidates.

The Sec secretion system is a protein translocase responsible for insertion of proteins into the inner membrane and periplasmic space (153, 154). The majority of T4SS components are likely Sec substrates, since they localize to the periplasm or OM (see Figure 1-1) and posses putative, if atypical, Sec signal peptides. In *B. subtilis* and *E. coli*, the Sec system reportedly has a helical punctate arrangement similar to the T4SS (133, 144). We hypothesized that assembly of T4SS components could be closely coupled with secretion through the Sec system, thus leading to the T4SS localization observed. However, GFP fusions to Sec components were much more diffuse than punctate, and did not appear to localize in a pattern similar to the T4SS (Cameron and Zambryski, unpublished results).

Our Sec localization results also argue against a potential role for anionic lipids in localizing the T4SS. In *B. subtilis*, anionic lipids and Sec components appear to localize to discrete foci around the cell periphery (133, 145), and the localization and activity of Sec components are closely tied to the presence of anionic lipids (133, 155). The lack of discrete Sec component localization in *A. tumefaciens* implies that anionic lipids are also evenly dispersed throughout these cells, and unlikely to contribute to a periodic spacing of T4SS complexes. The potential impact of anionic lipids on T4SS localization was not studied further.

Cytoskeletal proteins such as the cell elongation scaffold MreB were an attractive possibility due to the many existing examples of spatial organization by these proteins. However, unlike most other rod-shaped bacteria, *A. tumefaciens* lacks MreB, so other cytoskeletal protein such as the cell division scaffold FtsZ, the FtsZ-positioning proteins MinCDE, and others were pursued. Initial results suggested that MinCDE might have a role in T4SS positioning (129), however a subsequent deletion of the *minCDE* genes from *A. tumefaciens* failed to disrupt T4SS localization (Cameron and Zambryski, unpublished results).

MinD is closely related to ParA of the plasmid partitioning system, and ParA homologs have been implicated in numerous spatial organization roles (156). Reported functions include determining equidistant spacing of carboxysomes in cyanobacteria (142), controlling the localization of chemotaxis proteins in *Vibrio cholerae* and *Rhodobacter sphaeroides* (157, 158), and regulating the positioning of the cell division FtsZ ring in *Myxococcus xanthus* (159). ParA usually interacts with its partner protein ParB to facilitate plasmid partitioning; however the ParA proteins described above typically lack their respective ParB partners, or substitute it with different proteins (156). *A. tumefaciens* contains several ParA/B pairs, as well as one such orphan ParA. Its role in subcellular protein localization was not assessed in this study.

FtsZ is a major cytoskeletal protein found in most bacteria, and was examined early on for a potential role in T4SS localization. Preliminary efforts to localize FtsZ revealed multiple T4SS-like foci around the cell during *vir*-induction conditions, by both

FtsZ-GFP fluorescent fusions and immunolocalization of the native protein (Zupan, Cameron, and Zambryski, unpublished results). Given the lack of MreB, we hypothesized that FtsZ might facilitate PG synthesis at these foci during cell elongation in *vir*-induction conditions. Although FtsZ did not appear to consistently colocalize with T4SS components (Cameron and Zambryski, unpublished results), the striking similarities between their localization patterns prompted us to consider additional mechanisms. We hypothesized that the overall PG synthesis process might help facilitate the insertion and assembly of the 20x20x20 nm T4SS complexes in the bacterial cell envelope. Figure 1-1 illustrates the dimensions of the T4SS within the context of the PG layer, clearly showing that T4SS assembly must disrupt the PG layer.

Thus, initial research efforts focused on understanding the PG synthesis enzymes and scaffolding proteins in *A. tumefaciens*. We hypothesized that understanding this process was a necessary prerequisite before we could directly test its role in the periodic arrangement of T4SS complexes.

4.1.2 Localization of cell division scaffold proteins

A recent report had indicated that *A. tumefaciens* and other Rhizobiales grow from their poles (104). During this time we were actively interested in determining the molecular components in *A. tumefaciens* responsible for PG synthesis during cell elongation and division. A bioinformatics survey of PG synthesis enzymes and related proteins revealed that *A. tumefaciens* does not encode most of the well-studied elongase specific components (described in more detail in Chapter 5). In contrast, most cell division components were present, meaning that cell division components and/or novel proteins might contribute to polar growth. To determine if cell division proteins might be utilized in polar growth, we set out to test whether the scaffolding protein FtsZ and its cell division partner FtsA localize to the growth pole under regular, non-*vir* induction growth conditions.

Serendipitously, we found early on that the lipophilic membrane dye FM4-64 appeared to most intensely label the non-actively growing regions of *A. tumefaciens* cells. In shorter cells FM4-64 labeled one pole but not the other, but in cells undergoing cell division, FM4-64 labeled one pole strongly, the other weakly, and did not label at the midcell (Figure 4-1A). The lack of labeling at the septum in dividing cells strongly suggested that actively growing regions were poorly labeled by FM4-64. As described below, this finding was eventually confirmed through a series of experiments that demonstrated FtsA-GFP localization to the growing cell pole during unipolar growth. FM4-64 labeling became an important tool for identifying old and new cell poles in future studies.

When cells expressing FtsA-GFP were labeled with FM4-64, FtsA-GFP localized specifically to the regions that were poorly labeled with FM4-64, and occasionally to both the pole and the midcell, in an apparent transitional state prior to cell division (Figure 4-1B). Quantification of polar localization revealed that FtsA was present at one pole in ~ 80% of the population during cell elongation. To specifically test if the FtsA-GFP and dim FM4-64 labeled poles were the growth poles, cells expressing FtsA-GFP were briefly incubated with Texas Red-X succinimidyl ester (TRSE), which non-specifically labels extracellular proteins. When the cells are washed free of TRSE unlabeled new cell material is added at the growth pole during continued cell growth (104). Cells labeled with TRSE, washed, and grown 15 minutes (Figure 4-1C) or for 1-2

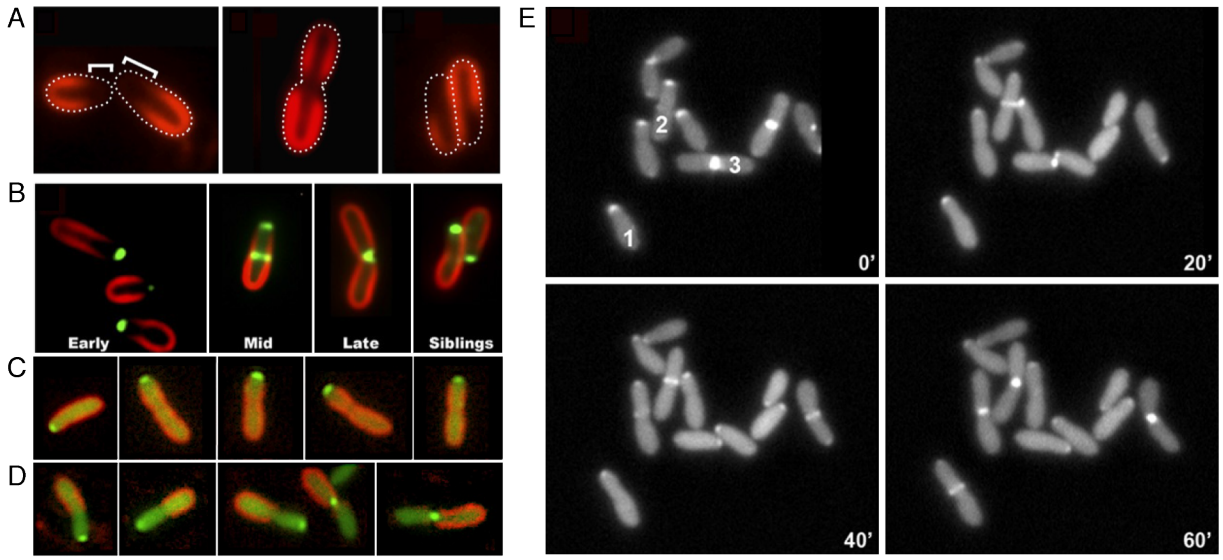

Figure 4-1 FtsA-GFP localization

(A) Differential labeling of old pole and growth pole by FM 4-64. Close-ups of FM 4-64 labeling: (left) more intense labeling of old pole; brackets indicate unlabeled growth poles; (middle) both poles labeled in a cell with midcell constriction; and (right) newly divided cells. White dots show the cell outlines. (B) Changes in FtsA-GFP localization correlated with early, mid, and late times of cell-cycle progression. Siblings are a pair of daughter cells that remained in contact with each other after cell division. C and D: cells expressing FtsA-GFP were incubated briefly with Texas red-X succinimidyl ester (TRSE) to label surface proteins. Cells grown for an additional (C) 15 minutes or (D) 120 minutes without TRSE revealed that FtsA-GFP was localized to the unlabeled growth pole. (E) Time-lapse microscopy of cells expressing FtsA-GFP. Actively growing bacteria were imaged using an ONIX live-cell imaging microfluidic flow chamber (CellASIC). Numbers highlight cells starting at (1) early, (2) mid, and (3) late cell cycle points in the timelapse

generations (Figure 4-1D) both showed that FtsA-GFP localized to the unlabeled new pole. These results demonstrated that FtsA-GFP localizes to the growth pole, i.e. to the pole without TRSE labeling. Since FtsA-GFP localization and FM4-64 labeling occur at opposite poles, we inferred that FM4-64 preferentially labels the old cell pole where there is no TRSE turnover. Time-lapse imaging of FtsA-GFP confirmed its localization to the growing pole (Figure 4-1E).

Since FtsA is a molecular marker for polar growth in *A. tumefaciens*, we asked whether FtsZ is likewise localized to the growth pole during vegetative growth. In contrast to our earlier experiments that examined FtsZ localization in very slow-growing *vir*-induced cells, during vegetative growth FtsZ-GFP localized to the growing poles in 40% of the cell population. However, the localization of FtsZ-GFP was more complex than FtsA-GFP or FM4-64 since 35% of cells had both polar and additional foci throughout the cell, and 25% exclusively exhibited a midcell foci or an FtsZ-GFP ring (Figure 4-2A). Similar patterns were again observed for the native FtsZ protein as detected by immunolocalization (Figure 4-2B). Like FtsA and FM4-64, the localization patterns of FtsZ appeared linked to the cell cycle, although the number of different localizations complicated the interpretation. The interpreted progression of FtsZ localization through the cell cycle is diagrammed in Figure 4-2C. Timelapse microscopy

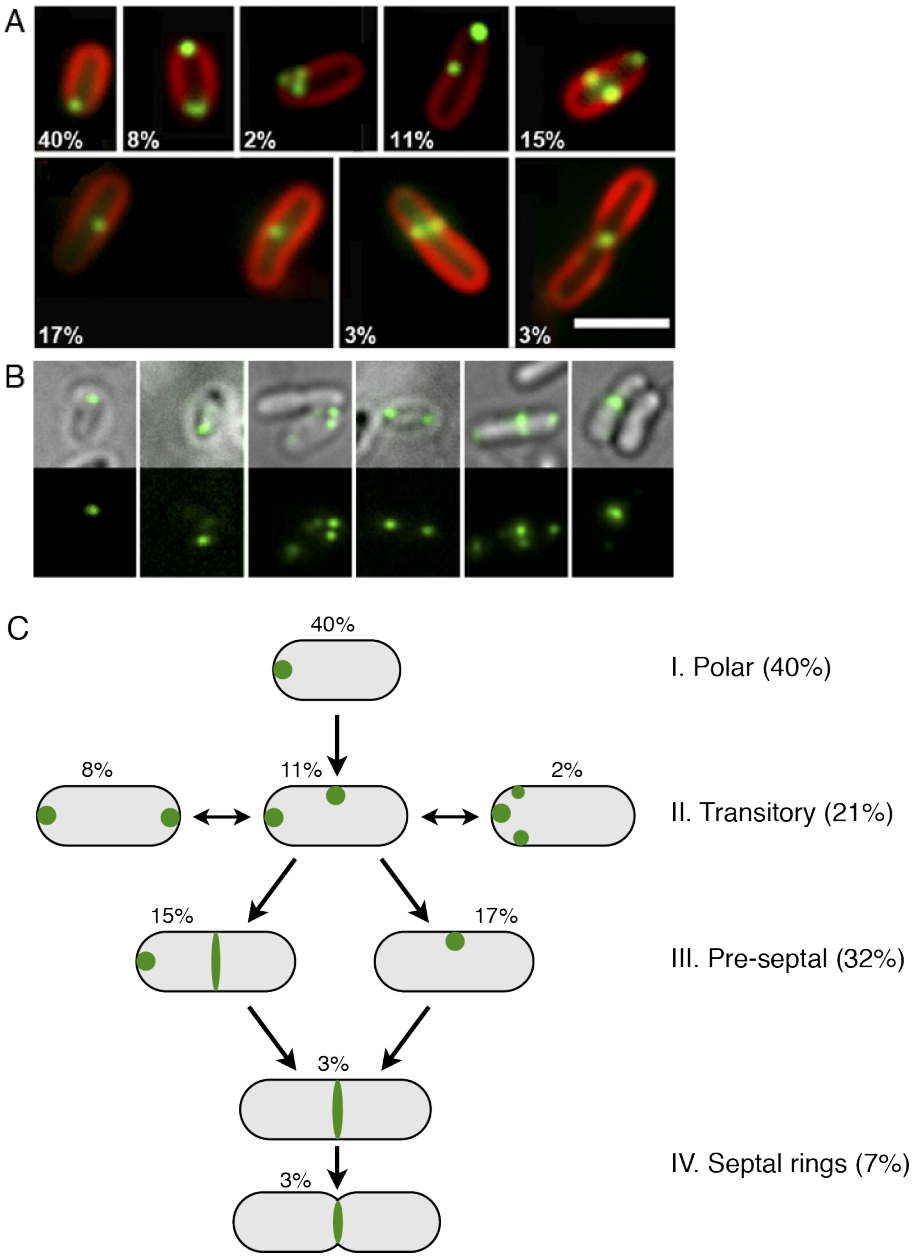

Figure 4-2 FtsZ localization and model

(A) Cells expressing FtsZ-GFP were quantified and categorized by localization pattern. Polar localization appeared most prominent in short cells, whereas midcell localization was most prominent in long or dividing cells. (B) Immunolocalization of native FtsZ revealed the same patterns observed for the FtsZ-GFP fusion, including midcell rings and polar and multiple foci. (C) A model of FtsZ localization through the cell cycle. Percentages indicate the proportion of cells observed with each localization pattern.

of FtsZ-GFP was unsuccessful, possibly due to long-term phototoxicity by the FtsZ-GFP fusion. Together these results indicate that the canonical cell division proteins FtsZ and FtsA localize to the growth pole. FtsA has a more consistent polar localization than FtsZ, suggesting that FtsA could play a major role in maintaining polar growth, may be more important for polar growth than FtsZ.

Additional experiments showed that treatment with sub-lethal concentrations of the penicillin derivative carbenicillin affects growth at the midcell, but not at the septum. Specifically, carbenicillin treatment resulted in dramatic bulging and other cell shape defects at the septum of nearly all the cells. Since most cells eventually reached the carbenicillin sensitive cell division stage, the preceding polar growth stage is likely insensitive to penicillin. Penicillin family antibiotics specifically target the active site serine residue of D,D-transpeptidase enzymes, thus the data suggested that a different type of PG synthesis enzyme is sufficient for polar growth. This hypothesis is described and tested further in the results presented in Chapter 5.

CHAPTER 5

Characterization of the peptidoglycan synthesis machinery in *Agrobacterium tumefaciens* during unipolar growth and cell division

The results presented in this chapter will shortly be submitted for consideration for publication in the journal mBio.

5.1 Introduction

Peptidoglycan (PG) is a fundamental feature of nearly all bacteria, and plays a primary role in maintaining cell integrity and cell shape. The PG layer is an interconnected mesh in the bacterial cell envelope, and when isolated intact from a cell, the sacculus it forms retains the overall, albeit deflated, shape of the original cell. PG is composed of glycan strands covalently bonded by short, periodic peptide crosslinks. In bacilli, the glycan strands run roughly perpendicular to the long axis of the cell, with peptide crosslinks arranged parallel to the cell axis (81, 85-87). This architecture allows bacteria to withstand significant osmotic pressure, and thicker cell walls confer greater resistance: typical Gram negative strains can withstand several atm, whereas the thicker Gram positives can withstand upwards of 20 atm (66, 67).

To grow and divide, bacteria must enlarge and remodel this PG mesh. For cell division, most bacteria share the same strategy: PG is synthesized at the midcell in a decreasing diameter, until the cell is completely bisected and two separate cells are formed (89). In *Escherichia coli*, septal PG synthesis is conducted by a divisome consisting of the transpeptidase PBP3, the transglycosylase/transpeptidase PBP1b, various PG-remodeling enzymes, and an assortment of regulatory and structural proteins (79). These components are all organized along a large scaffolding ring formed by the tubulin homolog FtsZ, and contraction of this ring provides the force that propels the division process (90-92). In most bacteria, FtsZ is anchored to the cytoplasmic membrane by FtsA, although γ-proteobacteria such as *E. coli* utilize both ZipA and FtsA for this purpose.

While bacteria employ a variety of strategies to expand their cell wall prior to division, in general new PG is inserted in either a laterally dispersed fashion along the cell length, or at specific landmarks such as the cell pole(s) (93). The most popular bacterial model systems, including *E. coli*, *Bacillus subtilis*, and *Caulobacter crescentus*, utilize the laterally dispersed mode of PG insertion, leading to a substantial body of research and understanding of this type of cell elongation. In *E. coli,* lateral PG synthesis is conducted by an elongasome consisting primarily of the transpeptidase PBP2 and the transglycosylase/transpeptidase PBP1a plus several accessory proteins. These are likely organized by short filaments of the actin homolog MreB and associated structural proteins (94, 95).

In contrast, relatively little is known about the components and processes that facilitate polar growth even though this growth strategy is utilized by several orders of bacteria, notably the Actinomycetales and the Rhizobiales, and sporadically among other bacterial species (93, 103-105). Polar growth in the Gram negative Rhizobiales has only recently been explored, and unlike the Actinomycetales, the Rhizobiales grow only from one pole. Although unipolar growth produces new and old cells that are roughly equivalent in size after division, some asymmetries are present; for example the old poles of *Agrobacterium tumefaciens* can produce a holdfast (104). The Rhizobiales also lack the lateral PG synthesis scaffold MreB that is essential in the well-studied model systems mentioned above (112). However the cell division proteins FtsA and FtsZ both localize to the growth pole and the septum in *A. tumefaciens*, suggesting that these well known cell division components may also participate in polar growth (113).

Here we investigated whether other classical divisome-specific PG synthesis components might also localize to the growth pole in *A. tumefaciens*. Surprisingly, FtsZ

and FtsA were the only cell division components to exhibit robust localization to the growth pole. Several PBPs with D,D-transpeptidase (DDT) activity exhibited only transient polar localization. However, *A. tumefaciens* and other Rhizobiales are enriched in genes encoding L,D-transpeptidases (LDTs), one of which showed strong localization to the growing pole. Finally, the area of PG synthesis activity at the polar tip gradually expanded distally as cells elongated, such that most of the new cell compartment was engaged in PG synthesis. This expanded activity appeared concomitant with an increase in the width of the entire new cell compartment, and resulted in old and new cell compartments with approximately equivalent lengths and widths just prior to cell division.

5.2 Results

5.2.1 Agrobacterium lacks the rod-shaped cell elongation machinery

To understand the molecular components responsible for polar growth in *A. tumefaciens*, the genome of the wild-type strain C58 first was examined for homologs of the well studied cell elongation machinery of *C. crescentus* and *E. coli*. Surprisingly, and in addition to MreB, the canonical cell elongation scaffold proteins MreC, MreD, RodA, and RodZ were absent. This result prompted us to perform an exhaustive bioinformatics search through the *A. tumefaciens* genome for all types of proteins reportedly involved in bacterial cell growth; a survey of over 70 of these proteins is presented in Table 5-1.

Our bioinformatics analyses revealed there were clear or likely homologs of the highly conserved cytoplasmic PG precursor synthesis machinery, most cell division components, and a suite of carboxy- and endopeptidases, lytic transglycosylases, and amidases. Most notably, there was an unusual enrichment in putative LD-transpeptidase enzymes, three copies of FtsZ (113), and two copies each of PBP3, PBP1B, and FtsK. In further support that polar elongation utilizes a novel pathway, we found no homologs of the cell elongation-specific transpeptidase PBP2. Of all the canonical cell elongation components, only the transglycosylase/transpeptidase PBP1a remained present in *A. tumefaciens*, perhaps reflecting an especially critical function of PBP1a.

Further phylogenetic analyses of the PBP1/2/3 homologs of *A. tumefaciens* compared to homologs in related Proteobacteria confirmed the duplication of PBP3 and PBP1b, the presence of PBP1a and PBP1c, and the absence of PBP2. Surprisingly, the presumed PBP1b of *A. tumefaciens* and other α-proteobacteria formed a distinct clade that was paraphyletic with PBP1b of *E. coli*. Within the α-proteobacteria these proteins form a third major clade beside PBP1a and PBP1c, and are therefore here referred to as PBP1b.

5.2.2 FtsZ and FtsA likely contribute to polar growth

Since *A. tumefaciens* lacks the expected cell elongation machinery, the polar growth process is likely mediated by some combination of cell division components and novel proteins. To investigate this hypothesis, we first focused on localizing two important cell division scaffolding proteins: the actin homolog FtsA and the tubulin homolog FtsZ. Our previous studies monitored snapshots of cells at different stages of the cell cycle and revealed that FtsA-GFP and FtsZ-GFP both localize to the cell pole during polar growth and to the midcell during cell division. Since FtsZ localization

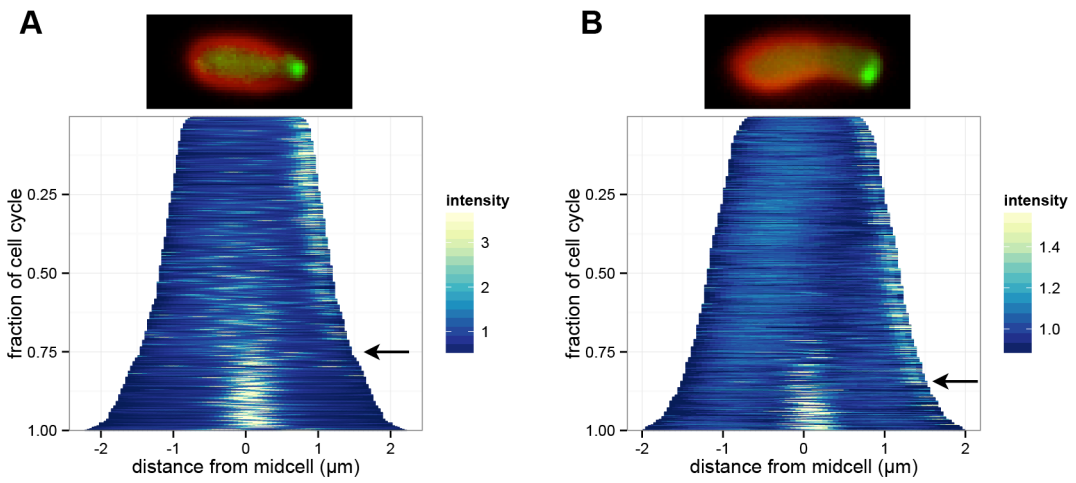

Figure 5-1 FtsZ and FtsA cell cycle localization

FtsZ and FtsA colocalize to the growth pole over most of the cell cycle, but exhibit different timings in the transition to midcell localization. Upper panels: example cells labeled with FM4-64 expressing (A) FtsZ-GFP or (B) FtsA-GFP. FM4-64 most intensely labeled the old pole opposite the FtsZ and FtsA fluorescent foci. Lower panels: demographs of cells expressing (A) FtsZ-GFP or (B) FtsA-GFP. Arrows indicate transition to consistent midcell localization. Demographs are oriented with the growing pole on the right, using FM4-64 old pole labeling as a reference.

appeared more variable than FtsA, here we asked to what degree their localization is coordinated over the cell cycle, and whether they sometimes have distinct localization patterns or potentially independent roles.

To this end we performed a quantitative study of FtsA-GFP and FtsZ-GFP localization over the cell cycle by representing whole-cell fluorescence profiles of mixed populations as composite demographs. To construct demographs, fluorescent profiles of several hundred cells were collected and represented as single lines stacked according to cell length. Given sufficient sampling, such a graph is expected to roughly represent progression through the cell cycle, starting from the shortest (new) cells and ending at the longest (dividing) cells; the relative timings of cell cycle-dependent localization can inferred from this ordered distribution of cell lengths. To orient old versus new poles for the demographs presented herein, we used the lipophilic dye FM4-64 that preferentially labels old poles in *A. tumefaciens* (113). As shown in Figure 5-1A, FtsZ-GFP progressed through three overall localization patterns: an initial polar localization, a mix of lateral and diminishing polar foci, and finally intense midcell localization.

In contrast, the FtsA-GFP demograph (Figure 5-1B) shows that FtsA-GFP remained exclusively at the growth pole until just prior to cell division. These results agree with our previous time-lapse data (113), and demonstrate the validity of the demograph approach. Comparison of the FtsA-GFP and FtsZ-GFP demographs revealed that FtsA-GFP consistently remained at the growth pole during the times when FtsZ-GFP localized to numerous sites throughout the cell and at cell poles. Furthermore, once FtsZ-GFP localized to the midcell in longer cells (representing the latter stages of the cell cycle), it no longer localized to the poles or other locations in the cell. In contrast, FtsA-GFP localized briefly to both the pole and the midcell as cells

transitioned to septal growth. Furthermore, FtsZ-GFP appeared at the midcell slightly before FtsA-GFP (black arrows, Figure 5-1), although the longest 15% of cells showed similar midcell localization of both FtsA-GFP and FtsZ-GFP just prior to cell division. These data together suggest the two proteins may contribute differently to the polar growth process.

5.2.3 Contributions of PBPs to polar growth

Given that the cell division scaffolding proteins FtsA and FtsZ both localize to the growth pole, we next investigated whether cell division PG synthesis proteins also localize to the growth pole. To gain a global perspective of the localization of all *A. tumefaciens* PBPs, cells were treated briefly with BocillinFL, a fluorescent penicillin derivative commonly used for *in vitro* detection of PBPs. BocillinFL treatment revealed weak but consistent polar labeling and stronger midcell labeling (Figure 5-2A,B). Midcell BocillinFL labeling occurred in the longest ~25% of cells, coincident with the frequency and distribution of midcell localization of FtsZ-GFP (see Figure 5-1A).

We hypothesized that *A. tumefaciens* may still utilize PBP1a as a transglycosylase for polar elongation, despite lacking the cell elongation transpeptidase PBP2. Indeed, a citrine-PBP1a fusion demonstrated a distinct preference for the growth pole over most of the cell cycle (Figure 5-2 C,D), and likely accounts for some of the polar BocillinFL labeling observed. Unlike FtsA-GFP or FtsZ-GFP, citrine-PBP1a did not

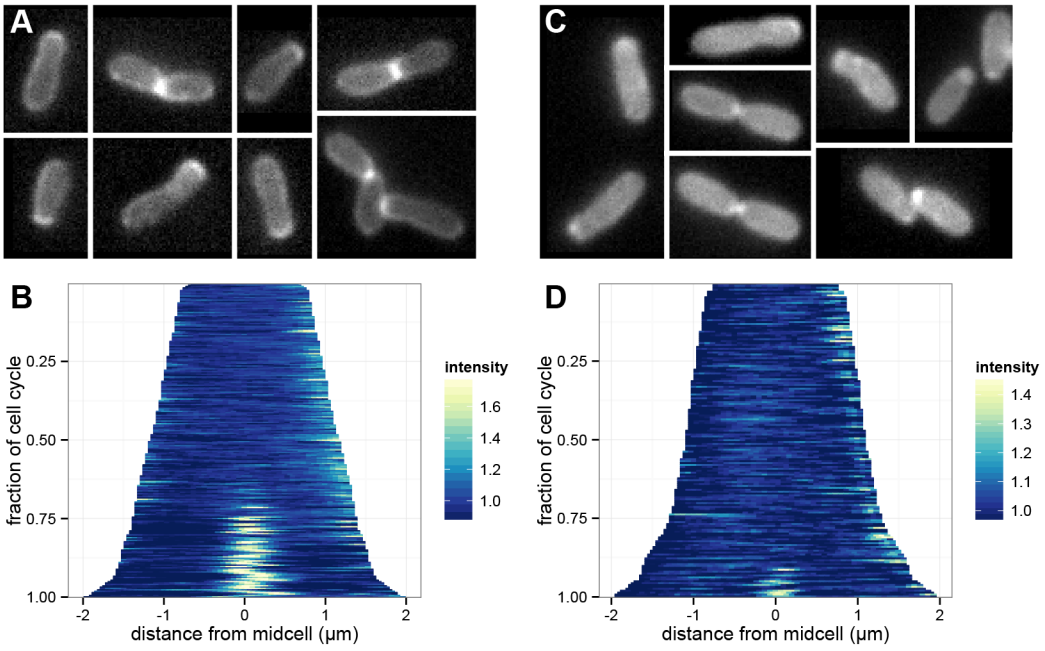

Figure 5-2 BocillinFL and citrine-PBP1a exhibit growth pole and midcell fluorescence

A and B: (A) Single cells and (B) demograph of cells labeled with BocillinFL. Midcell fluorescence is much more intense than growth pole fluorescence, suggesting that a minority of PBPs are involved in polar growth. C and D: (C) Single cells and (D) demograph of cells expressing citrine-PBP1a. Citrine-PBP1a shows a faint, but consistent, growth pole localization. Demographs are oriented with the growing pole on the right, using FM4-64 old pole labeling as a reference.

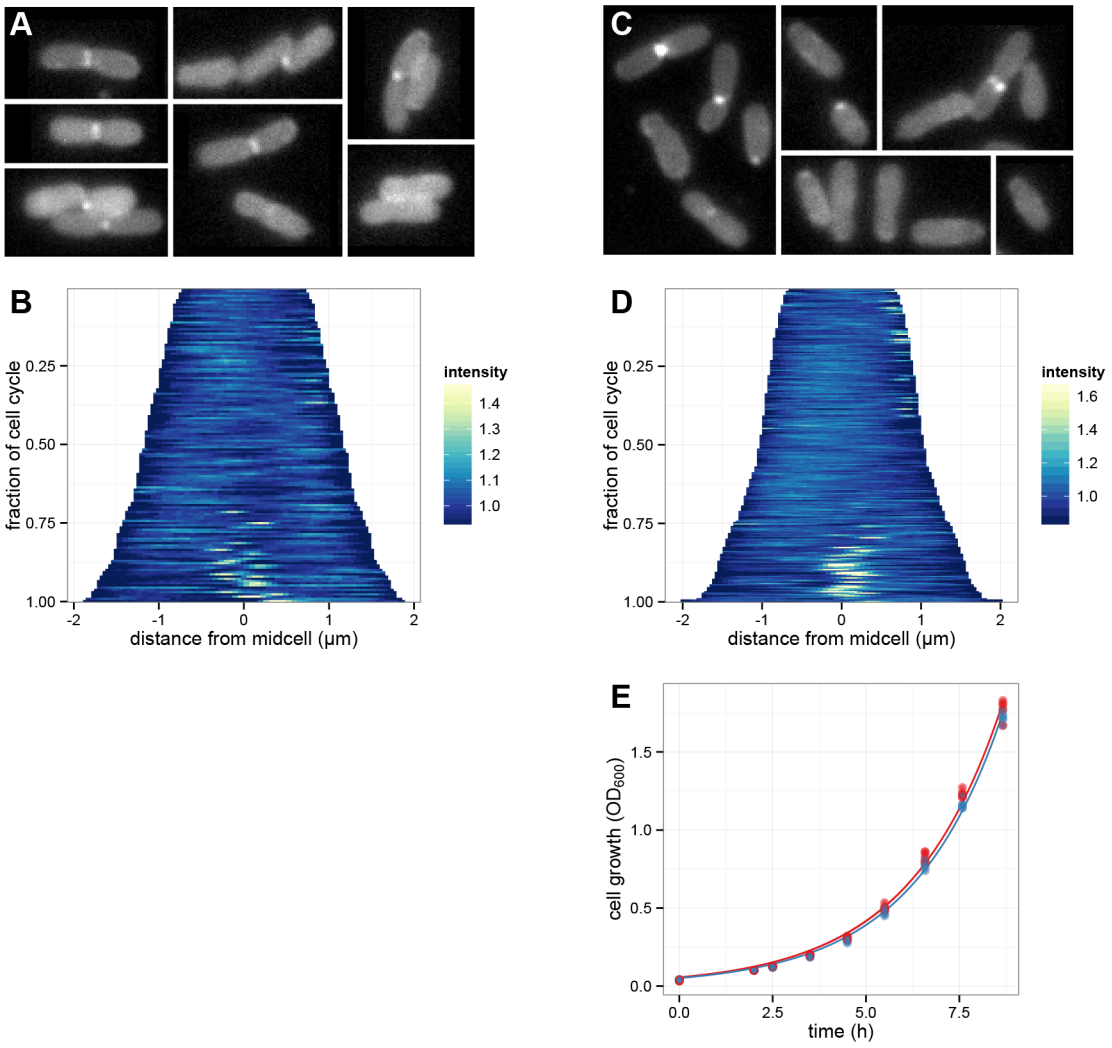

Figure 5-3 PBP3a and PBP3b do not exhibit strong polar localization

A and B: (A) Single cells and (B) demograph of cells expressing citrine-PBP3a. C and D: (C) Single cells and (D) demograph of cells expressing citrine-PBP3b. Intense fluorescence only occurred at the septum, or at the growth pole in very short cells. The growth pole is oriented on the right of the demographs. (E) Exponential growth of wildtype C58 (red) and C58 Δ*PBP3b* (blue). Each curve represents an exponential fit to five independent cultures.

relocalize to the midcell until the final 5-10% of the cell cycle, suggesting it is not needed to initiate cell division.

As noted above, *A. tumefaciens* has two PBP3 transpeptidases, referred to here as PBP3a (Atu2100) and PBP3b (Atu1067). The gene encoding PBP3a is located adjacent to *murE, ftsZ,* and *ftsA*, in the same position as *ftsI* (PBP3) in *E. coli*, while the gene for PBP3b is located elsewhere in the genome. To test if either copy of PBP3 might serve as a transpeptidase for polar cell growth, citrine fusions for each protein were examined. Both proteins primarily localized at the septum in long cells with occasional weak localization to the growth pole in shorter cells (Figure 5-3A,C).

Demographs revealed that citrine-PBP3a very rarely localized to the pole, whereas citrine-PBP3b exhibited polar localization through the first third of the cell cycle

(Figure 5-3B,D). However a deletion of PBP3b had no apparent effect on growth rate (Figure 5-3E), suggesting that neither PBP3b nor its localization to the pole are essential features of polar growth. Since neither PBP3a nor PBP3b remained at the cell poles over the entire cell cycle, most likely additional transpeptidases are required for polar growth.

5.2.4 L,D-transpeptidases have a major role in polar growth

As noted, *A. tumefaciens* and other members of the polar-growing Rhizobiales contain an unusual abundance of putative LD-transpeptidase (LDT) proteins (Table 5-2), suggesting a possible link between LDTs and polar growth. Unlike the PBP2 & PBP3 DD-transpeptidases (DDTs) that form 4,3 crosslinks between D-alanine and m-Dap in two PG stem peptides, LDTs catalyze 3,3 crosslinks directly between two m-Dap residues and are insensitive to most penicillins. More than 50% of the peptide crosslinks in *A. tumefaciens* and the related Rhizobiales *Sinorhizobium meliloti* are 3,3 crosslinks (104), compared to only 10% in *E. coli* (160). As reported previously, treatment of *A. tumefaciens* with sublethal concentrations of carbenicillin, a penicillin derivative that targets DDTs results in morphology defects at the midcell, but does not affect the cell poles (113). Thus, DDTs do not play a major role in polar growth. These results prompt the hypothesis that instead LDTs play a role in polar growth.

To understand how the LDTs of the Rhizobiales are related to those found in other bacteria, we constructed a phylogenetic tree of the LDTs from over forty bacterial

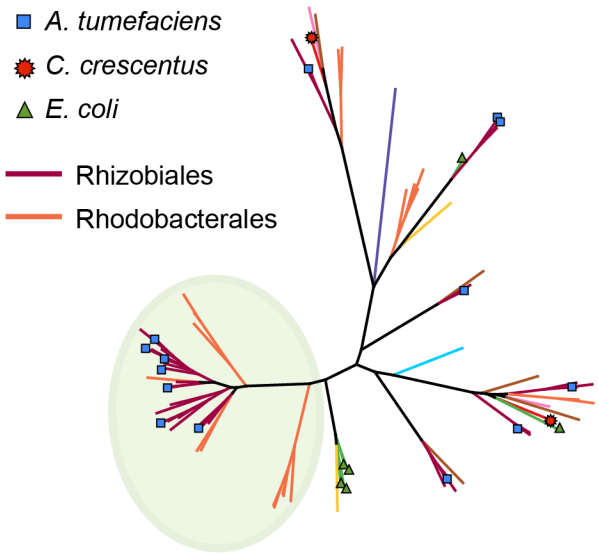

Figure 5-4 Unrooted phylogenetic tree of LDTs from representative Proteobacteria species.

The green shaded area highlights a clade composed only of the Rhizobiales and Rhodobacterales orders. The LDTs from *A. tumefaciens* (blue squares), *C. crescentus* (red stars), and *E. coli* (green triangles) are indicated on the tree. Branches are colored according the the taxonomic order of the strains: multiple orders (black), Rhizobiales (burgundy), Rhodobacterales (orange), Sphingomonadales (brown), Caulobacterales (red), Rhodospirillales (pink), Neisseriales (turquoise), Pseudomonadales (yellow), Enterobacteriales (green), Campylobacterales (purple).

species, primarily representing α-proteobacterial strains and select representatives from other Proteobacteria and more divergent species. Table 5-2 lists the strains used to construct this tree. For clarity, a smaller tree of the LDTs from twelve Proteobacteria is presented in Figure 5-4. Notably, although the LDTs of *A. tumefaciens* (Figure 5-4, blue boxes) and other Rhizobiales are distributed throughout the tree, they are particularly clustered in a few adjacent branches. Closer inspection revealed these branches (Figure 5-4, within green oval) are specifically composed of LDTs found in the two closely related orders of Rhizobiales and Rhodobacterales. The Rhizobiales strains examined typically include about five to eight LDTs in this group, or roughly half the total number of LDTs in each strain.

A subset of the *A. tumefaciens* LDTs were selected for localization studies to sample the various phylogenetic branches and to test the LDTs that were most highly expressed in transcriptome studies (161). A C-terminal sfGFP fusion to Atu0845, one of the Rhizobiales/Rhodobacterales specific LDTs, exhibited a striking localization to the growth pole (Figure 5-5). Furthermore, the intensity of the growth-pole localized Atu0845-sfGFP appeared to increase gradually over the cell cycle (Figure 5-5B, compare the poles of long versus short cells) and remained at the growth pole despite the appearance of additional septal labeling just prior to cell division. This polar

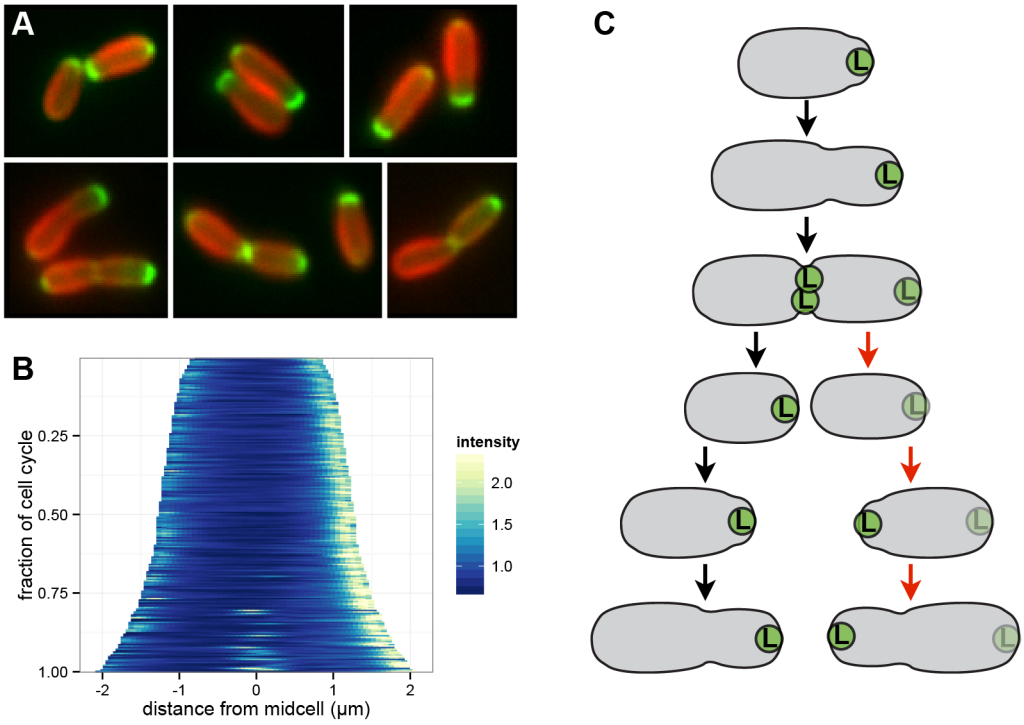

Figure 5-5 LDT Atu0845 localizes intensely to the growth pole

(A) Single cells expressing Atu0845-sfGFP and labeled with FM4-64. (B) Demograph of cells expressing Atu0845-sfGFP. Growth poles are oriented to the right, using FM4-64 old pole labeling as a reference. (C) A model for the generation of Atu0845-sfGFP fluorescence at the old pole. Atu0845 (green "L") localizes at the growth pole, but does not completely leave the pole during cell division. The newly generated cell (descent by red arrows) temporarily retains this Atu0845 at its old pole, but this feature is absent from the original progenitor cell (descent by black arrows).

retention may explain the presence of the less intense fluorescence also visible at the old poles in many cells. Figure 5-5C diagrams how such bipolar fluorescence could arise as cells divide.

The other LDTs tested did not exhibit strong polar localization when fused to sfGFP. Instead, these LDTs tended to predominantly localize to the midcell at cell division, then localize temporarily at the new pole in newly divided cells (Figure 5-6A-E), much like the citrine-PBP3b fusion. One fusion, Atu1164-sfGFP localized simply as multiple foci around the cell periphery (Figure 5-6E). Atu0669-sfGFP, the other Rhizobiales/Rhodobacterales clade representative, gained localization to the growth pole immediately prior to cell division (Figure 5-6B, red circle). In contrast, every other protein with cell cycle-dependent localization lost or reduced growth pole localization

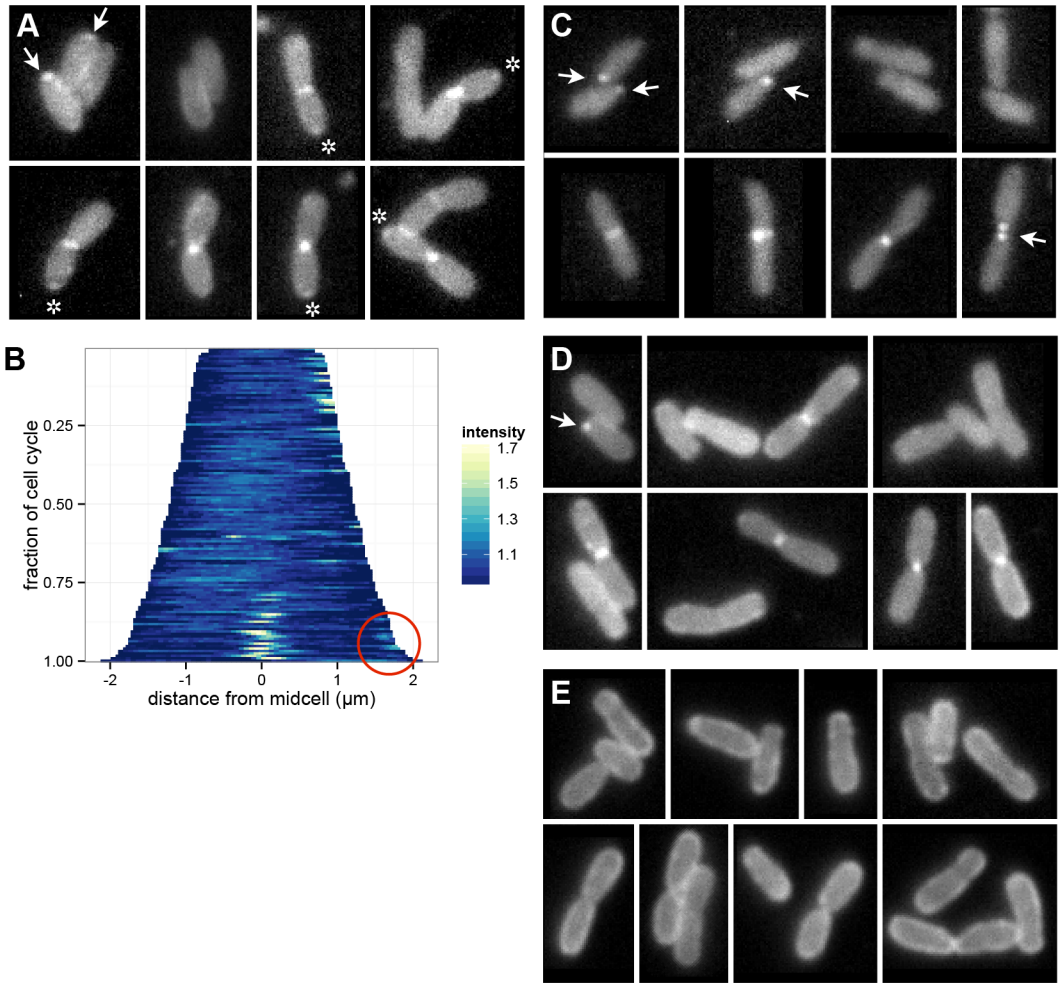

Figure 5-6 Localization of additional LDTs

A,C-E: Images of cells expressing (A) Atu0669-sfGFP, (C) Atu3332-sfGFP, (D) Atu2133-sfGFP, (E) Atu1164-sfGFP. A,C,D: Fluorescence foci primarily localize to the septum and occasionally to new poles in recently divided cells (arrows). E: Faint foci are primarily visible along the cell periphery. (A) Foci of Atu0669-sfGFP also faintly localized to the growth pole during cell division (✲). (B) A demograph of cells expressing Atu0669-sfGFP shows that growth pole localization was lost shortly after cell division (i.e. it is only present in very short cells at the top of the demograph), and then returned (red circle) just prior to the next cell division.

immediately prior to cell division. The weaker and more diffuse localization of these four LDTs contrasts with the strong polar localization of Atu0845-sfGFP.

5.2.5 Localization of PG synthesis activity

The above results indicate that PG synthesis enzymes and scaffolding proteins localize to the growth pole, or midcell, and in the case of FtsZ to multiple sites throughout *A. tumefaciens*, yet it is not clear at which location(s) PG synthesis is most active. To address this question, we took advantage of the fact that many bacteria readily incorporate exogenous D-amino acids into their PG (162, 163). This exchange is mediated by either DDTs, which exchange the exogenous amino acid with the fifth D-alanine in the stem peptide, or by LDTs, which act on the fourth position D-alanine (163). In *A. tumefaciens*, mass spectrometry studies indicate that exogenous D-amino acid analogs are specifically incorporated by LDTs into the fourth stem peptide position (164).

To directly visualize where LDTs are most active, we grew cells with exogenously added alkyne-D-alanine (alkDala), a D-alanine analog that can readily be covalently linked *in-situ* to an azido-fluorophore using a simple copper-catalyzed click chemistry protocol (165). Fluorescence microscopy revealed cells were labeled at one pole, or at the midcell in obviously constricting cells (Figure 5-7A). Similar results were reported using both azido-D-alanine and pre-labeled fluorescent D-alanine probes in *A. tumefaciens* (164).

Growth pole labeling of alkDala was confirmed using a pulse chase with Texas red succinimidyl ester (TRSE). TRSE non-specifically labels surface proteins, and is retained specifically with previously synthesized cell material in *A. tumefaciens* (104). After incubation with TRSE, AlkDala labeling specifically targeted the regions of new growth that were unlabeled by TRSE (Figure 5-7D). Additionally, fluorescent vancomycin, a commonly used probe for nascent PG, demonstrated the same labeling patterns (polar and midcell) as alkDala when combined with a TRSE chase (Figure 5-7E). Thus, alkDala exchange occurs in proximity to nascent PG synthesis.

Unexpectedly, despite that cells were all incubated with alkDala for the same length of time, the labeled region was noticeably larger in longer cells compared to shorter cells (Figure 5-7A). This change was quantified by measuring the length of the region of alkDala labeling, from the growth pole to the point where the fluorescence labeling plateaued to cellular background intensities. In cells without midcell alkDala labeling (cells less than ~3.0 μm), the labeling region increased linearly in relation to cell length, and roughly doubled in size as cells grew (red line, Figure 5-7B). After the appearance of midcell labeling (cells greater than ~3.0 μm), the labeling area appeared to increase at a slightly faster rate, perhaps reflecting additional septal PG synthesis activity (blue line, Figure 5-7B). A demograph of these cells displays dramatically increased alkDala labeling along the length of the new cell compartments prior to cell division (Figure 5-7C). Thus, growth of the new pole appears to be considerably more complex than realized in previous studies.

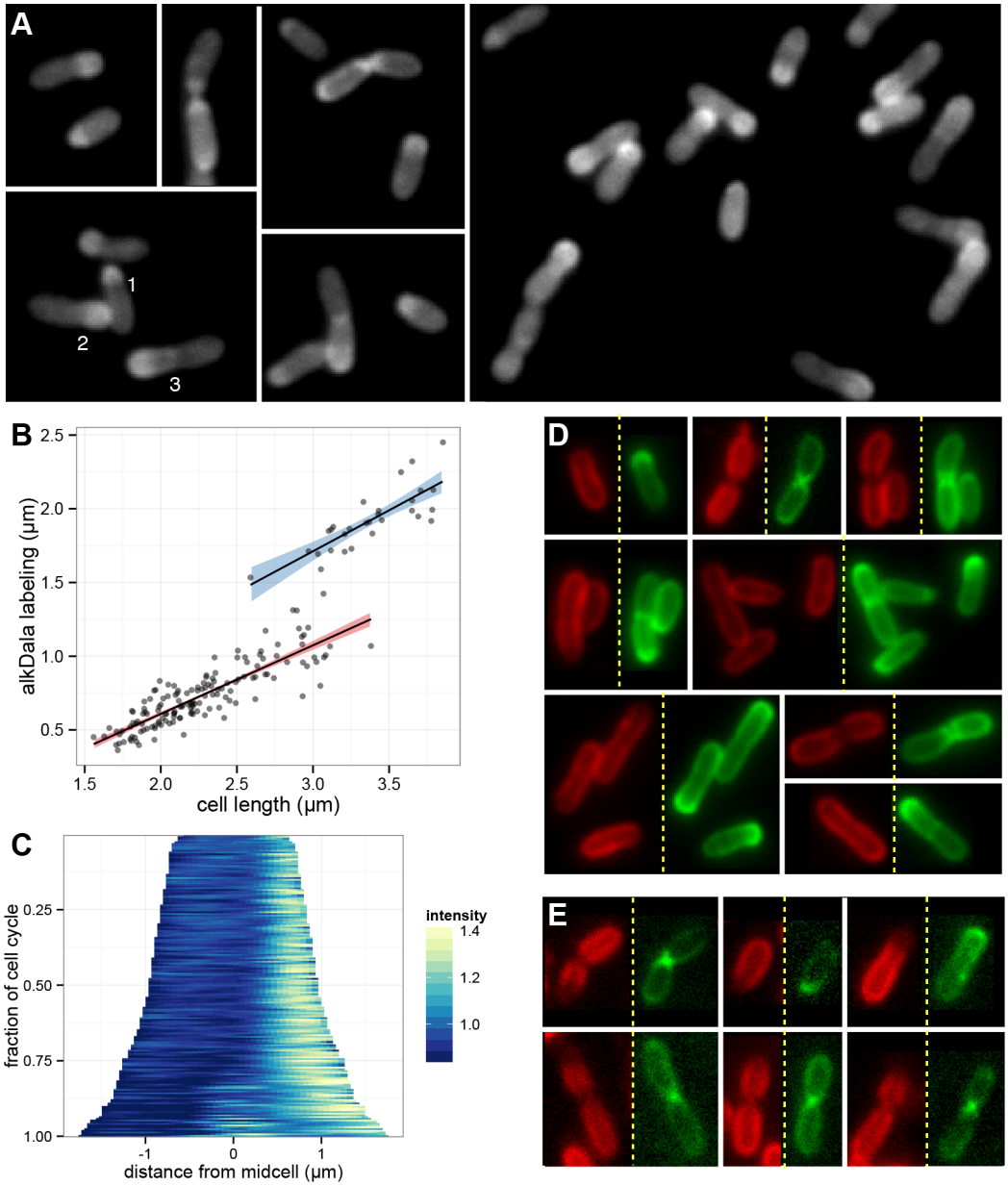

Figure 5-7 LDTs are active over an increasing area of the new cell compartment

(A) Individual cells allowed to incorporate alkDala for 20 minutes. Shorter cells display a shorter region of labeling than longer cells; compare labeling in cells 1-3. (B) scatterplot of the length of the labeled region versus total cell length. The labeled region length increases linearly with cell length in cells before (red line) and after (blue line) the appearance of septal labeling in cells ~3.0 µm and longer. Red and blue shaded areas indicate 95% confidence intervals. C, demograph of alkDala labeled cells, with the growing cell poles oriented on the right. D and E: AlkDala controls. (D) Exponentially growing cells were first labeled with TRSE (red), washed to remove the TRSE, and then labeled for 20 minutes with alkDala (green). AlkDala labeling coincided with the lightest TRSE signal, indicating that alkDala was incorporated into regions of new growth. (E) exponentially growing cells were labeled with TRSE (red), washed to remove the TRSE, and then labeled for 20 minutes with VanFL (green); VanFL labeled the regions of the cells with the lightest TRSE signal.

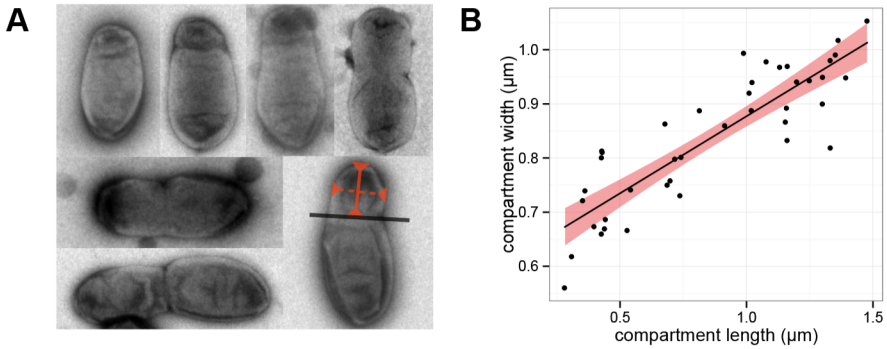

Figure 5-8 New cell compartments increase in width as they grow in length

(A) Examples of whole-cell TEM images of exponentially growing *A. tumefaciens*. Note the slight indentation/constriction (see also black line in lower right panel) demarking the boundary between the old and new cell compartments. Lower right panel, lengths and widths of new cell compartments (red) were measured. (B) scatter plot of compartment lengths and width of new cell compartments. Shaded area indicates 95% confidence interval.

5.2.6 Polar growth involves expansion in cell width and length

The above results prompted us to examine the dimensions of *A. tumefacien*s over the cell cycle for evidence of growth that might correspond to the increased alkDala labeling area (Figure 5-7B). New *A. tumefaciens* cell compartments frequently appear narrower than their parent old cell compartments, even at the resolution afforded by light microscopy (see cells in Figure 5-2A,C and Figure 5-5A). Presumably such new cell compartments must eventually increase in width to maintain cell diameters over successive generations. However it was not clear if this increase occurred before or after cell division, or if it could be related to the observed increase in alkDala labeling area.

To investigate changes in cell dimensions over the cell cycle, whole-cell transmission electron microscopy was performed on mixed cultures of exponentially growing *A. tumefaciens*, and the lengths and widths of each new cell compartment were measured (Figure 5-8A). Much like the alkDala labeling, there was a linear relationship between the lengths and widths of new cell compartments (Figure 5-8B). Thus, although new poles are initially narrower than their parent old cell compartments, new cell compartments increase in both length and width as the cell matures.

5.3 Discussion

To better understand polar growth in the Rhizobiales, fluorescent fusions were constructed to predicted cell elongation and division components in *A. tumefaciens*. We refer to cell elongation and division proteins based on their canonical homologs in well-studied systems like *E. coli*. While the cell division scaffold proteins FtsZ and FtsA exhibited strong localization to the growth pole, the cell division-associated PBP3s did not. Instead the LDT Atu0845 displayed significant polar localization and may play a major role in polar growth. This latter finding is consistent with the unusual abundance of LDTs (see Figure 5-4 and Table 5-2) and LDT-mediated 3,3-crosslinks in *A. tumefaciens* and other Rhizobiales (104). PBP1a, the only canonical cell elongation protein in *A. tumefaciens,* also exhibited modest polar localization. Finally, polar growth

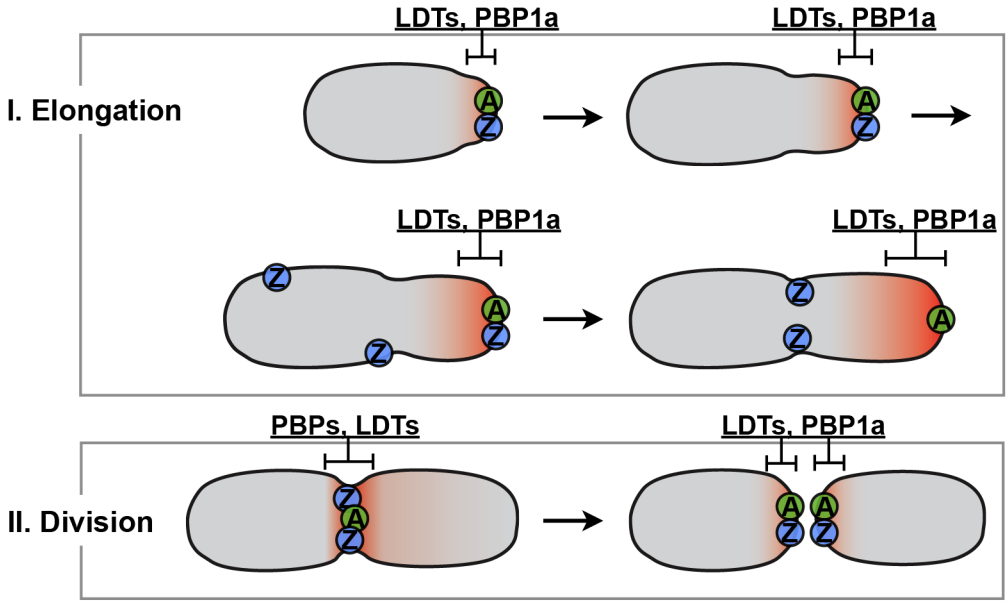

Figure 5-9 Model of *A. tumefaciens* cell growth dynamics

The new cell compartment emerges from the new pole, and gradually increases in length and width along with the region of active PG synthesis (red shading). FtsZ (blue "Z") and FtsA (green "A") localize to the growth pole along with PBP1a and the LDT Atu0845. Prior to cell division, FtsZ relocalizes to the septum, where it is joined by the PBP3s, FtsA, PBP1a, and various LDTs for cell division. All these proteins remain at the division site and are ready to direct new cell polar growth in daughter cells. Square brackets illustrate the relative positions and lengths of regions of localization for LDTs and PBP1.

was found to involve substantial cell shape remodeling and LDT-mediated PG synthesis activity over the entire new cell compartment.

A model of cell growth and division in *A. tumefaciens* is presented in Figure 5-9. Cell elongation involves several stages during which a new cell compartment emerges and increases in length and width as it matures. Initially, the scaffold proteins FtsA and FtsZ localize to the growing pole tip along with PBP1a and LDT Atu0845. Over time an increasing proportion of the new cell compartment engages in LDT-mediated PG synthesis activity (Figure 5-9, red shading), implicating additional LDTs in this process. Prior to cell division, FtsZ leaves the growth pole before FtsA (Figure 5-9), perhaps highlighting different functional roles for these proteins in polar growth. FtsZ, FtsA, PBP1a, PBP3s, and LDTs all localize to the midcell during cell division. Once the cell divides, the former septum becomes the site of new polar growth, utilizing the assortment of proteins already localized to the new pole.

Polar growth in the Rhizobiales may have co-evolved with the large number of LDTs within this order. The phylogenetic clustering of Rhizobiales and Rhodobacterales LDTs is particularly intriguing, since some members of Rhodobacterales also grow by budding. Unlike the Rhizobiales, the Rhodobacterales still retain MreB. However, MreB in *Rhodobacter sphaeroides* has atypical localization to the midcell (166), suggesting that Rhodobacterales may be an evolutionary intermediate between the polar-growing Rhizobiales and other α-proteobacteria. The phylogenetically divergent LDTs shared by these orders could help enable polar and other atypical growth in these organisms.

LDTs are also central components of the PG synthesis machinery in the Gram positive, bi-polar-growing Actinomycetales. LDT-mediated 3,3 crosslinks represent 38% of the PG crosslinks in *Corynebacterium jeikeium* (111), 30% in *Mycobacterium smegmatis* (167), and 80% in *Mycobacterium tuberculosis* grown to stationary phase (168). In contrast, 3,3 crosslinks represent less than 10% of total crosslinks in *E .coli* PG (160), and strains deleted of the LDTs contributing to 3,3 crosslinks exhibit no growth defects (169). The apparent association between polar growth and LDTs is intriguing and warrants future research to understand the nature of this relationship.

How the Rhizobiales direct PG synthesis specifically to the new cell compartment is currently unknown. Polar growth is potentially influenced by one or more of the many well studied mechanisms that control polar differentiation and the cell cycle in α-proteobacteria. For example, disruption or overexpression of CcrM, CpdR1, DivJ, DivK, PdhS1, PleC, or PodJ produces bulging, branching, and other cell shape and integrity defects in *Brucella abortus, S. meliloti,* or *A. tumefaciens* (170-175). Similar phenotypes are observed when cell division proteins are disrupted in the Rhizobiales; a partial deletion of MinCDE or over expression of MinCDE or FtsZ generates swollen and branched cells in *S. meliloti* (176, 177). These similarities may indicate a critical shared pathway that is sensitive to overexpression.

The mechanisms governing the insertion of nascent PG strands into established PG are not yet understood for any type of cell growth. Lateral expansion of the PG likely involves localized PG remodeling to allow insertion of new glycan strands into the existing PG mesh. However, since polar growth also involves a sustained expansion of the cell diameter, it may require considerably more PG synthesis and remodeling activity. Polar growth may represent a reversal of the highly regulated PG remodeling that occurs during cell division, where successively smaller rings of PG are generated at the septum (178-182). Since At0845 only showed polar localization during cell growth, additional LDTs are likely responsible for the PG synthesis and remodeling activities that lead to increased cell width. Subpolar PG synthesis implies many aspects of polar growth in the Rhizobiales remain to be uncovered.

5.4 Materials and Methods

5.4.1 Strains and Growth Conditions

Strains and plasmids used in this study are listed in Table 5-3. *A. tumefaciens* C58 containing nopaline pTiC58 was transformed with the plasmids described, and cultured at 28ºC on LB media supplemented with appropriate antibiotics. To obtain exponential growth, overnight cultures were diluted to ~10^8 cells / mL in LB containing 10 mM IPTG and antibiotics, then grown for 4-5 hours at 28ºC and 250 RPM.

5.4.2 Cloning and Genomic Deletions

Plasmids were constructed using standard protocols, and all clones were verified by DNA sequencing. Strain ATC107 with *Δpbp3b::npt* was constructed through allelic exchange by transforming wild type C58 with pTC092, selecting for kanamycin resistant clones, then counter selecting for sucrose resistant colonies. Deletion of *pbp3b* was confirmed by PCR and sequencing.

5.4.3 Homology Searches & Phylogenetic Analyses

Phylogenetic trees of the PBP proteins were constructed by first gathering homologs to the *E. coli* K12 PBP3 or PBP1b proteins within the desired species using NCBI Delta-BLAST. Significant hits were roughly aligned using MAFFT (183), and the PBP2/3 or PBP1a/b/c clusters were selected for a full alignment in MAFFT. LDT homologs were gathered on the basis of the ykud Pfam domain, and then aligned using MAFFT. Columns containing more than 75% gaps were removed using trimAl (184). PhyML (185) was used to calculate maximum likelihood trees, using aLRT SH-like estimates of branch support. Trees were visualized using Archaeopteryx (186) and Adobe Illustrator CS6 (Adobe Systems).

5.4.4 Fluorescence Labeling

All centrifugations of cells were conducted for 5 minutes at 8000 X g, and all manipulations were performed at room temperature unless otherwise noted. Cells were labeled with FM4-64 (Life Technologies) immediately prior to imaging, by adding 8 mg/mL of FM4-64 to ~$5x10^8$ cells / mL in growth media and incubating for 10 minutes. Cells were centrifuged, and the supernatant was used to adjust to a final concentration prior to imaging. BocillinFL (Life Technologies) was added at a concentration of 167 µg / mL to cultures concentrated to ~10^9 cells / mL in LB. Cells were incubated at 28ºC and 250 RPM for 10 minutes, pelleted and washed twice with pH 7.4 PBS, then labeled with FM4-64 as described.

Alkyne-D-alanine labeling was conducted essentially as previously described (165). In brief, (R)-a-propargylglycine “AlkDala” (Fisher Scientific) was added to a final concentration of 1 mM to growing cultures of ~$4x10^8$ cells / mL, and allowed to incorporate during 20 minutes of exponential growth. Cells were pelleted and washed once with pH 7.4 PBS + 0.01% BSA (PBSB), then fixed in ice-cold 70% ethanol for 20 minutes. After three additional washes, cells were incubated for 30 minutes in PBSB containing 1 mM copper sulfate, 128 µM Tris[(1-benzyl-1H-1,2,3-triazol-4-yl) methyl]amine “TBTA” (Sigma-Aldrich), 1.3 mM copper sulfate, and 20 µM tetramethylrhodamine azide “TAMRA” (Life Technologies). Cells were washed five times in PBSB prior to imaging.

For combined alkDala and Texas red succinimidyl ester “TRSE” labeling, cells were first concentrated to ~$8x10^9$ cells / mL in pH 8.5 PBS containing ~70 µg / mL TRSE (Life Technologies). After a 10 minute incubation, the reaction was quenched by addition of lysine to 57 mM. Cells were washed once with LB, then resuspended to ~$1.2x10^9$ cells / mL with 1 mM alkDala. After 20 minutes of incubation at 28ºC and 250 RPM, cells were washed three times with PBSB and fixed for 15 minutes in 2% formaldehyde. The remaining protocol was performed as described above, except that Alexa Fluor 488 azide was substituted in place of TAMRA.

For combined vancomycin-FL and TRSE labeling, cells were resuspended to $4x10^8$ cells / mL in LB and grown for 45 minutes following TRSE labeling. The culture was then concentrated to ~10^{10} cells / mL in LB, and vancomycin-BODIPY FL (Life Technologies) and unlabeled vancomycin were each added to a concentration of 10 ng/µl. Cells were incubated for 6 minutes, then washed twice prior to imaging.

5.4.5 Microscopy and Data Analysis

Slides were prepared by first covering a microscope slide with thin (~340 μm) layer of 1.5% agarose in pH 7.4 PBS. Once solidified, the agarose was trimmed to the size of a coverslip. Cells were resuspended at a final concentration of ~$3x10^9$ cells / mL, then 2 μl was placed on top of each agarose pad, covered with a coverslip and sealed with nail polish. Images were taken with an Applied Precision DeltaVision Elite deconvolution microscope and processed using Fiji/ImageJ (151). Demographs were constructed by first measuring fluorescence intensity profiles in Fiji, then processing the data in R (187) using a custom script designed to sort cells by length and normalize intensity profiles by each cell's average fluorescence. The script and a user guide are available at http://github.com/ta-cameron/Cell-Profiles. Demographs and all other plotted figures were generated in R using the ggplot2 package (188).

5.4.6 Whole-cell TEM

Exponentially growing cultures were concentrated to ~$8x10^9$ cells / mL. Droplets of cell suspension were placed on formvar-coated 200 mesh copper grids for two minutes. The grids were washed twenty times by passing them through drops of double distilled water on parafilm. Excess water was wicked from the grids using filter paper. Grids were incubated with 5 uL of 0.5% uranyl acetate in water for 30 seconds; then excess liquid was wicked away using filter paper. Grids were air dried and subjected to electron microscopy using a Philips/Tecnai 12 TEM.

Table 5-1 Peptidoglycan synthesis and cell division genes in *A. tumefaciens*

E. coli / C. crescentus gene	Atu locus	Name used	Notes
CELL ELONGATION SCAFFOLD			
MreB	NP		actin scaffold
MreC	NP		associate with MreB & IM
MreD	NP		associate with MreB & IM
RodA	NP		lipid II flipase (PG precursor)
RodZ	NP		
CELL DIVISION SCAFFOLD			
FtsZ	Atu2086	FtsZ	Z-ring scaffold. Full-length α-Proteobacteria version.
	Atu4673		lacks extra C-terminal domains typically found in α-Proteobacteria
	Atu4215		partial tubulin domain only
FtsA	Atu2087	FtsA	interact/stabilize Z-ring
ZapA	Atu8191†		interact/stabilize Z-ring
ZapB	NP		
ZapC	NP		
FtsK (SpoIIIE)	Atu2759		coordination of division & chromosome segregation
	Atu3210		
FzlA	Atu0293†		interact/stabilize Z-ring
FzlC	Atu2824		
KidO	Atu5198†		may be recruited to z-ring to prevent assembly of adjacent rings
FtsQ (DivIB)	Atu2088		stabilizes divisome interactions
FtsL	NP		stabilizes divisome interactions
FtsB (DivIC)	Atu1428		stabilizes divisome interactions
FtsN	Atu1710†		stabilizes divisome interactions
DamX	NP		PG binding
DedD	NP		PG binding
RlpA	Atu1500		PG binding
	Atu0290		
PEPTIDOGLYCAN PRECURSOR SYNTHESIS			
MurA-G	present		PG precursor synthesis
Ddl	Atu2089		PG precursor synthesis
Alr	NP		racemases (synthesis of D-ala & D-Glu)
DadX	Atu3292		racemases (synthesis of D-ala & D-Glu)
MurI	Atu1867		racemases (synthesis of D-ala & D-Glu)
MraY	Atu2097		PG precursor synthesis
FtsW	Atu2095		lipid II flipase (PG precursor)
PEPTIDOGLYCAN SYNTHESIS / HYDROLYSIS / REMODELING			
MtgA	Atu2720		transglycosylase only; to division site/PBP3
HMW PBPs			
PBP1a	Atu1341	PBP1a	1º cell elongation transglycosylase
PBP1b	Atu0103	PBP1b1	1º cell division transglycosylase
	Atu0931	PBP1b2	
PBP1c	Atu3694	PBP1c	
PBP2	NP		1º cell elongation transpeptidase in typical bacilli
PBP3	Atu2100	PBP3a	1º cell division transpeptidase
	Atu1067	PBP3b	
LMW PBPs			
PBP5	Atu1499		
PBP4B	Atu3077		

E. coli / C. crescentus gene	Atu locus	Name used	Notes
	Atu0933		
PBP6	NP		
PBP6B	NP		
	Atu2321†		
	Atu1505†		
	Atu3634†		
PBP4	NP		
PBP7	NP		
LD-transpeptidases			
YcbB	Atu1615		
	Atu1164†	Atu1164	
	Atu1293†		
	Atu2133†	Atu2133	
YbiS	Atu2336†		Rhizobiales/Rhodobacterales LDT
	Atu5196†		Rhizobiales/Rhodobacterales LDT
	Atu0048†		Rhizobiales/Rhodobacterales LDT
	Atu0845†	Atu0845	Rhizobiales/Rhodobacterales LDT
	Atu0669†	Atu0669	Rhizobiales/Rhodobacterales LDT
	Atu3331†		Rhizobiales/Rhodobacterales LDT
	Atu0844†		Rhizobiales/Rhodobacterales LDT
	Atu2764†		
YafK	Atu3332	Atu3332	
	Atu3631		
YnhG	NP		
ErfK	NP		
YcfS	NP		
DD- & LD-endopeptidases			
MepA	Atu0186		
Lytic transglycosylases			
Slt70	NP		septum cleavage w/ PBP7
MltA	Atu0009		septum cleavage w/ PBP1B
MltB	Atu0092†		septum cleavage
	Atu3779†		
	Atu2122†		
MitC	NP		septum cleavage
MltD	NP		septum cleavage
MltE (EmtA)	Atu2112		
MltF	NP		
Amidases			
AmiA	NP		LytC-type PG amidase
AmiB	NP		LytC-type PG amidase
AmiC	Atu1340		LytC-type PG amidase
AmiD	Atu2113		
PEPTIDOGLYCAN REGULATION			
LpoA	NP		regulates PBP1a
LpoB	NP		regulates PBP1b
FtsE	Atu3606		FtsE/X ABC system interacts with EnvC protein to activate AmiA/B
FtsX	Atu3607†		FtsE/X ABC system interacts with EnvC protein to activate AmiA/B
EnvC	Atu2775		activates AmiA/B
	Atu1832†		
NlpD / DipM	Atu1700		activates AmiC, LytM factor
YgeR	NP		
YebA	NP		

E. coli / C. crescentus gene	Atu locus	Name used	Notes
Ivy	NP		inhibits MltB
OM-PG LINKAGE			
TolABRQ-Pal	present		OM invagination during septation / PG linkage
Lpp	NP		links PG tightly to OM (in γ-proteobacteria)
ADDITIONAL GENES			
PopZ	Atu1720†		cell polarity
TipN	NP		cell polarity
PodJ	Atu0499†		cell polarity
MipZ	NP		inhibits FtsZ at pole (Caulobacter)
SlmA	NP		nucleoid occlusion (E coli)
MinCDE	present		z-ring positioning
SulA	NP		inhibits cell division during SOS

† Lower confidence matches, with low sequence similarity, matching primarily by shared domains, altered domain architecture, or other ambiguities.

NP indicates the corresponding gene was not present in the *A. tumefaciens* genome.

Table 5-2 Strains used in phylogenetic studies

phylum	class	order	strain	LDTs
Actinobacteria	Actino-	Actinomycetales	*Mycobacterium tuberculosis H37Rv*	6
Actinobacteria	Actino-	Actinomycetales	*Streptomyces coelicolor A3(2)*	8
Firmicutes	Bacilli	Bacillales	*Bacillus subtilis 168*	3
Firmicutes	Bacilli	Lactobacillales	*Enterococcus faecium DO*	1
Proteobacteria	α-proteo	Caulobacterales	*Asticcacaulis biprosthecum C19*	1
Proteobacteria	α-proteo	Caulobacterales	*Asticcacaulis excentricus CB 48*	1
Proteobacteria	α-proteo	Caulobacterales	*Brevundimonas subvibrioides 15264*	2
Proteobacteria	α-proteo	Caulobacterales	†*Caulobacter crescentus CB15*	2
Proteobacteria	α-proteo	Caulobacterales‡	*Hirschia baltica ATCC 49814*	1
Proteobacteria	α-proteo	Caulobacterales‡	*Hyphomonas neptunium ATCC 15444*	2
Proteobacteria	α-proteo	Caulobacterales	*Phenylobacterium zucineum HLK1*	5
Proteobacteria	α-proteo	Magnetococcales	*Magnetococcus marinus MC-1*	3
Proteobacteria	α-proteo	Parvularculales	*Parvularcula bermudensis HTCC2503*	1
Proteobacteria	α-proteo	Rhizobiales	†*Agrobacterium tumefaciens str. C58*	14
Proteobacteria	α-proteo	Rhizobiales	†*Bradyrhizobium japonicum USDA 110*	21
Proteobacteria	α-proteo	Rhizobiales	†*Brucella suis 1330*	10
Proteobacteria	α-proteo	Rhizobiales	*Hyphomicrobium denitrificans 51888*	15
Proteobacteria	α-proteo	Rhizobiales	†*Mesorhizobium loti MAFF303099*	18
Proteobacteria	α-proteo	Rhizobiales	*Methylosinus trichosporium OB3b*	14
Proteobacteria	α-proteo	Rhizobiales	*Rhodomicrobium vannielii ATCC 17100*	11
Proteobacteria	α-proteo	Rhizobiales	†*Rhodopseudomonas palustris TIE-1*	13
Proteobacteria	α-proteo	Rhizobiales	†*Sinorhizobium meliloti 1021*	13
Proteobacteria	α-proteo	Rhodobacterales	†*Rhodobacter sphaeroides 2.4.1*	9
Proteobacteria	α-proteo	Rhodobacterales	*Roseobacter denitrificans OCh 114*	6
Proteobacteria	α-proteo	Rhodobacterales	*Roseobacter litoralis Och 149*	11
Proteobacteria	α-proteo	Rhodobacterales	*Roseovarius nubinhibens ISM*	10
Proteobacteria	α-proteo	Rhodobacterales	*Sagittula stellata E-37*	8
Proteobacteria	α-proteo	Rhodobacterales	*Sulfitobacter sp. EE-36*	7
Proteobacteria	α-proteo	Rhodospirillales	†*Magnetospirillum magneticum AMB-1*	1
Proteobacteria	α-proteo	Rhodospirillales	†*Rhodospirillum rubrum ATCC 11170*	2
Proteobacteria	α-proteo	Sphingomonadales	*Novosphingobium nitrogenifigens 19370*	4
Proteobacteria	α-proteo	Sphingomonadales	*Sphingobium chlorophenolicum L-1*	5
Proteobacteria	α-proteo	Sphingomonadales	*Sphingomonas wittichii RW1*	4
Proteobacteria	β-proteo	Neisseriales	†*Neisseria meningitidis MC58*	1
Proteobacteria	δ-proteo	Myxococcales	†*Myxococcus xanthus DK 1622*	2
Proteobacteria	ε -proteo	Campylobacterales	†*Campylobacter jejuni NCTC 11168*	1
Proteobacteria	ε -proteo	Campylobacterales	†*Helicobacter pylori 26695*	1
Proteobacteria	γ-proteo	Enterobacteriales	†*Escherichia coli str. K-12 MG1655*	6
Proteobacteria	γ-proteo	Enterobacteriales	†*Klebsiella pneumoniae MGH 78578*	6
Proteobacteria	γ-proteo	Legionellales	†*Coxiella burnetii RSA 493*	8
Proteobacteria	γ-proteo	Pseudomonadales	†*Pseudomonas syringae B728a*	2
Proteobacteria	γ-proteo	Vibrionales	†*Vibrio cholerae O1 biovar El Tor N16961*	3
Proteobacteria	γ-proteo	Xanthomonadales	†*Xanthomonas oryzae KACC 10331*	1

† Strains included in both the PBP and LDT analyses

‡ These strains are officially classified as Rhodobacterales but have better support through multi-gene analyses for placement in Caulobacterales (189).

Table 5-3 Strains and plasmids used in this study

Strains	Relevant genotype	Source
XL1-Blue	*E. coli* cloning strain, *endA1 gyrA96(nalR) thi-1 recA1 relA1 lac glnV44 F'[::Tn10 proAB+ lacIq Δ(lacZ)M15] hsdR17(rK- mK+),* Tet^R	lab stock
C58	wild-type *A. tumefaciens* strain C58	lab stock
ATC107	*A. tumefaciens* C58 *Δpbp3b::npt*, Kan^R	this study
Plasmids	**Relevant gene(s) and construction**	**Source**
pACYC-Duet-1	*E. coli* cloning vector, Cm^R	Novagen
pDW029	broad host-range vector, *vir*-inducible, $Strep^R$ $Spec^R$	(23)
pSRK-Km	broad host-range vector, lac-inducible, Kan^R	(190)
pJZ207	pSRK-Km encoding FtsZ-GFP	(113)
pJZ208	pSRK-Km encoding FtsA-GFP	(113)
pJZ124	pDW029 encoding mRFP1, cloned with BspHI and AvrII-TAA-SalI sites	this study
pJZ146	pJZ124 encoding FtsZ-RFP, with *atu2086* cloned with BspHI sites	this study
pTC060	pSRK-Km encoding FtsZ-RFP, cloned from pJZ146 with NdeI & XbaI sites	this study
pTC077	pDW029 encoding lacI and lac-inducible FtsZ-RFP, cloned by blunt ligating the pDW029 AflII & SacII fragment with the pTC060 EcoRI fragment, $Strep^R$ $Spec^R$	this study
pTC059	pSRK-Km encoding citrine, cloned with NdeI & SacI-TAA-XbaI sites	this study
pTC135	pTC059 encoding citrine-PBP1a, with *atu1341* cloned with SacI & SmaI sites	this study
pTC074	pTC059 encoding citrine-PBP3a, with *atu2100* cloned with SacI & SmaI sites	this study
pTC062	pTC059 encoding citrine-PBP3b, with *atu1067* cloned with SacI & SmaI sites	this study
pJAF026	pSRK-Km encoding sfGFP cloned with NdeI & AvrII-TAA-HindIII sites	this study
pTC122	pJAF026 encoding Atu0845-sfGFP, with *atu0845* cloned with NdeI sites	this study
pTC123	pJAF026 encoding Atu1164-sfGFP, with *atu1164* cloned with NdeI sites	this study
pTC127	pSRK-Km carrying *sfGFP*, cloned from pJAF026 with SmaI & XhoI sites	this study
pTC130	pTC127 encoding Atu3332-sfGFP, with *atu3322* cloned with NdeI & SmaI sites	this study
pTC132	pTC127 encoding Atu2133-sfGFP, with *atu2133* cloned with NdeI & SmaI sites	this study
pTC140	pTC127 encoding Atu0669-sfGFP, with *atu0669* cloned with NdeI & SmaI sites	this study
pTC092	pACYC Duet-1 carrying a *pbp3b* deletion cassette consisting of 1038 nt upstream of *pbp3b*, npt, 1047 nt downstream of *pbp3b*, and *sacB*	this study

CHAPTER 6

Concluding Remarks

6.1 Summary of findings

6.1.1 Type IV secretion system localization

The subcellular localization of the *virB* T4SS of *A. tumefaciens* was re-examined using higher resolution deconvolution microscopy, with the intention of addressing conflicting data in the field, and better understanding the role of the type IV secretion (T4SS) in attachment of *A. tumefaciens* to host plant cells. GFP fusions to many T4SS components did not complement deletions of the native protein, presumably because the bulky GFP interferes with proper assembly of the T4SS complex. However, GFP-VirB8 was fully functional and localized as multiple foci around the cell periphery (129). For this construct, GFP was fused to the cytoplasmic tail of VirB8, leaving the major periplasmic domain of VirB8 intact for T4SS assembly and function. Immunolocalization of the native VirB8 and eight additional VirB proteins confirmed that numerous T4SS components localized as multiple foci across the cell surface (64).

By visual inspection, GFP-VirB8 and other T4SS components appeared as if they might be localized in a helical pattern. If true, this would imply the existence of a T4SS organizing factor in the cell, and a biological purpose for such organization. To specifically test if T4SS localization is organized, the localization of GFP-VirB8 foci was examined quantitatively. When measured along the sides of cells, GFP-VirB8 had a characteristic, preferred spacing of roughly 0.5 μm. Examination of this spacing by Fourier analysis demonstrated a non-random, periodic signal. Monte Carlo simulations of foci placement along a helical scaffold replicated the observed spacing distribution, and were distinct from simulations of random placement. Maximum likelihood model fits and quantitative model comparisons further supported that GFP-VirB8 foci are periodically arranged in the cell.

Although the T4SS organizing factor was not identified, this periodic arrangement may serve biological purpose during *A. tumefaciens* host cell attachment. When *vir*-induced bacteria were incubated with plant protoplasts, *A. tumefaciens* predominantly attached to the protoplasts along its lateral length (64). In contrast, *A. tumefaciens* without the T4SS genes present did not bind well in any orientation. Surprisingly, the unipolar holdfast did not appear to contribute significantly to plant cell binding and polar associations were infrequently observed, perhaps indicating that this holdfast is ineffective in attaching to plant cell membranes. Since the T4SS facilitates lateral host cell attachment, the arrangement of these complexes on the plant cell surface is likely an important factor influencing the chances that an *A. tumefaciens* cell will successfully initiate contact and substrate transfer to host cells.

6.1.2 Unipolar growth components

As part of a long-term plan to assess peptidoglycan (PG) synthesis for a role in establishing periodic T4SS localization, the unipolar cell growth process of *A. tumefaciens* was examined. These studies initially focused on the two classical cell division scaffold proteins FtsZ and FtsA. Through a combination of colocalization and pulse-chase labeling experiments, both proteins were found to localize to the growing cell pole. Conversely, the lipophilic membrane dye FM4-64 was found to label the old cell pole most intensely, and therefore served as an important tool in distinguishing the old and growth poles. FtsA-GFP was amenable to timelapse studies, and consistently localized at the growing cell tip or at the midcell in dividing cells. Since FtsZ-GFP

timelapses were unsuccessful, its localization over the cell cycle was instead studied using demographs. A custom R script was used to construct a demograph (a composite kymograph) from the localization of FtsZ-GFP in hundreds of individual cells ordered by length. The demograph showed that FtsZ transitioned from exclusively unipolar localization to include additional FtsZ foci throughout the cells as they grew. FtsZ retained polar localization until it transitioned to strong midcell localization for the final ~ 25% of the cell cycle. FtsA appeared to lag behind FtsZ in midcell relocalization.

Using the demograph approach, the localization of various PG synthesis enzymes over the *A. tumefaciens* cell cycle was examined. The only canonical cell elongation protein present, PBP1a, consistently localized to the growth pole. In other well-studied systems PBP1a requires an additional transpeptidase for PG synthesis; however neither of the canonical PBP3 transpeptidases localized to the growth pole long enough to account for polar growth. A bioinformatics survey of the PG synthesis components in *A. tumefaciens* revealed an unusual enrichment of L,D-transpeptidase (LDT) proteins, and therefore several were chosen for additional localization studies. Remarkably, one LDT robustly localized to the growing pole, and it may therefore serve an important role in polar growth.

Unipolar growth was further characterized by directly examining PG synthesis activity at the growing poles. PG synthesis activity was visualized by briefly incubating cultures with an exogenous D-amino acid, which is exchanged in place with existing D-amino acids in the *A. tumefaciens* PG through an LDT-mediated mechanism (164). Although LDT activity was limited to the new poles in new cells, it gradually expanded in area as the new cell compartment grew. Examination of new cell compartments by whole-cell TEM revealed that new poles expand in both length and width as they grow, in striking contrast to typical rod shaped growth where cells maintain a single, tightly constrained width. Both cell width and the area of LDT activity gradually increased over the cell cycle.

6.2 Conclusions and future directions

6.2.1 Does PG synthesis lead to a periodic localization of T4SS complexes?

This work lays the groundwork for future studies testing for a role of PG synthesis in T4SS localization. However, before those studies can be fully pursued, additional analysis will be needed to confirm the putative cell elongation roles of FtsZ, FtsA, PBP1a, and Atu0845. Ideally, interactions between these proteins should be shown (by biochemical pull-downs or yeast two hybrid assays), and their functional roles should be established through gene deletions, depletions, or by adding or inducing specific inhibitors. The uncharacterized predicted tranglycosylases PBP1b1, PBP1b2, and MtgA should also be localized to determine if they might participate in polar growth.

Preliminary results of FtsZ-RFP localization in a Δ*minCDE* construct cast doubt on a major role for FtsZ in polar elongation, as FtsZ-RFP appears to spend only the initial ~ 25% of the early cell cycle (defined by the shortest cells) associated with the growth pole in this deletion strain (Figure 6-1). These results are intriguing, and if reproducible, would warrant a full examination of the localization of FtsA, Atu0845, PBP1a, and PG synthesis activities in the Δ*minCDE* background. In *S. meliloti* (176) and *A. tumefaciens* (Cameron and Zambryski, unpublished results), Δ*minCDE* constructs appear to have normal morphology and growth characteristics. If FtsZ were

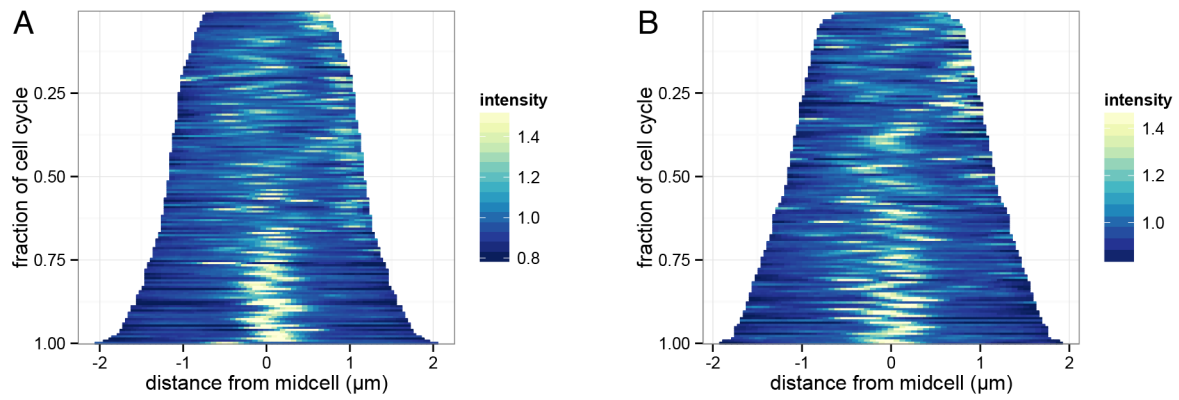

Figure 6-1 Effect of Δ*minCDE* on FtsZ localization

(A) FtsZ-RFP in wild-type *A. tumefaciens.* FtsZ maintains polar localization for the first ~ 75% of the cell cycle, as reported for FtsZ-GFP. (B) FtsZ-RFP in a Δ*minCDE* background. FtsZ-RFP rapidly disassociates from the growth pole after cell division.

the only component with altered localization in Δ*minCDE*, this would argue that FtsZ is only needed during the early stages of polar growth, with the remaining components still playing roles during the entire elongation process.

Once confirmed, all identified components of the polar elongasome would need to be localized under *vir*-induction conditions to test if they exhibit the same multiple foci observed for FtsZ-GFP. In this scenario, the slowed cell elongation and division that occurs during optimal *vir*-induction might result in numerous sites of paused PG synthesis or possibly weakened PG that would enable insertion of T4SSs. Targeted protein-protein interaction studies or pull-downs between these PG synthesis proteins and T4SS components would provide strong support for a role of PG synthesis in establishing a periodic T4SS localization pattern.

Even if polar elongation components do not localize or interact with T4SS complexes, polar growth may still have an instrumental role in establishing a periodic distribution of T4SS complexes. In this alternate hypothesis, the continued addition of new cell material at the growth pole would serve to create a spacing effect between T4SS complexes. This hypothesis relies on a periodic assembly of new T4SS complexes at the growth pole, an aspect that has not yet been specifically investigated. The generation of unlabeled growth poles following Texas red-X succinimidyl ester (TRSE) labeling offers limited support that outer membrane components may be inserted at the growth pole in *A. tumefaciens*, although further experiments would be needed to confirm. Long-term time-lapse studies of the localization T4SS components in cells undergoing early stages of *vir*-induction would easily test this periodic polar insertion hypothesis. Addition of new T4SS foci at the growth pole would provide support, whereas addition of T4SS foci throughout the cell would argue otherwise. If true, this mechanism could have the added benefit of providing another possible explanation for the discrepancies between reports of polar and lateral T4SS.

6.2.2 How are cell width, length, and division controlled?

As recently reviewed by Young (191), the factors controlling bacterial cell width are poorly understood. Under normal, steady growth both width and length appear linked to the nutritional state of the cell, where faster growing cells are generally longer and wider than slower growing cells. Cell length is also controlled by mechanisms, such as the MinCDE system, that ultimately modulate the timing of cell division. In contrast, while cell width is affected by mutations to cell elongation components, the underlying control mechanism is unknown. Strong evidence for the existence of such a regulatory mechanism was demonstrated with *E. coli*, in which cells were able to grow through a narrow channel half their normal width, then emerge and eventually recover their original dimensions (192).

In *A. tumefaciens*, the concept of cell width control needs to be viewed from a new perspective. The average width of new cell compartment continues to linearly increase, without stopping or slowing, until the cell eventually divides (Figure 5-8). However, the width of the new cell compartment must still be regulated; indeed, treatment of cells with nalidixic acid to delay DNA replication and cell division does not appear to result in obviously wider new cell compartments in *A. tumefaciens* (Figure 6-2A,B) or *S. meliloti* (177) cells observed by light microscopy. Closer inspection of nalidixic acid-treated cells by whole-cell TEM or by microscopy combined with cell analysis software capable of sub-pixel resolution (i.e. MicrobeTracker (193)) may help illuminate precisely what width *A. tumefaciens* prefers, and how cell growth is modulated to achieve this preferred width.

Cell length in *A. tumefaciens* appears to be quite variable. Previous studies indicated that new cell compartments can be considerably shorter than old cell compartments upon division (104, 194). When the sizes of old and new cell compartments were compared using whole-cell TEM images (Figure 5-8), at least some new cell compartments reached dimensions approximately equivalent to their old cell

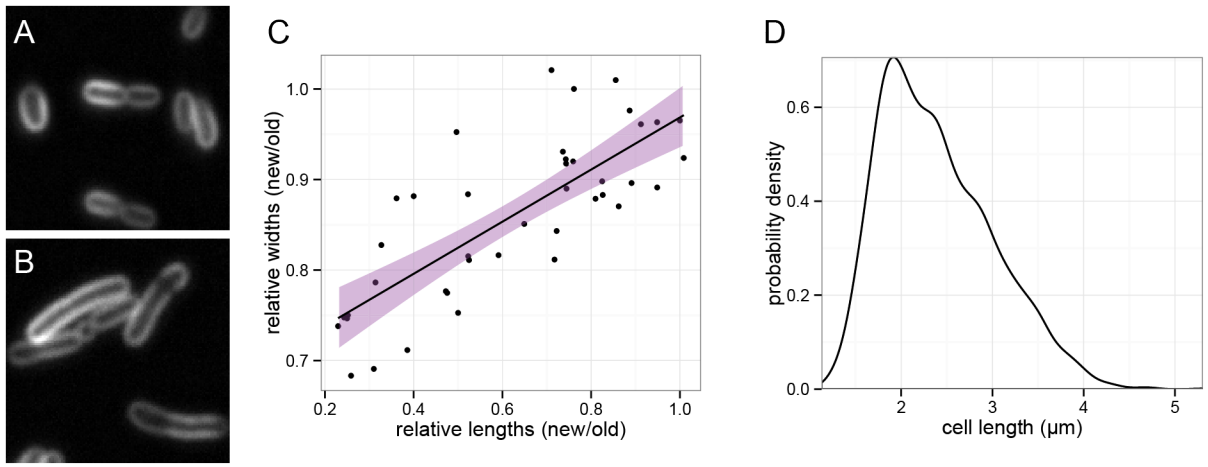

Figure 6-2 *A. tumefaciens* growth characteristics

A and B: (A) untreated and (B) nalidixic acid treated cells, labeled with FM4-64. Treated cells increase in length without apparent effect on cell width. (C) Relative lengths and widths of new and old cell compartments, as measured from whole-cell TEM images. New cell compartments are capable of reaching the same dimensions as their parent old cell compartments. (D) Gaussian kernel density estimate plot of the cell lengths of 2760 cells. The 'step-like' distribution is not predicted by exponential or linear growth rate models.

compartments (Figure 6-2C). With static images such as these however, old and new cell compartments of similar size may be mis-identified, and some new cell compartments may have *exceeded* the size of their parent old cell compartments. Since *A. tumefaciens* appears to exclusively grow from the new pole / cell compartment, it must occasionally produce new cells larger than the parent old cell compartments; a growth model that produced cells only less than or equal in size to current cells would not maintain cell dimensions over many rounds of cell division. Time-lapse imaging and sub-pixel quantification of the dimensions of old and new cells over several generations would help address this question.

Such cell dimension data would be relevant to several other questions as well. When the lengths of 2760 cells (measured for the demographs presented in Chapter 5) are graphed as a Gaussian kernel density estimate plot (Figure 6-2D), the distribution of cell sizes does not replicate the predicted distributions for either exponential or linear growth rates (195), particularly in the appearance of multiple 'steps' of cell lengths over the distribution (see "bumps' on right side of the curve in Figure 6-2D). These multiple defined lengths may reflect multiple distinct growth rates through the cell cycle, and preliminary experiments with MicrobeTracker demonstrated the feasibility of a growth rate analysis. Alternatively, *A. tumefaciens* could produce old and new cells that undergo different life cycles, and the cumulative distribution of these populations produces the step-like pattern of cell lengths. Comparison of the growth rates and lifecycle of individual old and new cells by time lapse imaging would help determine if this were the case.

There is some evidence to suggest *A. tumefaciens* and other members of the Rhizobiales may share differentiated old and new cell life cycles with their notable fellow α-proteobacterium *C. crescentus.* In *B. abortus*, old cell compartments specifically inherit an assortment of proteins during cell division, including DivK-P, PdhS, and FumC, whereas new cells must generate these proteins *de novo* (172, 196, 197). Likewise, the old poles of *A. tumefaciens* can produce a polysaccharide holdfast, resulting in stationary old cells and mobile new cells (104). These types of bacterial differentiations could produce distinctly different life cycles between old and new cells, with potential implications for cell growth, virulence, and the distribution of the T4SS.

References

1. **Alvarez-Martinez CE**, **Christie PJ**. 2009. Biological diversity of prokaryotic type IV secretion systems. Microbiol Mol Biol Rev **73**:775–808.
2. **Backert S**, **Fronzes R**, **Waksman G**. 2008. VirB2 and VirB5 proteins: specialized adhesins in bacterial type-IV secretion systems? Trends Microbiol **16**:409–413.
3. **Carey KL**, **Newton HJ**, **Lührmann A**, **Roy CR**. 2011. The Coxiella burnetii Dot/Icm system delivers a unique repertoire of type IV effectors into host cells and is required for intracellular replication. PLoS Pathog. **7**:e1002056.
4. **Ben-Tekaya H**, **Gorvel J-P**, **Dehio C**. 2013. Bartonella and Brucella--weapons and strategies for stealth attack. Cold Spring Harb Perspect Med **3**.
5. **De Block M**, **Herrera-Estrella L**, **Van Montagu M**, **Schell J**, **Zambryski PC**. 1984. Expression of foreign genes in regenerated plants and in their progeny. EMBO J **3**:1681–1689.
6. **Horsch RB**, **Fry JE**, **Hoffmann NL**, **Eichholtz D**, **Rogers SG**, **Fraley RT**. 1985. A Simple and General Method for Transferring Genes into Plants. Science **227**:1229–1231.
7. **Hulse M**, **Johnson S**, **Ferrieri P**. 1993. Agrobacterium Infections in Humans: Experience at One Hospital and Review. Clinical Infectious Diseases **16**:112–117.
8. **Middelveen MJ**, **Stricker RB**. 2011. Filament formation associated with spirochetal infection: a comparative approach to Morgellons disease. Clin Cosmet Investig Dermatol **4**:167–177.
9. **Bundock P**, **Dulk-Ras den A**, **Beijersbergen A**, **Hooykaas PJ**. 1995. Trans-kingdom T-DNA transfer from Agrobacterium tumefaciens to Saccharomyces cerevisiae. EMBO J **14**:3206–3214.
10. **Kunik T**, **Tzfira T**, **Kapulnik Y**, **Gafni Y**, **Dingwall C**, **Citovsky V**. 2001. Genetic transformation of HeLa cells by Agrobacterium. PNAS **98**:1871–1876.
11. **Schröder G**, **Schuelein R**, **Quebatte M**, **Dehio C**. 2011. Conjugative DNA transfer into human cells by the VirB/VirD4 type IV secretion system of the bacterial pathogen Bartonella henselae. PNAS **108**:14643–14648.
12. **Fernández-González E**, **de Paz HD**, **Alperi A**, **Agúndez L**, **Faustmann M**, **Sangari FJ**, **Dehio C**, **Llosa M**. 2011. Transfer of R388 derivatives by a pathogenesis-associated type IV secretion system into both bacteria and human cells. J Bacteriol **193**:6257–6265.
13. **Llosa M**, **Schröder G**, **Dehio C**. 2012. New perspectives into bacterial DNA transfer to human cells. Trends Microbiol **20**:355–359.
14. **Vernade D**, **Herrera-Estrella A**, **Wang K**, **Montagu MV**. 1988. Glycine betaine allows enhanced induction of the Agrobacterium tumefaciens vir genes by acetosyringone at low pH. J Bacteriol **170**:5822–5829.
15. **Cangelosi GA**, **Ankenbauer RG**, **Nester EW**. 1990. Sugars induce the Agrobacterium virulence genes through a periplasmic binding protein and a transmembrane signal protein. PNAS **87**:6708–6712.
16. **Stachel SE**, **Messens E**, **Van Montagu M**, **Zambryski P**. 1985. Identification of the signal molecules produced by wounded plant cells that activate T-DNA

transfer in Agrobacterium tumefaciens. Nature **318**:624–629.
17. **Stachel SE**, **Nester EW**, **Zambryski PC**. 1986. A plant cell factor induces Agrobacterium tumefaciens vir gene expression. PNAS **83**:379–383.
18. **Braun AC**. 1952. The crown-gall disease. Ann. N. Y. Acad. Sci. **54**:1153–1161.
19. **Stachel SE**, **Zambryski PC**. 1986. virA and virG control the plant-induced activation of the T-DNA transfer process of A. tumefaciens. Cell **46**:325–333.
20. **Berger BR**, **Christie PJ**. 1994. Genetic complementation analysis of the Agrobacterium tumefaciens virB operon: virB2 through virB11 are essential virulence genes. J Bacteriol **176**:3646–3660.
21. **Cascales E**, **Christie PJ**. 2004. Definition of a bacterial type IV secretion pathway for a DNA substrate. Science **304**:1170–1173.
22. **Vergunst AC**, **Schrammeijer B**, **Dulk-Ras den A**, **de Vlaam CM**, **Regensburg-Tuïnk TJ**, **Hooykaas PJ**. 2000. VirB/D4-dependent protein translocation from Agrobacterium into plant cells. Science **290**:979–982.
23. **Zupan JR**, **Hackworth CA**, **Aguilar J**, **Ward DV**, **Zambryski PC**. 2007. VirB1* promotes T-pilus formation in the vir-Type IV secretion system of Agrobacterium tumefaciens. J Bacteriol **189**:6551–6563.
24. **Atmakuri K**, **Cascales E**, **Burton OT**, **Banta LM**, **Christie PJ**. 2007. Agrobacterium ParA/MinD-like VirC1 spatially coordinates early conjugative DNA transfer reactions. EMBO J **26**:2540–2551.
25. **Pitzschke A**, **Hirt H**. 2010. New insights into an old story: Agrobacterium-induced tumour formation in plants by plant transformation. EMBO J **29**:1021–1032.
26. **Schulein R**, **Guye P**, **Rhomberg TA**, **Schmid MC**, **Schröder G**, **Vergunst AC**, **Carena I**, **Dehio C**. 2005. A bipartite signal mediates the transfer of type IV secretion substrates of Bartonella henselae into human cells. PNAS **102**:856–861.
27. **Vergunst AC**, **van Lier MCM**, **Dulk-Ras den A**, **Stüve TAG**, **Ouwehand A**, **Hooykaas PJJ**. 2005. Positive charge is an important feature of the C-terminal transport signal of the VirB/D4-translocated proteins of Agrobacterium. PNAS **102**:832–837.
28. **Akiyoshi DE**, **Morris RO**, **Hinz R**, **Mischke BS**, **Kosuge T**, **Garfinkel DJ**, **Gordon MP**, **Nester EW**. 1983. Cytokinin/auxin balance in crown gall tumors is regulated by specific loci in the T-DNA. PNAS **80**:407–411.
29. **Thompson J**, **Donkersloot JA**. 1992. Biosynthesis and distribution of N-carboxyalkyl amino acids (opines) in bacteria. Res Microbiol **143**:127–131.
30. **White CE**, **Winans SC**. 2007. Cell-cell communication in the plant pathogen Agrobacterium tumefaciens. Philos Trans R Soc Lond, B, Biol Sci **362**:1135–1148.
31. **Fronzes R**, **Schäfer E**, **Wang L**, **Saibil HR**, **Orlova EV**, **Waksman G**. 2009. Structure of a type IV secretion system core complex. Science **323**:266–268.
32. **Chandran V**, **Fronzes R**, **Duquerroy S**, **Cronin N**, **Navaza J**, **Waksman G**. 2009. Structure of the outer membrane complex of a type IV secretion system. Nature.
33. **Walldén K**, **Williams R**, **Yan J**, **Lian PW**, **Wang L**, **Thalassinos K**, **Orlova EV**, **Waksman G**. 2012. Structure of the VirB4 ATPase, alone and bound to the core

complex of a type IV secretion system. PNAS **109**:11348–11353.
34. **Atmakuri K**, **Cascales E**, **Christie PJ**. 2004. Energetic components VirD4, VirB11 and VirB4 mediate early DNA transfer reactions required for bacterial type IV secretion. Mol Microbiol **54**:1199–1211.
35. **Banta LM**, **Kerr JE**, **Cascales E**, **Giuliano ME**, **Bailey ME**, **McKay C**, **Chandran V**, **Waksman G**, **Christie PJ**. 2011. An Agrobacterium VirB10 mutation conferring a type IV secretion system gating defect. J Bacteriol **193**:2566–2574.
36. **Cascales E**, **Christie PJ**. 2004. Agrobacterium VirB10, an ATP energy sensor required for type IV secretion. PNAS **101**:17228–17233.
37. **Eisenbrandt R**, **Kalkum M**, **Lai E-M**, **Lurz R**, **Kado CI**, **Lanka E**. 1999. Conjugative pili of IncP plasmids, and the Ti plasmid T pilus are composed of cyclic subunits. J Biol Chem **274**:22548–22555.
38. **Lai E-M**, **Chesnokova O**, **Banta LM**, **Kado CI**. 2000. Genetic and environmental factors affecting T-pilin export and T-pilus biogenesis in relation to flagellation of Agrobacterium tumefaciens. J Bacteriol **182**:3705–3716.
39. **Ahmed Aly K**, **Baron C**. 2007. The VirB5 protein localizes to the T-pilus tips in Agrobacterium tumefaciens. Microbiology (Reading, Engl) **153**:3766–3775.
40. **Shirasu K**, **Koukolíková-Nicola Z**, **Hohn B**, **Kado CI**. 1994. An inner-membrane-associated virulence protein essential for T-DNA transfer from Agrobacterium tumefaciens to plants exhibits ATPase activity and similarities to conjugative transfer genes. Mol Microbiol **11**:581–588.
41. **Jones AL**, **Shirasu K**, **Kado CI**. 1994. The product of the virB4 gene of Agrobacterium tumefaciens promotes accumulation of VirB3 protein. J Bacteriol **176**:5255–5261.
42. **Shamaei-Tousi A**, **Cahill R**, **Frankel G**. 2004. Interaction between protein subunits of the type IV secretion system of Bartonella henselae. J Bacteriol **186**:4796–4801.
43. **Mossey P**, **Hudacek A**, **Das A**. 2010. Agrobacterium tumefaciens type IV secretion protein VirB3 is an inner membrane protein and requires VirB4, VirB7, and VirB8 for stabilization. J Bacteriol **192**:2830–2838.
44. **Yuan Q**, **Carle A**, **Gao C**, **Sivanesan D**, **Ahmed Aly K**, **Höppner C**, **Krall L**, **Domke N**, **Baron C**. 2005. Identification of the VirB4-VirB8-VirB5-VirB2 pilus assembly sequence of type IV secretion systems. J Biol Chem **280**:26349–26359.
45. **Baron C**, **Llosa M**, **Zhou S**, **Zambryski PC**. 1997. VirB1, a component of the T-complex transfer machinery of Agrobacterium tumefaciens, is processed to a C-terminal secreted product, VirB1. J Bacteriol **179**:1203–1210.
46. **Lin T-S**, **Kado CI**. 1993. The virD4 gene is required for virulence while virD3 and orf5 are not required for virulence of Agrobacterium tumefaciens. Mol Microbiol **9**:803–812.
47. **Sagulenko E**, **Chen J**, **Christie PJ**. 2001. Role of Agrobacterium VirB11 ATPase in T-pilus assembly and substrate selection. J Bacteriol **183**:5813–5825.
48. **Jakubowski SJ**, **Cascales E**, **Krishnamoorthy V**, **Christie PJ**. 2005. Agrobacterium tumefaciens VirB9, an outer-membrane-associated component of a type IV secretion system, regulates substrate selection and T-pilus

biogenesis. J Bacteriol **187**:3486–3495.
49. **Jakubowski SJ**, **Kerr JE**, **Garza I**, **Krishnamoorthy V**, **Bayliss R**, **Waksman G**, **Christie PJ**. 2009. Agrobacterium VirB10 domain requirements for type IV secretion and T pilus biogenesis. Mol Microbiol **71**:779–794.
50. **Garza I**, **Christie PJ**. 2013. A putative transmembrane leucine zipper of agrobacterium VirB10 is essential for t-pilus biogenesis but not type IV secretion. J Bacteriol **195**:3022–3034.
51. **Baron C**. 2010. Antivirulence drugs to target bacterial secretion systems. Curr Opin Microbiol **13**:100–105.
52. **Cegelski L**, **Marshall GR**, **Eldridge GR**, **Hultgren SJ**. 2008. The biology and future prospects of antivirulence therapies. Nat Rev Micro **6**:17–27.
53. **Kauppi AM**, **Nordfelth R**, **Uvell H**, **Wolf-Watz H**, **Elofsson M**. 2003. Targeting bacterial virulence: inhibitors of type III secretion in Yersinia. Chemistry & Biology **10**:241–249.
54. **Pinkner JS**, **Remaut H**, **Buelens F**, **Miller E**, **Aberg V**, **Pemberton N**, **Hedenström M**, **Larsson A**, **Seed P**, **Waksman G**, **Hultgren SJ**, **Almqvist F**. 2006. Rationally designed small compounds inhibit pilus biogenesis in uropathogenic bacteria. PNAS **103**:17897–17902.
55. **Paschos A**, **Patey G**, **Sivanesan D**, **Gao C**, **Bayliss R**, **Waksman G**, **O'Callaghan D**, **Baron C**. 2006. Dimerization and interactions of Brucella suis VirB8 with VirB4 and VirB10 are required for its biological activity. PNAS **103**:7252–7257.
56. **Paschos A**, **Hartigh den A**, **Smith MA**, **Atluri VL**, **Sivanesan D**, **Tsolis RM**, **Baron C**. 2011. An in vivo high-throughput screening approach targeting the type IV secretion system component VirB8 identified inhibitors of Brucella abortus 2308 proliferation. Infect Immun **79**:1033–1043.
57. **Smith MA**, **Coinçon M**, **Paschos A**, **Jolicoeur B**, **Lavallée P**, **Sygusch J**, **Baron C**. 2012. Identification of the binding site of Brucella VirB8 interaction inhibitors. Chemistry & Biology **19**:1041–1048.
58. **Bhatty M**, **Laverde Gomez JA**, **Christie PJ**. 2013. The expanding bacterial type IV secretion lexicon. Res Microbiol **164**:620–639.
59. **Chen L**, **Chen Y**, **Wood DW**, **Nester EW**. 2002. A new type IV secretion system promotes conjugal transfer in Agrobacterium tumefaciens. J Bacteriol **184**:4838–4845.
60. **Li PL**, **Everhart DM**, **Farrand SK**. 1998. Genetic and sequence analysis of the pTiC58 trb locus, encoding a mating-pair formation system related to members of the type IV secretion family. J Bacteriol **180**:6164–6172.
61. **Tegtmeyer N**, **Wessler S**, **Backert S**. 2011. Role of the cag-pathogenicity island encoded type IV secretion system in Helicobacter pylori pathogenesis. FEBS J. **278**:1190–1202.
62. **Hiroki Nagai TK**. 2011. Type IVB Secretion Systems of Legionella and Other Gram-Negative Bacteria. Frontiers in Microbiology **2**.
63. **Cameron TA**, **Roper M**, **Zambryski PC**. 2012. Quantitative Image Analysis and Modeling Indicate the Agrobacterium tumefaciens Type IV Secretion System Is Organized in a Periodic Pattern of Foci. PLoS ONE **7**:e42219.
64. **Aguilar J**, **Cameron TA**, **Zupan J**, **Zambryski PC**. 2011. Membrane and core

periplasmic Agrobacterium tumefaciens virulence Type IV secretion system components localize to multiple sites around the bacterial perimeter during lateral attachment to plant cells. MBio **2**:e00218–11.
65. **Guttenplan SB**, **Shaw S**, **Kearns DB**. 2013. The cell biology of peritrichous flagella in Bacillus subtilis. Mol Microbiol **87**:211–229.
66. **Cayley DS**, **Guttman HJ**, **Record MT**. 2000. Biophysical characterization of changes in amounts and activity of Escherichia coli cell and compartment water and turgor pressure in response to osmotic stress. Biophysical Journal **78**:1748–1764.
67. **Whatmore AM**, **Reed RH**. 1990. Determination of turgor pressure in Bacillus subtilis: a possible role for K+ in turgor regulation. J. Gen. Microbiol. **136**:2521–2526.
68. **Balish MF**, **Krause DC**. 2006. Mycoplasmas: a distinct cytoskeleton for wall-less bacteria. J. Mol. Microbiol. Biotechnol. **11**:244–255.
69. **Kürner J**, **Frangakis AS**, **Baumeister W**. 2005. Cryo-electron tomography reveals the cytoskeletal structure of Spiroplasma melliferum. Science **307**:436–438.
70. **Razin S**, **Masover GK**, **Palant M**, **Hayflick L**. 1977. Morphology of Ureaplasma urealyticum (T-mycoplasma) organisms and colonies. J Bacteriol **130**:464–471.
71. **Pavelka MS**. 2007. Another brick in the wall. Trends Microbiol **15**:147–149.
72. **Errington J**. 2013. L-form bacteria, cell walls and the origins of life. Open Biol **3**:120143.
73. **Domínguez-Cuevas P**, **Mercier R**, **Leaver M**, **Kawai Y**, **Errington J**. 2012. The rod to L-form transition of Bacillus subtilis is limited by a requirement for the protoplast to escape from the cell wall sacculus. Mol Microbiol **83**:52–66.
74. **Mercier R**, **Kawai Y**, **Errington J**. 2013. Excess membrane synthesis drives a primitive mode of cell proliferation. Cell **152**:997–1007.
75. **Fleming A**. 1929. On the Antibacterial Action of Cultures of a Penicillium, with Special Reference to their Use in the Isolation of B. influenzæ. British journal of experimental pathology **10**:226.
76. **Chain E**, **Florey HW**, **Gardner AD**, **Heatley NG**, **Jennings MA**, **Orr-Ewing J**, **Sanders AG**. 1940. Penicillin as a Chemotherapeutic Agent. Originally published as Volume 2, Issue 6104 **236**:226–228.
77. **Abraham EP**, **Chain E**. 1940. An Enzyme from Bacteria able to Destroy Penicillin. Nature **146**:837–837.
78. **Boucher HW**, **Talbot GH**, **Benjamin DK**, **Bradley J**, **Guidos RJ**, **Jones RN**, **Murray BE**, **Bonomo RA**, **Gilbert D**, **Infectious Diseases Society of America**. 2013. 10 x '20 Progress--development of new drugs active against gram-negative bacilli: an update from the Infectious Diseases Society of America. Clin. Infect. Dis. **56**:1685–1694.
79. **Vollmer W**, **Bertsche U**. 2008. Murein (peptidoglycan) structure, architecture and biosynthesis in Escherichia coli. Biochim Biophys Acta **1778**:1714–1734.
80. **Typas A**, **Banzhaf M**, **Gross CA**, **Vollmer W**. 2011. From the regulation of peptidoglycan synthesis to bacterial growth and morphology. Nat Rev Micro **10**:123–136.
81. **Vollmer W**, **Seligman SJ**. 2010. Architecture of peptidoglycan: more data and

more models. Trends Microbiol.
82. **Meroueh SO**, **Bencze KZ**, **Hesek D**, **Lee M**, **Fisher JF**, **Stemmler TL**, **Mobashery S**. 2006. Three-dimensional structure of the bacterial cell wall peptidoglycan. PNAS **103**:4404–4409.
83. **Magnet S**, **Dubost L**, **Marie A**, **Arthur M**, **Gutmann L**. 2008. Identification of the L,D-transpeptidases for peptidoglycan cross-linking in Escherichia coli. J Bacteriol **190**:4782–4785.
84. **Koch AL**. 1998. Orientation of the peptidoglycan chains in the sacculus of Escherichia coli. Res Microbiol **149**:689–701.
85. **Gan L**, **Chen S**, **Jensen GJ**. 2008. Molecular organization of Gram-negative peptidoglycan. PNAS **105**:18953–18957.
86. **Beeby M**, **Gumbart JC**, **Roux B**, **Jensen GJ**. 2013. Architecture and assembly of the Gram-positive cell wall. Mol Microbiol **88**:664–672.
87. **Wang S**, **Furchtgott L**, **Huang KC**, **Shaevitz JW**. 2012. Helical insertion of peptidoglycan produces chiral ordering of the bacterial cell wall. PNAS **109**:E595–604.
88. **Vollmer W**, **Höltje JV**. 2004. The Architecture of the Murein (Peptidoglycan) in Gram-Negative Bacteria: Vertical Scaffold or Horizontal Layer(s)? J Bacteriol **186**:5978–5987.
89. **Blaauwen Den T**, **de Pedro MA**, **Nguyen-Distèche M**, **Ayala JA**. 2008. Morphogenesis of rod-shaped sacculi. FEMS Microbiology Reviews **32**:321–344.
90. **Li Y**, **Hsin J**, **Zhao L**, **Cheng Y**, **Shang W**, **Huang KC**, **Wang H-W**, **Ye S**. 2013. FtsZ protofilaments use a hinge-opening mechanism for constrictive force generation. Science **341**:392–395.
91. **Lan G**, **Daniels BR**, **Dobrowsky TM**, **Wirtz D**, **Sun SX**. 2009. Condensation of FtsZ filaments can drive bacterial cell division. PNAS **106**:121–126.
92. **Osawa M**, **Anderson DE**, **Erickson HP**. 2009. Curved FtsZ protofilaments generate bending forces on liposome membranes. EMBO J **28**:3476–3484.
93. **Margolin W**. 2009. Sculpting the bacterial cell. Curr Biol **19**:R812–22.
94. **Swulius MT**, **Chen S**, **Jane Ding H**, **Li Z**, **Briegel A**, **Pilhofer M**, **Tocheva EI**, **Lybarger SR**, **Johnson TL**, **Sandkvist M**, **Jensen GJ**. 2011. Long helical filaments are not seen encircling cells in electron cryotomograms of rod-shaped bacteria. Biochem Biophys Res Commun **407**:650–655.
95. **van Teeffelen S**, **Wang S**, **Furchtgott L**, **Huang KC**, **Wingreen NS**, **Shaevitz JW**, **Gitai Z**. 2011. The bacterial actin MreB rotates, and rotation depends on cell-wall assembly. PNAS **108**:15822–15827.
96. **García del Portillo F**, **de Pedro MA**. 1990. Differential effect of mutational impairment of penicillin-binding proteins 1A and 1B on Escherichia coli strains harboring thermosensitive mutations in the cell division genes ftsA, ftsQ, ftsZ, and pbpB. J Bacteriol **172**:5863–5870.
97. **Charpentier X**, **Chalut C**, **Rémy M-H**, **Masson J-M**. 2002. Penicillin-binding proteins 1a and 1b form independent dimers in Escherichia coli. J Bacteriol **184**:3749–3752.
98. **Müller P**, **Ewers C**, **Bertsche U**, **Anstett M**, **Kallis T**, **Breukink E**, **Fraipont C**, **Terrak M**, **Nguyen-Distèche M**, **Vollmer W**. 2007. The essential cell division protein FtsN interacts with the murein (peptidoglycan) synthase PBP1B in

Escherichia coli. J Biol Chem **282**:36394–36402.
99. **Banzhaf M**, **van den Berg van Saparoea B**, **Terrak M**, **Fraipont C**, **Egan A**, **Philippe J**, **Zapun A**, **Breukink E**, **Nguyen-Distèche M**, **Blaauwen Den T**, **Vollmer W**. 2012. Cooperativity of peptidoglycan synthases active in bacterial cell elongation. Mol Microbiol **85**:179–194.
100. **van der Ploeg R**, **Verheul J**, **Vischer NOE**, **Alexeeva S**, **Hoogendoorn E**, **Postma M**, **Banzhaf M**, **Vollmer W**, **Blaauwen Den T**. 2013. Colocalization and interaction between elongasome and divisome during a preparative cell division phase in Escherichia coli. Mol Microbiol **87**:1074–1087.
101. **Varma A**, **de Pedro MA**, **Young KD**. 2007. FtsZ directs a second mode of peptidoglycan synthesis in Escherichia coli. J Bacteriol **189**:5692–5704.
102. **Fenton AK**, **Gerdes K**. 2013. Direct interaction of FtsZ and MreB is required for septum synthesis and cell division in Escherichia coli. EMBO J **32**:1953–1965.
103. **Brown PJB**, **Kysela DT**, **Brun YV**. 2011. Polarity and the diversity of growth mechanisms in bacteria. Semin. Cell Dev. Biol. **22**:790–798.
104. **Brown PJB**, **de Pedro MA**, **Kysela DT**, **Van der Henst C**, **Kim J**, **De Bolle X**, **Fuqua C**, **Brun YV**. 2012. Polar growth in the Alphaproteobacterial order Rhizobiales. PNAS **109**:1697–1701.
105. **Kysela DT**, **Brown PJB**, **Huang KC**, **Brun YV**. 2013. Biological Consequences and Advantages of Asymmetric Bacterial Growth. Annu Rev Microbiol **67**:130628184403000.
106. **Flärdh K**. 2003. Essential role of DivIVA in polar growth and morphogenesis in Streptomyces coelicolor A3(2). Mol Microbiol **49**:1523–1536.
107. **Holmes NA**, **Walshaw J**, **Leggett RM**, **Thibessard A**, **Dalton KA**, **Gillespie MD**, **Hemmings AM**, **Gust B**, **Kelemen GH**. 2013. Coiled-coil protein Scy is a key component of a multiprotein assembly controlling polarized growth in Streptomyces. PNAS **110**:E397–406.
108. **Fuchino K**, **Bagchi S**, **Cantlay S**, **Sandblad L**, **Wu D**, **Bergman J**, **Kamali-Moghaddam M**, **Flärdh K**, **Ausmees N**. 2013. Dynamic gradients of an intermediate filament-like cytoskeleton are recruited by a polarity landmark during apical growth. PNAS **110**:E1889–97.
109. **Flärdh K**. 2010. Cell polarity and the control of apical growth in Streptomyces. Curr Opin Microbiol **13**:758–765.
110. **Letek M**, **Fiuza M**, **Ordóñez E**, **Villadangos AF**, **Ramos A**, **Mateos LM**, **Gil JA**. 2008. Cell growth and cell division in the rod-shaped actinomycete Corynebacterium glutamicum. Antonie Van Leeuwenhoek **94**:99–109.
111. **Lavollay M**, **Arthur M**, **Fourgeaud M**, **Dubost L**, **Marie A**, **Riegel P**, **Gutmann L**, **Mainardi J-L**. 2009. The beta-lactam-sensitive D,D-carboxypeptidase activity of Pbp4 controls the L,D and D,D transpeptidation pathways in Corynebacterium jeikeium. Mol Microbiol **74**:650–661.
112. **Jones LJ**, **Carballido-López R**, **Errington J**. 2001. Control of cell shape in bacteria: helical, actin-like filaments in Bacillus subtilis. Cell **104**:913–922.
113. **Zupan JR**, **Cameron TA**, **Anderson-Furgeson J**, **Zambryski PC**. 2013. Dynamic FtsA and FtsZ localization and outer membrane alterations during polar growth and cell division in Agrobacterium tumefaciens. PNAS **110**:9060–9065.

114. **Matthysse AG**, **Holmes KV**, **Gurlitz RH**. 1981. Elaboration of cellulose fibrils by Agrobacterium tumefaciens during attachment to carrot cells. J Bacteriol **145**:583–595.
115. **Thorstenson YR**, **Zambryski PC**. 1994. The essential virulence protein VirB8 localizes to the inner membrane of Agrobacterium tumefaciens. J Bacteriol **176**:1711–1717.
116. **Kumar RB**, **Xie YH**, **Das A**. 2000. Subcellular localization of the Agrobacterium tumefaciens T-DNA transport pore proteins: VirB8 is essential for the assembly of the transport pore. Mol Microbiol **36**:608–617.
117. **Kumar RB**, **Das A**. 2002. Polar location and functional domains of the Agrobacterium tumefaciens DNA transfer protein VirD4. Mol Microbiol **43**:1523–1532.
118. **Atmakuri K**, **Ding Z**, **Christie PJ**. 2003. VirE2, a type IV secretion substrate, interacts with the VirD4 transfer protein at cell poles of Agrobacterium tumefaciens. Mol Microbiol **49**:1699–1713.
119. **Jakubowski SJ**, **Krishnamoorthy V**, **Cascales E**, **Christie PJ**. 2004. Agrobacterium tumefaciens VirB6 domains direct the ordered export of a DNA substrate through a type IV secretion System. J Mol Biol **341**:961–977.
120. **Judd PK**, **Kumar RB**, **Das A**. 2005. The type IV secretion apparatus protein VirB6 of Agrobacterium tumefaciens localizes to a cell pole. Mol Microbiol **55**:115–124.
121. **Judd PK**, **Kumar RB**, **Das A**. 2005. Spatial location and requirements for the assembly of the Agrobacterium tumefaciens type IV secretion apparatus. PNAS **102**:11498–11503.
122. **Xu J**, **Kim J**, **Danhorn T**, **Merritt PM**, **Fuqua C**. 2012. Phosphorus limitation increases attachment in Agrobacterium tumefaciens and reveals a conditional functional redundancy in adhesin biosynthesis. Res Microbiol **163**:674–684.
123. **Xu J**, **Kim J**, **Koestler BJ**, **Choi J-H**, **Waters CM**, **Fuqua C**. 2013. Genetic analysis of Agrobacterium tumefaciens unipolar polysaccharide production reveals complex integrated control of the motile-to-sessile switch. Mol Microbiol **89**:929–948.
124. **Tomlinson AD**, **Fuqua C**. 2009. Mechanisms and regulation of polar surface attachment in Agrobacterium tumefaciens. Curr Opin Microbiol **12**:708–714.
125. **Li G**, **Smith CS**, **Brun YV**, **Tang JX**. 2005. The elastic properties of the caulobacter crescentus adhesive holdfast are dependent on oligomers of N-acetylglucosamine. J Bacteriol **187**:257–265.
126. **Bardy SL**, **Maddock JR**. 2007. Polar explorations Recent insights into the polarity of bacterial proteins. Curr Opin Microbiol **10**:617–623.
127. **Gilmour MW**, **Lawley TD**, **Rooker MM**, **Newnham PJ**, **Taylor DE**. 2001. Cellular location and temperature-dependent assembly of IncHI1 plasmid R27-encoded TrhC-associated conjugative transfer protein complexes. Mol Microbiol **42**:705–715.
128. **Gunton JE**, **Gilmour MW**, **Alonso G**, **Taylor DE**. 2005. Subcellular localization and functional domains of the coupling protein, TraG, from IncHI1 plasmid R27. Microbiology (Reading, Engl) **151**:3549–3561.
129. **Aguilar J**, **Zupan J**, **Cameron TA**, **Zambryski PC**. 2010. Agrobacterium type IV

secretion system and its substrates form helical arrays around the circumference of virulence-induced cells. PNAS **107**:3758–3763.
130. **Backert S**, **Meyer TF**. 2006. Type IV secretion systems and their effectors in bacterial pathogenesis. Curr Opin Microbiol **9**:207–217.
131. **Thomashow MF**, **Hugly S**, **Buchholz WG**, **Thomashow LS**. 1986. Molecular basis for the auxin-independent phenotype of crown gall tumor tissues. Science **231**:616–618.
132. **Li G**, **Brown PJB**, **Tang JX**, **Xu J**, **Quardokus EM**, **Fuqua C**, **Brun YV**. 2012. Surface contact stimulates the just-in-time deployment of bacterial adhesins. Mol Microbiol **83**:41–51.
133. **Campo N**, **Tjalsma H**, **Buist G**, **Stepniak D**, **Meijer M**, **Veenhuis M**, **Westermann M**, **Müller JP**, **Bron S**, **Kok J**, **Kuipers OP**, **Jongbloed JDH**. 2004. Subcellular sites for bacterial protein export. Mol Microbiol **53**:1583–1599.
134. **Shih Y-L**, **Le T**, **Rothfield L**. 2003. Division site selection in Escherichia coli involves dynamic redistribution of Min proteins within coiled structures that extend between the two cell poles. PNAS **100**:7865–7870.
135. **Thanedar S**, **Margolin W**. 2004. FtsZ exhibits rapid movement and oscillation waves in helix-like patterns in Escherichia coli. Curr Biol **14**:1167–1173.
136. **Domínguez-Escobar J**, **Chastanet A**, **Crevenna AH**, **Fromion V**, **Wedlich-Söldner R**, **Carballido-López R**. 2011. Processive movement of MreB-associated cell wall biosynthetic complexes in bacteria. Science **333**:225–228.
137. **Garner EC**, **Bernard R**, **Wang W**, **Zhuang X**, **Rudner DZ**, **Mitchison T**. 2011. Coupled, Circumferential Motions of the Cell Wall Synthesis Machinery and MreB Filaments in B. subtilis. Science **333**:222–225.
138. **Akaike H**. 1974. A new look at the statistical model identification. IEEE Trans. Automat. Contr. **19**:716–723.
139. **Ingerson-Mahar M**, **Briegel A**, **Werner JN**, **Jensen GJ**, **Gitai Z**. 2010. The metabolic enzyme CTP synthase forms cytoskeletal filaments. Nat Cell Biol **12**:739–746.
140. **Foulquier E**, **Pompeo F**, **Bernadac A**, **Espinosa L**, **Galinier A**. 2011. The YvcK protein is required for morphogenesis via localization of PBP1 under gluconeogenic growth conditions in Bacillus subtilis. Mol Microbiol **80**:309–318.
141. **Pérez-Núñez D**, **Briandet R**, **David B**, **Gautier C**, **Renault P**, **Hallet B**, **Hols P**, **Carballido-López R**, **Guédon E**. 2011. A new morphogenesis pathway in bacteria: unbalanced activity of cell wall synthesis machineries leads to coccus-to-rod transition and filamentation in ovococci. Mol Microbiol **79**:759–771.
142. **Savage DF**, **Afonso B**, **Chen AH**, **Silver PA**. 2010. Spatially ordered dynamics of the bacterial carbon fixation machinery. Science **327**:1258–1261.
143. **López D**, **Kolter R**. 2010. Functional microdomains in bacterial membranes. Genes Dev **24**:1893–1902.
144. **Shiomi D**, **Yoshimoto M**, **Homma M**, **Kawagishi I**. 2006. Helical distribution of the bacterial chemoreceptor via colocalization with the Sec protein translocation machinery. Mol Microbiol **60**:894–906.
145. **Barák I**, **Muchová K**, **Wilkinson AJ**, **O'Toole PJ**, **Pavlendová N**. 2008. Lipid spirals in Bacillus subtilis and their role in cell division. Mol Microbiol **68**:1315–1327.

146. **Pichoff S**, **Shen B**, **Sullivan B**, **Lutkenhaus J**. 2012. FtsA mutants impaired for self-interaction bypass ZipA suggesting a model in which FtsA's self-interaction competes with its ability to recruit downstream division proteins. Mol Microbiol **83**:151–167.
147. **Cabelli RJ**, **Dolan KM**, **Qian LP**, **Oliver DB**. 1991. Characterization of membrane-associated and soluble states of SecA protein from wild-type and SecA51(TS) mutant strains of Escherichia coli. J Biol Chem **266**:24420–24427.
148. **Szeto TH**. 2002. Membrane localization of MinD is mediated by a C-terminal motif that is conserved across eubacteria, archaea, and chloroplasts. Proceedings of the National Academy of Sciences **99**:15693–15698.
149. **Salje J**, **van den Ent F**, **de Boer P**, **Löwe J**. 2011. Direct membrane binding by bacterial actin MreB. Mol Cell **43**:478–487.
150. **Brandon LD**, **Goehring N**, **Janakiraman A**, **Yan AW**, **Wu T**, **Beckwith J**, **Goldberg MB**. 2003. IcsA, a polarly localized autotransporter with an atypical signal peptide, uses the Sec apparatus for secretion, although the Sec apparatus is circumferentially distributed. Mol Microbiol **50**:45–60.
151. **Schindelin J**, **Arganda-Carreras I**, **Frise E**, **Kaynig V**, **Longair M**, **Pietzsch T**, **Preibisch S**, **Rueden C**, **Saalfeld S**, **Schmid B**, **Tinevez J-Y**, **White DJ**, **Hartenstein V**, **Eliceiri K**, **Tomancak P**, **Cardona A**. 2012. Fiji: an open-source platform for biological-image analysis. Nat Methods **9**:676–682.
152. **Schermelleh L**, **Heintzmann R**, **Leonhardt H**. 2010. A guide to super-resolution fluorescence microscopy. J Cell Biol **190**:165–175.
153. **Driessen AJM**, **Nouwen N**. 2008. Protein translocation across the bacterial cytoplasmic membrane. Annu Rev Biochem **77**:643–667.
154. **Xie K**, **Dalbey RE**. 2008. Inserting proteins into the bacterial cytoplasmic membrane using the Sec and YidC translocases. Nat Rev Micro **6**:234–244.
155. **Lill R**, **Dowhan W**, **Wickner W**. 1990. The ATPase activity of SecA is regulated by acidic phospholipids, SecY, and the leader and mature domains of precursor proteins. Cell **60**:271–280.
156. **Lutkenhaus J**. 2012. The ParA/MinD family puts things in their place. Trends Microbiol **20**:411–418.
157. **Ringgaard S**, **Schirner K**, **Davis BM**, **Waldor MK**. 2011. A family of ParA-like ATPases promotes cell pole maturation by facilitating polar localization of chemotaxis proteins. Genes Dev **25**:1544–1555.
158. **Roberts MAJ**, **Wadhams GH**, **Hadfield KA**, **Tickner S**, **Armitage JP**. 2012. ParA-like protein uses nonspecific chromosomal DNA binding to partition protein complexes. PNAS **109**:6698–6703.
159. **Treuner-Lange A**, **Aguiluz K**, **van der Does C**, **Gómez-Santos N**, **Harms A**, **Schumacher D**, **Lenz P**, **Hoppert M**, **Kahnt J**, **Muñoz-Dorado J**, **Søgaard-Andersen L**. 2013. PomZ, a ParA-like protein, regulates Z-ring formation and cell division in Myxococcus xanthus. Mol Microbiol **87**:235–253.
160. **Glauner B**, **Höltje JV**, **Schwarz U**. 1988. The composition of the murein of Escherichia coli. J Biol Chem **263**:10088–10095.
161. **Klüsener S**, **Hacker S**, **Tsai Y-L**, **Bandow JE**, **Gust R**, **Lai E-M**, **Narberhaus F**. 2010. Proteomic and transcriptomic characterization of a virulence-deficient phosphatidylcholine-negative Agrobacterium tumefaciens mutant. Molecular

Genetics and Genomics **283**:575–589.
162. **Lam H**, **Oh D-C**, **Cava F**, **Takacs CN**, **Clardy J**, **de Pedro MA**, **Waldor MK**. 2009. D-amino acids govern stationary phase cell wall remodeling in bacteria. Science **325**:1552–1555.
163. **Cava F**, **de Pedro MA**, **Lam H**, **Davis BM**, **Waldor MK**. 2011. Distinct pathways for modification of the bacterial cell wall by non-canonical D-amino acids. EMBO J **30**:3442–3453.
164. **Kuru E**, **Hughes HV**, **Brown PJ**, **Hall E**, **Tekkam S**, **Cava F**, **de Pedro MA**, **Brun YV**, **VanNieuwenhze MS**. 2012. In Situ probing of newly synthesized peptidoglycan in live bacteria with fluorescent D-amino acids. Angew. Chem. Int. Ed. Engl. **51**:12519–12523.
165. **Siegrist MS**, **Whiteside S**, **Jewett JC**, **Aditham A**, **Cava F**, **Bertozzi CR**. 2013. (D)-amino acid chemical reporters reveal peptidoglycan dynamics of an intracellular pathogen. ACS Chem. Biol. **8**:500–505.
166. **Slovak PM**, **Wadhams GH**, **Armitage JP**. 2005. Localization of MreB in Rhodobacter sphaeroides under conditions causing changes in cell shape and membrane structure. J Bacteriol **187**:54–64.
167. **Wietzerbin J**, **Das BC**, **Petit JF**, **Lederer E**, **Leyh-Bouille M**, **Ghuysen JM**. 1974. Occurrence of D-alanyl-(D)-meso-diaminopimelic acid and meso-diaminopimelyl-meso-diaminopimelic acid interpeptide linkages in the peptidoglycan of Mycobacteria. Biochemistry **13**:3471–3476.
168. **Lavollay M**, **Arthur M**, **Fourgeaud M**, **Dubost L**, **Marie A**, **Veziris N**, **Blanot D**, **Gutmann L**, **Mainardi J-L**. 2008. The peptidoglycan of stationary-phase Mycobacterium tuberculosis predominantly contains cross-links generated by L,D-transpeptidation. J Bacteriol **190**:4360–4366.
169. **Sanders AN**, **Pavelka MS**. 2013. Phenotypic analysis of Eschericia coli mutants lacking L,D-transpeptidases. Microbiology **159**:1842–1852.
170. **Kahng LS**, **Shapiro L**. 2001. The CcrM DNA methyltransferase of Agrobacterium tumefaciens is essential, and its activity is cell cycle regulated. J Bacteriol **183**:3065–3075.
171. **Kobayashi H**, **De Nisco NJ**, **Chien P**, **Simmons LA**, **Walker GC**. 2009. Sinorhizobium meliloti CpdR1 is critical for co-ordinating cell cycle progression and the symbiotic chronic infection. Mol Microbiol **73**:586–600.
172. **Hallez R**, **Mignolet J**, **Van Mullem V**, **Wery M**, **Vandenhaute J**, **Letesson J-J**, **Jacobs-Wagner C**, **De Bolle X**. 2007. The asymmetric distribution of the essential histidine kinase PdhS indicates a differentiation event in Brucella abortus. EMBO J **26**:1444–1455.
173. **Fields AT**, **Navarrete CS**, **Zare AZ**, **Huang Z**, **Mostafavi M**, **Lewis JC**, **Rezaeihaghighi Y**, **Brezler BJ**, **Ray S**, **Rizzacasa AL**, **Barnett MJ**, **Long SR**, **Chen EJ**, **Chen JC**. 2012. The conserved polarity factor podJ1 impacts multiple cell envelope-associated functions in Sinorhizobium meliloti. Mol Microbiol **84**:892–920.
174. **Kim J**, **Heindl JE**, **Fuqua C**. 2013. Coordination of division and development influences complex multicellular behavior in Agrobacterium tumefaciens. PLoS ONE **8**:e56682.
175. **Pini F**, **Frage B**, **Ferri L**, **De Nisco NJ**, **Mohapatra SS**, **Taddei L**, **Fioravanti A**,

Dewitte F, **Galardini M**, **Brilli M**, **Villeret V**, **Bazzicalupo M**, **Mengoni A**, **Walker GC**, **Becker A**, **Biondi EG**. 2013. The DivJ, CbrA and PleC system controls DivK phosphorylation and symbiosis in Sinorhizobium meliloti. Mol Microbiol **90**:54–71.

176. **Cheng J**, **Sibley CD**, **Zaheer R**, **Finan TM**. 2007. A Sinorhizobium meliloti minE mutant has an altered morphology and exhibits defects in legume symbiosis. Microbiology (Reading, Engl) **153**:375–387.
177. **Latch JN**, **Margolin W**. 1997. Generation of buds, swellings, and branches instead of filaments after blocking the cell cycle of Rhizobium meliloti. J Bacteriol **179**:2373–2381.
178. **Heidrich C**, **Templin MF**, **Ursinus A**, **Merdanovic M**, **Berger J**, **Schwarz H**, **de Pedro MA**, **Höltje JV**. 2001. Involvement of N-acetylmuramyl-L-alanine amidases in cell separation and antibiotic-induced autolysis of Escherichia coli. Mol Microbiol **41**:167–178.
179. **Priyadarshini R**, **Popham DL**, **Young KD**. 2006. Daughter cell separation by penicillin-binding proteins and peptidoglycan amidases in Escherichia coli. J Bacteriol **188**:5345–5355.
180. **Priyadarshini R**, **de Pedro MA**, **Young KD**. 2007. Role of peptidoglycan amidases in the development and morphology of the division septum in Escherichia coli. J Bacteriol **189**:5334–5347.
181. **Peters NT**, **Dinh T**, **Bernhardt TG**. 2011. A fail-safe mechanism in the septal ring assembly pathway generated by the sequential recruitment of cell separation amidases and their activators. J Bacteriol **193**:4973–4983.
182. **Yang DC**, **Tan K**, **Joachimiak A**, **Bernhardt TG**. 2012. A conformational switch controls cell wall-remodelling enzymes required for bacterial cell division. Mol Microbiol **85**:768–781.
183. **Katoh K**, **Standley DM**. 2013. MAFFT multiple sequence alignment software version 7: improvements in performance and usability. Mol. Biol. Evol. **30**:772–780.
184. **Capella-Gutiérrez S**, **Silla-Martínez JM**, **Gabaldón T**. 2009. trimAl: a tool for automated alignment trimming in large-scale phylogenetic analyses. Bioinformatics **25**:1972–1973.
185. **Guindon S**, **Dufayard J-F**, **Lefort V**, **Anisimova M**, **Hordijk W**, **Gascuel O**. 2010. New algorithms and methods to estimate maximum-likelihood phylogenies: assessing the performance of PhyML 3.0. Syst. Biol. **59**:307–321.
186. **Han MV**, **Zmasek CM**. 2009. phyloXML: XML for evolutionary biology and comparative genomics. BMC Bioinformatics **10**:356.
187. **R Core Team**. 2013. R: A Language and Environment for Statistical Computing. R Foundation for Statistical Computing, Vienna, Austria.
188. **Wickham H**. 2009. ggplot2. Springer.
189. **Badger JH**, **Eisen JA**, **Ward NL**. 2005. Genomic analysis of Hyphomonas neptunium contradicts 16S rRNA gene-based phylogenetic analysis: implications for the taxonomy of the orders “Rhodobacterales” and Caulobacterales. Int. J. Syst. Evol. Microbiol. **55**:1021–1026.
190. **Khan SR**, **Gaines J**, **Roop RM**, **Farrand SK**. 2008. Broad-host-range expression vectors with tightly regulated promoters and their use to examine the

influence of TraR and TraM expression on Ti plasmid quorum sensing. Appl Environ Microbiol **74**:5053–5062.
191. **Young KD**. 2010. Bacterial shape: two-dimensional questions and possibilities. Annu Rev Microbiol **64**:223–240.
192. **Mannik J**, **Driessen R**, **Galajda P**, **Keymer JE**, **Dekker C**. 2009. Bacterial growth and motility in sub-micron constrictions. PNAS **106**:14861–14866.
193. **Sliusarenko O**, **Heinritz J**, **Emonet T**, **Jacobs-Wagner C**. 2011. High-throughput, subpixel precision analysis of bacterial morphogenesis and intracellular spatio-temporal dynamics. Mol Microbiol **80**:612–627.
194. **Hallez R**, **Bellefontaine A-F**, **Letesson J-J**, **De Bolle X**. 2004. Morphological and functional asymmetry in alpha-proteobacteria. Trends Microbiol **12**:361–365.
195. **Koch AL**, **Higgins ML**. 1984. Control of wall band splitting in Streptococcus faecalis. J. Gen. Microbiol. **130**:735–745.
196. **Mignolet J**, **Van der Henst C**, **Nicolas C**, **Deghelt M**, **Dotreppe D**, **Letesson J-J**, **De Bolle X**. 2010. PdhS, an old-pole-localized histidine kinase, recruits the fumarase FumC in Brucella abortus. J Bacteriol **192**:3235–3239.
197. **Van der Henst C**, **de Barsy M**, **Zorreguieta A**, **Letesson J-J**, **De Bolle X**. 2013. The Brucella pathogens are polarized bacteria. Microbes Infect.